

Towards Double Parton Distributions from First Principles using Large Momentum Effective Theory

Max Jaarsma,^{a,b} Rudi Rahn,^{a,b,c} Wouter J. Waalewijn^{a,b}

^a*Nikhef, Theory Group, Science Park 105, 1098 XG, Amsterdam, The Netherlands*

^b*Institute for Theoretical Physics Amsterdam and Delta Institute for Theoretical Physics, University of Amsterdam, Science Park 904, 1098 XH Amsterdam, The Netherlands*

^c*Department of Physics and Astronomy, University of Manchester, Manchester, M13 9PL, United Kingdom*

E-mail: m.jaarsma@uva.nl, rudi.rahn@manchester.ac.uk,
w.j.waalewijn@uva.nl

ABSTRACT: In double parton scattering (DPS), two partonic collisions take place between one pair of colliding hadrons. The effect of DPS can be significant for precision measurements due to the additional radiation from secondary partonic collisions, and especially for specific processes such as same-sign WW production. Its effect is usually included through Monte Carlo parton showers. In a factorization approach to DPS, the initial state is described by double parton distributions (DPDs). These are currently poorly constrained by experiment, but provide a view on interesting correlations between partons in the hadron. Here we show that the Large Momentum Effective Theory approach can be applied to DPDs. Specifically, we present a general matching relation between DPDs and lattice-calculable quasi-DPDs for general flavor, spin and color structures. We furthermore calculate the one-loop matching coefficients for the quark-quark DPDs, verifying that the infrared logarithms and divergences cancel in the matching. While we restrict to the flavor-non-singlet case, we do take color and spin correlations into account. Interestingly, quasi-DPDs combines non-trivial features from both the collinear and transverse momentum dependent quasi-parton distribution functions. This represents a first step in extending the quasi-PDF approach to DPDs, opening up a new way to constrain these distributions using lattice QCD.

Contents

1	Introduction	1
2	Quasi-PDFs, TMDs, and LaMET	3
2.1	Notation and conventions	3
2.2	Lightcone PDFs and TMDs	4
2.3	Quasi-PDFs and matching with lightcone-PDFs	6
2.4	Quasi-TMDs and matching with physical TMDs	8
2.5	Lattice calculability of the quasi-soft function	10
3	Double parton distribution functions	11
3.1	Introduction to double parton scattering	11
3.2	Field-theoretical definition of DPDs	13
3.3	Renormalization of DPDs	15
4	Quasi-double parton distributions	16
4.1	Defining quasi-DPDs	16
4.2	Lattice calculability of the DPD quasi-soft function	18
4.3	Factorization for quasi-DPDs	19
5	One-loop matching for the flavor-non-singlet case	22
5.1	Handling divergences in calculating DPDs for partonic states	22
5.2	Constructing the one-loop matching kernel	24
5.3	Lightcone- and quasi-DPDs at one-loop	27
5.4	Result for one-loop matching kernel	30
6	Conclusions	32
A	Plus distributions	33
B	One-loop diagrams	33

1 Introduction

Experimental studies at hadron colliders largely focus on hard scattering processes, in which heavy particles (such as Higgs bosons or top quarks) or jets with large transverse momenta are produced. In the theoretical description of these processes, one usually considers a single partonic scattering between a pair of colliding hadrons. Monte Carlo parton showers account for the underlying event through multiple parton interactions [1–4] to describe

the data. These additional partonic collisions are much less energetic, but the resulting radiation may e.g. affect jet measurements such as the jet mass [5, 6].

In a factorization approach to double parton scattering (DPS), the initial state is described by double parton distributions (DPDs). DPS was already considered in the early days of the parton model [7–11], and since then there has been substantial progress in formalizing the theoretical framework [11–20], see ref. [21] for a comprehensive review. DPDs describe the possibility of extracting two partons out of a hadron, in direct analogy to the parton distribution functions (PDFs) that describe the extraction of a single parton. DPDs depend on the transverse separation of the partons, as well as their flavor, spin and color states, opening up the exciting possibility of studying correlations between the partons in the hadron [10, 13, 14, 16].

While there is clear experimental evidence for double parton scattering, the result of such measurements is often expressed in terms of a single number: the effective cross section σ_{eff} . This assumes that both scatterings are independent of each other, as summarized in the “pocket formula” for the DPS cross section: $\sigma_{\text{DPS}} = \sigma_1 \sigma_2 / (S \sigma_{\text{eff}})$, where $\sigma_{1,2}$ are the cross sections of the individual partonic scatterings and S is a symmetry factor [11]. Though there are many measurements of σ_{eff} from different processes [22–36], the field has not progressed to the point that an extraction of DPDs is within reach. In the meantime, sum rules [37, 38] and positivity bounds have been investigated [39, 40], DPDs have been studied using various models of the proton [41–47], and moments of the DPDs have been extracted from lattice data [48–50] (similar to the lattice extraction of moments of parton distributions).

In recent years, a new method of obtaining PDFs from lattice QCD has been proposed [51–59], which makes use of Large Momentum Effective Theory (LaMET) and has been referred to the quasi-PDF approach (alternatively, there is the pseudo-PDF approach based on short-distance factorization). In this method one defines an analogue of the PDF in which the fields are now space-like separated, known as the quasi-PDF, which corresponds to the PDF under an infinite Lorentz boost. The quasi-PDF is defined such that it can be calculated using lattice methods. It agrees with the PDF in the infrared (nonperturbative) limit, and the difference in the ultraviolet limit can be encoded by a perturbative matching correction, in principle providing access to the entire momentum fraction dependence of the PDF. More recently, this method has been extended to the case of transverse momentum dependent parton distributions (TMDs) [60–69]. This extension was rather non-trivial because the definition of the physical TMDs, the ones that enter the factorization formulae, contains a soft function. The soft function involves two opposite light-like directions, which presents a difficulty to implement on a Euclidean lattice. Fortunately, it has been shown that the soft function can be split up into a rapidity independent part and a part that only involves the Collins-Soper kernel and that each individual part can be calculated on the lattice [61, 63, 70–73].

In this paper, we extend the quasi-PDF approach to the case of DPDs. We define lattice-calculable quasi-DPDs and construct a matching formula that relates them to their physical counterparts. The matching relation we present is general: it holds for DPDs of all flavor combinations, spin structures and color structures. We further present a one-loop

calculation of the matching kernels that are relevant to the quark flavor non-singlet case, and we include results for spin and color correlations. This calculation verifies, at least to one-loop order, that the quasi-DPDs and the physical DPDs share the same infrared behaviour, which is a necessary condition for the matching to apply. With this matching relation, DPD and the nonperturbative correlations of partons in a hadron they encode, can be accessed through lattice QCD.

The outline of this paper is as follows: In sec. 2 we provide a brief introduction to LaMET and its application to quasi-PDFs and TMDs. Similarly, in sec. 3 we provide a brief introduction on DPDs, including their field-theoretic definition. (These sections can be skipped by those familiar with these topics.) The matching between quasi-DPDs and physical DPDs is discussed in sec. 4, and an explicit one-loop calculation for the quark flavor non-singlet case is carried out in sec. 5, with expressions for individual diagrams relegated to app. B. We conclude in sec. 6. Notation regarding plus distributions are summarized in app. A.

2 Quasi-PDFs, TMDs, and LaMET

After establishing our notation and conventions in sec. 2.1, we start in sec. 2.2 with a recap of the field-theoretic definition of parton distribution functions (PDFs) and transverse-momentum-dependent parton distribution functions (TMDs). We review the current approach to extract PDFs (sec. 2.3) and TMDs (sec. 2.4) from lattice calculations using Large Momentum Effective Theory (LaMET).

We refer the reader to the original literature on LaMET [51, 52, 56], as well as a paper [65] proving the possibility of determining TMDs using lattice calculations, on which much of our understanding is based. We generally follow the notation established in ref. [65].

2.1 Notation and conventions

In defining parton distribution functions, it is useful to work in lightcone coordinates. We denote the components of a vector in lightcone coordinates by $(v^+, v^-, \mathbf{v}_\perp)$, where

$$v^\pm = \frac{v^0 \pm v^z}{\sqrt{2}}, \quad \mathbf{v}_\perp = (v^x, v^y). \quad (2.1)$$

The dot product takes the following form

$$v \cdot w = v^+ w^- + v^- w^+ - \mathbf{v}_\perp \cdot \mathbf{w}_\perp, \quad (2.2)$$

and the factors of $\sqrt{2}$ ensure that the Jacobian of the coordinate transformation is unity, $d^4x = dx^+ dx^- d^2\mathbf{x}_\perp$. Corresponding to a transverse vector \mathbf{b}_\perp , we write

$$b_\perp = (0, 0, \mathbf{b}_\perp), \quad (2.3)$$

and we will use \mathbf{b}_\perp and b_\perp interchangeably when there is no potential for confusion. We will use $n_a = (1^+, 0^-, \mathbf{0}_\perp)$, $n_b = (0^+, 1^-, \mathbf{0}_\perp)$ to denote the light-like basis vectors.

The definition of parton distributions involve Wilson lines, which are path ordered exponentials of gauge field operators. For a general path γ , the Wilson line is defined as

$$W[\gamma] = P \exp \left(i g \int_{\gamma} dx^{\mu} \mathcal{A}_{\mu}^a(x) t^a \right). \quad (2.4)$$

In general the t^a depends on the $SU(3)$ representation of the partons, but in this work we restrict ourselves to quarks and therefore only need the fundamental representation. Hence there is no need for a label to indicate the representation.

In the TMDs we will encounter Wilson lines that follow a staple-shaped path, for which we introduce the following notation

$$W_{\sqsubset}(b, \eta v, \delta) = W \left[b \leftarrow b + \eta v - \frac{\delta}{2} \leftarrow \eta v + \frac{\delta}{2} \leftarrow 0 \right]. \quad (2.5)$$

This describes a Wilson line consisting of straight-line segments going from the origin to b along a staple-shaped path, where the sides of the staple have length η and lie in the direction of v . Note that our convention for the direction of the arrows is opposite that of [65], i.e. our “ \leftarrow ” corresponds to their “ \rightarrow ”. The argument δ concerns the shape of the transverse segment of the Wilson line and is chosen such that the transverse segment is perpendicular to the longitudinal pieces (to avoid angle-dependence in the renormalization of the soft function). Besides the staple-shaped Wilson line, the definition of TMDs also involves a Wilson loop that is obtained by gluing together two staple-shaped Wilson lines at their end-points, which we denote by

$$S_{\gg}(b, \eta v, \bar{\eta} \bar{v}) = \text{tr} [W[b \leftarrow b + \bar{\eta} \bar{v} \leftarrow \bar{\eta} \bar{v} \leftarrow 0 \leftarrow \eta v \leftarrow b + \eta v \leftarrow b]]. \quad (2.6)$$

2.2 Lightcone PDFs and TMDs

The (bare) parton distribution functions are defined as hadronic matrix elements of fields separated along the lightcone. For quarks,

$$f_q(x, \epsilon) = \int \frac{db^-}{4\pi} e^{-i x P^+ b^-} \langle P | \bar{\psi}(b^-) \gamma^+ W[b^- \leftarrow 0] \psi(0) | P \rangle, \quad (2.7)$$

where $(0^+, b^-, \mathbf{0}_{\perp})$ is abbreviated to b^- and ϵ regulates the UV divergences. Here, $W[b^- \leftarrow 0]$ is a straight Wilson line from 0 to b^- that ensures the gauge invariance of the parton distribution, and is defined in eq. (2.4). The finite length Wilson line in eq. (2.7) can be regarded as the remnant of two Wilson lines extending to infinity with opposite orientation,

$$W[b^- \leftarrow 0] = W[b^- \leftarrow -\infty n_b] W[-\infty n_b \leftarrow 0], \quad (2.8)$$

describing the remaining color-charged objects in the process and accounting for the interactions of the extracted parton with their color-potential. The bare lightcone PDFs have ultraviolet divergences and require renormalization, leading to a dependence on a renormalization scale μ in the renormalized PDFs.

Next, we consider the field theoretic definition of lightcone TMDs, for which we will only consider the quark case and hence suppress flavor labels. Since TMDs also encode the

dependence on the transverse momentum of the parton, they naively correspond to PDFs in which the fields also have a separation along the transverse directions. This transverse gap prevents the cancellation of the anti-parallel Wilson lines in eq. (2.8). As a consequence, we encounter the rapidity divergences typically associated with infinite-length light-like Wilson lines. Many different regulators have been introduced to handle these rapidity divergences, see e.g. refs. [74–80]. In this work we consider two of these: the off-lightcone regulator used in the Collins scheme [76] and the δ -regulator [74, 79]. The off-lightcone regulator takes all light-like Wilson slightly off the lightcone,

$$\begin{aligned} W[a - \infty n_a \leftarrow a] &\rightarrow W[a - \infty n_A(y_A) \leftarrow a], \\ W[a - \infty n_b \leftarrow a] &\rightarrow W[a - \infty n_B(y_B) \leftarrow a], \end{aligned} \quad (2.9)$$

where $n_A(y_A)$ and $n_B(y_B)$ are space-like vectors with rapidities of respectively y_A and y_B ,

$$\begin{aligned} n_A(y_A) &= (1, -e^{-2y_A}, \mathbf{0}_\perp), \\ n_B(y_B) &= (-e^{2y_B}, 1, \mathbf{0}_\perp). \end{aligned} \quad (2.10)$$

The delta regulator is implemented by modifying the definition of infinite-length Wilson lines as follows,

$$\begin{aligned} W[a - \infty n_a \leftarrow a] &\rightarrow P \exp \left(ig \int_0^{-\infty} ds e^{s\delta^-} A^{c,-}(a + sn_a) t^c \right) \\ W[a - \infty n_b \leftarrow a] &\rightarrow P \exp \left(ig \int_0^{-\infty} ds e^{s\delta^+} A^{c,+}(a + sn_b) t^c \right). \end{aligned} \quad (2.11)$$

The effect of this regulator is that the $\pm i0$ in eikonal propagators get replaced by finite imaginary numbers.

To construct a lightcone TMD that is free of rapidity divergences, we begin by defining a *beam function*, also known as the unsubtracted TMD. In the Collins scheme the (bare) beam function is defined as

$$B(x, b_\perp, \epsilon, y_B, P^+) = \int \frac{db^-}{4\pi} e^{-ixP^+b^-} \langle P | \bar{\psi}(b) \gamma^+ W_\square(b, -\infty n_B(y_B), b^- n_b) \psi(0) | P \rangle, \quad (2.12)$$

where $b = (0, b^-, \mathbf{b}_\perp)$ and W_\square is a staple-shaped Wilson line defined in eq. (2.5). It extends from one quark field along the lightcone to minus infinity, bridges the transverse gap, and returns to connect to the second quark field in the correlator. The third argument in this Wilson line is chosen such that the transverse gap is perpendicular to the longitudinal segments of the Wilson line. In the above, y_B is associated with the rapidity of n_B , as given in eq. (2.10), and acts as a rapidity regulator by taking the Wilson line slightly off the lightcone.

The dependence on a rapidity regulator is indicative of a missing piece in our calculation, given here by a *soft function* encoding the dependence on soft emissions radiated by the energetic colour-charged particles in the process. In the Collins scheme, the (bare) soft function is defined as

$$S(b_\perp, \epsilon, y_A, y_B) = \frac{1}{N_c} \langle 0 | S_{\gg}(b_\perp, -\infty n_A(y_A), -\infty n_B(y_B)) | 0 \rangle, \quad (2.13)$$

with the Wilson loop $S_{\mathbb{S}}$ defined in eq. (2.6). The soft function encodes information about the full process, as soft emissions — isotropic and long-ranged — can mediate interactions between the different collinear sectors. For the definition of one single TMD, this means that only one Wilson staple’s direction is fixed to match the beam function (\sqcap), the other (\sqcap') must be matched up with the TMD describing the other incoming parton (or outgoing spray of hadrons, for semi-inclusive deep-inelastic scattering), such that the full cross-section is well-defined. As a result, the geometry encoded by the soft function resembles that of an open book, with the spine along the transverse separation between the partons (and with infinitely wide pages). It carries two rapidity regulators, y_A and y_B , due to the fact that there are two staple-shaped Wilson lines in its definition (the two open pages of the book).

The physical TMD is defined as the ratio of the beam function and the square root of the soft function¹. In the Collins scheme,

$$f(x, b_{\perp}, \mu, \zeta) = \lim_{\epsilon \rightarrow 0} Z_{\text{uv}}(\epsilon, \mu, \zeta) \lim_{y_B \rightarrow -\infty} \frac{B(x, b_{\perp}, \epsilon, y_B, P^+)}{\sqrt{S(b_{\perp}, \epsilon, y_A, y_B)}}, \quad (2.14)$$

which is free of rapidity divergences regularized by y_B , but depends on an auxiliary variable

$$y_n = \frac{1}{2}(y_A + y_B). \quad (2.15)$$

In eq. (2.14) it is implied that one takes $y_B \rightarrow -\infty$ and $y_A \rightarrow +\infty$ while keeping y_n fixed. The dependence on y_n cancels in the full cross-section, through a dependence on a rapidity scale

$$\zeta = 2(xP^+)^2 e^{-2y_n} \quad (2.16)$$

as a remnant of the rapidity regulator cancellation. After the rapidity divergences are cancelled, the UV divergences are regularized and renormalized through Z_{uv} , to arrive at a TMD that can be used in calculations.

2.3 Quasi-PDFs and matching with lightcone-PDFs

The PDFs and TMDs as defined above are, unfortunately, not compatible with calculations on the lattice. This is mainly due to the sign problem. Lattice QCD circumvents the sign problem by making use of a Euclidean lattice, prohibiting the calculation of matrix elements where operators are separated in time. Since the parton distributions in eqs. (2.7) and (2.12) involve fields that are separated along the lightcone, and hence also separated in time, they cannot be directly accessed on the lattice.

A solution arises from the insight that the ultra-relativistic limit of a space-like trajectory “looks” light-like, and so we may expect to be able to relate a highly-boosted off-lightcone parton distribution to a PDF (or TMD). This is the fundamental insight behind the quasi-PDF approach, and has its root in the view of the parton picture as envisioned by Large Momentum Effective Theory (LaMET) [51, 52, 56]. LaMET posits that in the large-momentum limit the structure of a proton (typically chosen to travel along the z -direction)

¹The reason we divide, rather than multiply, with by the square root of the soft function is due the zero-bin [81], that accounts for the overlap between the beam function and soft function. Here this overlap is equal to the inverse of the soft function [82–84].

is independent of the exact value for P^z — a Large Momentum symmetry — and so we should expect results for PDFs (or TMDs) defined with separation along the z -direction to agree with those separated along the lightcone up to corrections of $\mathcal{O}(\Lambda_{\text{QCD}}^2/P_z^2)$ ². As a consequence, we can define a quasi-PDF, with exactly this type of separation.

Quasi-PDFs have the same definition as their lightcone counterparts, but with the lightcone correlators replaced by correlators where the fields are only separated along the z -axis. For quarks, the (bare) quasi-PDF is defined as

$$\tilde{f}_q(x, \epsilon, P^z) = \int \frac{dz}{4\pi} e^{ixP^z z} \langle P | \bar{\psi}(z) \gamma^z W[z \leftarrow 0] \psi(0) | P \rangle. \quad (2.17)$$

where we use a tilde to distinguish it from the light-cone PDF in eq. (2.7). The time-independence of this matrix element makes the quasi-PDF well suited for lattice calculations. In contrast to the boost-invariant lightcone-PDF, the quasi-PDF is boost dependent, which is captured by its P^z dependence. Applying an infinite boost to the quasi-PDF is therefore identical to considering the $P^z \rightarrow \infty$ limit.

As $P^z \rightarrow \infty$, one naively expects the quasi-PDF to approach the lightcone-PDF. However, they are inherently different due the order of limits concerning the ultraviolet regulator and $P^z \rightarrow \infty$: For the lightcone-PDF that enters in factorization formulae, a UV regulator is introduced after already having taken the limit of infinite hadron momentum. For the quasi-PDF, the infinite boost is only performed after UV divergences have been regulated. Instead of equality, one can however derive a matching relation relating the lightcone- and quasi-PDFs in the limit that P^z is much larger than Λ_{QCD} and the mass of the hadron M [51, 52, 58]:

$$\tilde{f}_a(x, \mu, P^z) = \sum_{a'} \int_{-1}^1 \frac{dx'}{|x'|} \mathcal{C}_{aa'}\left(\frac{x}{x'}, \frac{\mu}{|x'|P^z}\right) f_{a'}(x', \mu) + \mathcal{O}\left(\frac{M^2}{P_z^2}, \frac{\Lambda_{\text{QCD}}^2}{x^2 P_z^2}, \frac{\Lambda_{\text{QCD}}^2}{(1-x)^2 P_z^2}\right). \quad (2.18)$$

Here \mathcal{C} is a perturbative matching kernel and the sum over a' accounts for mixing between parton species. This matching relation also holds for polarized PDFs ($a = \Delta q, \delta q$). It should be noted that the above equation relates the renormalized lightcone- and quasi-PDFs, so the matching kernel depends on the renormalization schemes for the lightcone- and quasi-PDFs. Though scale-invariance requires that the matching coefficient depends on the value of μ and the partonic momentum $|x'|P^z$, any perturbative expansion will involve $\alpha_s(\mu)$ as well.

The matching kernel for the quark flavor non-singlet case (\mathcal{C}_{qq}) was first calculated to one-loop order for all polarizations in ref. [59] and is now known up to two-loop order [85, 86]. The complete matching for all parton species and polarizations has been performed to one-loop order [87].

Much progress has been made in extracting parton distributions from lattice data. The unpolarized quark flavor non-singlet distribution was recently extracted from lattice data using the two-loop matching kernel [88] and the gluon PDF has been calculated using the

²The power corrections also depend on x, b_\perp and the mass of the hadron.

one-loop matching coefficient [57, 89–91]. Additionally, the above matching relation has been extended to the case of generalized parton distributions (GPDs) [92].

2.4 Quasi-TMDs and matching with physical TMDs

In this section we review the recent progress for quasi-TMDs. We start by providing their field-theoretic definition, present the matching relation with the physical TMDs, and then sketch the proof for this matching that was given in ref. [65].

The (bare) quasi-beam function corresponding to the beam function in eq. (2.12) is defined as,

$$\tilde{B}(x, b_\perp, a, \tilde{\eta}, x\tilde{P}^z) = \int \frac{dz}{4\pi} e^{ixP^z z} \langle \tilde{P} | \bar{\psi}(b) \gamma^z W_\square(b, \tilde{\eta}\hat{z}, b^z\hat{z}) \psi(0) | \tilde{P} \rangle, \quad (2.19)$$

where $b = (0, \mathbf{b}_\perp, z)$, a denotes a UV regulator (e.g. ϵ or the lattice spacing), and the Wilson staple is now along the z -axis. The finite length of the Wilson line $\tilde{\eta}$ renders this object calculable on the lattice. The limit of large $\tilde{\eta}$ is divergent, so $\tilde{\eta}$ has to be chosen large but finite for calculations on the lattice. The external proton state and choice of rapidity regulator influence each other as will be discussed below (see eq. (2.27)), which is the reason we write $|\tilde{P}\rangle$ and \tilde{P}^z in this section (which was not needed in sec. 2.3).

As for the physical TMD in eq. (2.14), the quasi-TMD requires a soft function. Defining a quasi-soft function that is related to the soft function by a Lorentz boost and is lattice calculable is challenging: the soft function knows about the color flow in the full process, as indicated by the two Wilson staples extending in *different* light-like directions. Here we contend ourselves to provide a definition of a soft function that leads to a consistent matching, deferring a discussion of how to calculate it on the lattice to sec. 2.5. The quasi-soft function can be defined by taking the Collins soft function, where the two staples are slightly off the lightcone, and boosting it such that one of its staples lies along the z -axis. Since the soft function is boost invariant, one does not have to make this boost explicit. One does, however, need to take into account that the quasi-soft function is to be calculated on the lattice, and therefore one has to impose a restriction on the length of the Wilson lines. This leads to the following definition

$$\tilde{S}(b_\perp, a, \tilde{\eta}, y_A, y_B) = \frac{1}{N_c} \langle 0 | S_\gg \left(b_\perp, -\tilde{\eta} \frac{n_A(y_A)}{|n_A(y_A)|}, -\tilde{\eta} \frac{n_B(y_B)}{|n_B(y_B)|} \right) | 0 \rangle, \quad (2.20)$$

Note that, because of the finite length $\tilde{\eta}$ of the Wilson lines, the quasi-soft function is rapidity finite. Rapidity divergences appear as $\tilde{\eta} \rightarrow \infty$.

The quasi-TMD is then defined as the ratio of the quasi-beam function in eq. (2.19) and the square root of the quasi-soft function in eq. (2.20),

$$\tilde{f}(x, b_\perp, \mu, \tilde{\zeta}, x\tilde{P}^z) = \lim_{a \rightarrow 0} \tilde{Z}_{\text{uv}}(a, \mu, y_A - y_B) \lim_{\tilde{\eta} \rightarrow \infty} \frac{\tilde{B}(x, b_\perp, a, \tilde{\eta}, x\tilde{P}^z)}{\sqrt{\tilde{S}(b_\perp, a, \tilde{\eta}, y_A, y_B)}}. \quad (2.21)$$

Here, the limit $\tilde{\eta} \rightarrow \infty$ is taken at fixed but arbitrarily large y_A and y_B , and the divergences that appear as $\tilde{\eta} \rightarrow \infty$ cancel between the beam and the soft function. Since the

quasi-beam and soft function can both be renormalized multiplicatively, we included one renormalization factor Z_{uv} for both. This renormalization factor only depends on the cusp of the Wilson lines, which can be expressed in terms of $y_A - y_B$. More notably, the renormalization does not depend on $\tilde{\eta}$ as this parameter only contains long-distance physics, and it is also insensitive to the parton momentum as is always the case for quasi parton distributions. Finally, note that the dependence on y_A and y_B on the right-hand side is hidden in the

$$\tilde{\zeta} = (2x\tilde{P}^z e^{y_B - y_n})^2 \quad (2.22)$$

on the left-hand side. This would seem to diverge as $y_A \rightarrow \infty$ and $y_B \rightarrow -\infty$ for fixed y_n , but this divergence can be shown to be spurious by expressing \tilde{P}^z in terms of the momentum P^+ for the physical TMD using eq. (2.27) given below.

The quasi-TMD in eq. (2.21) can be matched perturbatively onto the physical (Collins scheme) TMD,

$$\tilde{f}(x, b_\perp, \mu, \tilde{\zeta}, x\tilde{P}^z) = C(x\tilde{P}^z, \mu) \exp\left[\frac{1}{2}\gamma_\zeta(b_\perp, \mu) \ln\left(\frac{\tilde{\zeta}}{\zeta}\right)\right] f(x, b_\perp, \mu, \zeta), \quad (2.23)$$

where $C(x\tilde{P}^z, \mu)$ is a perturbative matching factor. This matching was proven in ref. [65] in two steps: First the quasi-TMD was related to a so-called large rapidity (LR) scheme TMD, which is then subsequently related to the physical (Collins scheme) TMD. The LR scheme can be viewed as an intermediate scheme between the quasi-TMD and the Collins-TMD, and is defined as the Collins scheme but with the order of the $y_B \rightarrow -\infty$ and $\epsilon \rightarrow 0$ limits reversed:

$$f^{\text{LR}}(x, b_\perp, \mu, \zeta, y_P - y_B) = \lim_{-y_B \gg 1} \lim_{\epsilon \rightarrow 0} Z_{\text{uv}}^{\text{LR}}(\epsilon, \mu, y_n - y_B) \frac{B(x, b_\perp, \epsilon, y_P - y_B)}{\sqrt{S(b_\perp, \epsilon, y_A, y_B)}}, \quad (2.24)$$

where

$$y_P = \frac{1}{2} \ln(P^+/P^-) = \ln[P^+ / (\sqrt{2}m_h)] \quad (2.25)$$

is the rapidity of the hadron momentum P . Here, both the left-hand-side and the right-hand-side depend on y_A and y_B , through either ζ as given in eq. (2.16) and eq. (2.15), or through y_n as given in eq. (2.15) directly. As ζ and y_n are assumed to be fixed the value of y_B therefore also determines the size of y_A . It was then shown, by an analysis of all Lorentz invariants that a TMD can depend on, that the quasi-TMD of eq. (2.21) and the LR-scheme TMD in eq. (2.24) are related by

$$\tilde{f}(x, b_\perp, \mu, \tilde{\zeta}, x\tilde{P}^z) = f^{\text{LR}}(x, b_\perp, \mu, \tilde{\zeta}, y_P - y_B). \quad (2.26)$$

Additionally, this analysis leads to the conclusion that

$$y_{\tilde{P}} = y_P - y_B, \quad (2.27)$$

where $y_{\tilde{P}}$ is the rapidity of \tilde{P} , which is the hadron momentum for the quasi-TMD. Consequently this equation illustrates why we take y_B to be large but finite.

Finally, the authors of [65] relate the LR scheme TMD to the Collins TMD, which differ only by the order of limits $y_B \rightarrow -\infty$ and $\epsilon \rightarrow 0$. Using asymptotic freedom, they argue that the difference between the two schemes can be accounted for by a perturbative matching factor. Combining this with the relation between the quasi- and LR scheme TMD of eq. (2.26), they arrive at the matching relation in eq. (2.23).

The first lattice calculation of the unpolarized flavor non-singlet quark TMD was carried out in [69] and an application to spin dependent TMDs can be found in [93]. Additionally, the matching relation in eq. (2.23) has been used to extract the Collins-Soper kernel from lattice calculations [71, 73]. The matching factor in eq. (2.23) is currently known to two-loops [68].

2.5 Lattice calculability of the quasi-soft function

Unfortunately, the quasi-TMD in eq. (2.21) that appears in the matching relation eq. (2.23) is not directly calculable on the lattice. The problem lies with the quasi-soft function that enters the definition of the quasi-TMD. The quasi-soft function consists of two Wilson line staples that are slightly off the lightcone staples, only one of which can be boosted to lie along the z -axis. Consequently, the matrix element defining the quasi-soft function is time dependent and cannot be calculated on the lattice directly.

In the literature this issue has been addressed by introducing a naive quasi-soft function. The (bare) naive quasi soft function is defined in terms of a rectangular Wilson loop, whose longitudinal sides lie along the z -axis,

$$\tilde{S}_{\text{naive}}(b_\perp, a, \tilde{\eta}) = \frac{1}{N_c} \langle 0 | S_{\gg}(b_\perp, \tilde{\eta}\hat{z}, -\tilde{\eta}\hat{z}) | 0 \rangle. \quad (2.28)$$

This soft factor can then be used to define a naive quasi-TMD that is directly calculable on the lattice,

$$\tilde{f}_{\text{naive}}(x, b_\perp, \mu, x\tilde{P}^z) = \lim_{\tilde{\eta} \rightarrow \infty} \frac{\tilde{B}(x, b_\perp, \mu, \tilde{\eta}, x\tilde{P}^z)}{\sqrt{\tilde{S}_{\text{naive}}(b_\perp, \mu, \tilde{\eta})}}, \quad (2.29)$$

and the structure of the renormalization is the same as in eq. (2.21). However, this naive quasi-TMD cannot directly be matched to the physical TMD, because it has different IR behavior.

The final step consists of relating the quasi- and naive quasi-TMD, by considering the ratio of the two functions

$$\frac{\tilde{f}(x, b_\perp, \mu, \tilde{\zeta}, x\tilde{P}^z)}{\tilde{f}_{\text{naive}}(x, b_\perp, \mu, x\tilde{P}^z)} = \lim_{\tilde{\eta} \rightarrow \infty} \sqrt{\frac{\tilde{S}_{\text{naive}}(b_\perp, \mu, \tilde{\eta})}{\tilde{S}(b_\perp, \mu, y_A, y_B, \tilde{\eta})}} = \sqrt{\frac{\tilde{S}_{\text{naive}}(b_\perp, \mu)}{S(b_\perp, \mu, y_A, y_B)}}, \quad (2.30)$$

where the dependence on y_A and y_B on the right-hand-side is hidden in the $\tilde{\zeta}$ and \tilde{P}^z , see eqs. (2.22) and (2.27). In the second equality the divergences as $\tilde{\eta} \rightarrow \infty$ cancel in the ratio. Crucially, the $S(b_\perp, \mu, y_A, y_B)$ in the final expression is the same soft function that enters the definition of the physical Collins scheme TMD. We can further reduce the above ratio by using the fact that for large y_A and y_B the Collins soft function behaves as

$$S(b_\perp, \mu, y_A, y_B) = S_I(b_\perp, \mu) e^{(y_A - y_B)\gamma_\zeta(b_\perp, \mu)}. \quad (2.31)$$

Here, $S_I(b_\perp, \mu)$ is the rapidity-independent part of the soft function. It is referred to in the literature as the intrinsic soft function, and has been related to a lattice-calculable meson form factor [63]. Furthermore, the Collins-Soper kernel can be calculated on the lattice by calculating ratios of quasi-beam functions at different hadron momenta [61]. Summarizing, the quasi-TMD is related to the naive quasi-TMD by

$$\tilde{f}(x, b_\perp, \mu, \tilde{\zeta}, x\tilde{P}^z) = \tilde{f}_{\text{naive}}(x, b_\perp, \mu, x\tilde{P}^z) \sqrt{\frac{\tilde{S}_{\text{naive}}(b_\perp, \mu)}{S_I(b_\perp, \mu)}} \exp\left[-\frac{1}{2}\gamma_\zeta(b_\perp, \mu) \ln\left(\frac{(2x\tilde{P}^z)^2}{\tilde{\zeta}}\right)\right], \quad (2.32)$$

where all ingredients on the right-hand-side can be calculated on the lattice. Results for lattice calculations of the soft function can be found in [70, 94].

3 Double parton distribution functions

We start with a brief introduction to double parton scattering in sec. 3.1, including a short overview of the theoretical framework. For a more comprehensive presentation, we refer to the book on this subject [21]. The definition of the double parton distributions are discussed in sec. 3.2, which is the starting point for their extracting from lattice QCD using LaMET, and their renormalization is treated in sec. 3.3.

3.1 Introduction to double parton scattering

Double parton scattering (DPS) refers to two partonic scatterings between the same colliding hadrons. In contrast to pile-up, in which there are collisions between different hadrons in the same bunch crossing, the two partonic collisions in DPS are *not* independent of each other. Within the area of multi-parton interactions, there are different kinematic regions of interest: For many LHC measurements, there is a single energetic collision and additional partonic scatterings take place at lower energies. These additional partonic scatterings still produce radiation that affect measurements and are modeled in Monte Carlo parton showers. On the other hand, there is also an interest in two energetic collisions, for which a field-theoretic description in terms of factorization formulae is available. This is the case we focus on, and the one investigated in measurements of DPS that extract σ_{eff} .

A given process, say double Drell-Yan for concreteness, can receive contributions from both DPS as well as single parton scattering (SPS). In the SPS contribution, only one parton is extracted from each of the colliding hadrons, and the two electroweak bosons are produced by a single hard scattering, rather than from two separate partonic scatterings. The contribution of DPS to the total cross section is suppressed by $\Lambda_{\text{QCD}}^2/Q^2$ compared to SPS, where Q is the typical energy scale of the hard collisions (the invariant mass of an electroweak boson in double Drell-Yan). To enhance the contribution of DPS, one can consider processes where the energies of the hard collisions are fairly low, such as charm production [95]. Alternatively, one can restrict to the region of phase-space where the total transverse momentum of each of the individual hard scatterings is small (for double Drell-Yan this is the transverse momentum of each of the electroweak bosons). For single parton

scattering the contribution is also power suppressed in this region as the two electroweak bosons are unlikely to each have a small transverse momentum, so the size of the SPS contribution will be of the same order as the DPS contribution [13].

The factorization formula for the double Drell-Yan cross section takes the following form [16, 19]

$$\begin{aligned} \frac{d\sigma_{\text{DPS}}}{dQ_1^2 dY_1 dQ_2^2 dY_2} &= \frac{1}{S} \sum_{a_1, a_2, a_3, a_4} \sum_{R_1, R_2, R_3, R_4} c_{R_1, R_2, R_3, R_4} \int \frac{dx_1}{x_1} \frac{dx_2}{x_2} \frac{dx_3}{x_3} \frac{dx_4}{x_4} \int d^2\mathbf{b}_\perp \Phi^2(|\mathbf{b}_\perp|, \nu) \\ &\times \sigma_{a_1 a_3}(x_1, x_3, Q_1, Y_1, \mu) \sigma_{a_2 a_4}(x_2, x_4, Q_2, Y_2, \mu) \\ &\times {}^{R_1 R_2}F_{a_1 a_2}(x_1, x_2, \mathbf{b}_\perp, \mu, \zeta_p) {}^{R_3 R_4}F_{a_3 a_4}(x_3, x_4, \mathbf{b}_\perp, \mu, \bar{\zeta}_p). \end{aligned} \quad (3.1)$$

Here ${}^{R_1 R_2}F_{a_1 a_2}(x_1, x_2, \mathbf{b}_\perp, \mu, \zeta)$ is the double parton distribution (DPD) describing the probability of extracting partons a_1 and a_2 from a proton with moment fraction x_1 and x_2 and transverse separation \mathbf{b}_\perp . The superscripts R_i label the color representation of the partons, and in principle there are also interference effects in fermion number (that we will not consider). Because color singlets are produced, the dependence on the color representation can simply be encoded in an overall coefficient c_{R_1, R_2, R_3, R_4} . The regulator $\Phi^2(|\mathbf{b}_\perp|, \nu)$ will be discussed below.

The partonic cross section $\sigma_{a_1 a_3}(x_1, x_3, Q_1, Y_1, \mu)$ in eq. (3.1) describes the scattering process in which the partons a_1 and a_3 collide to form an electroweak boson with invariant mass Q_1 and rapidity Y_1 . Beyond leading order in perturbation theory, additional partons are produced in the final state and infrared poles in the partonic cross sections need to be subtracted. The coefficient S describes a symmetry factor. The parton flavors a_i and representations R_i are summed over, and the momentum fractions x_i and the transverse separation \mathbf{b}_\perp between the two collisions are integrated over.

Even for unpolarized protons, the cross section in eq. (3.1) receives contributions from DPDs such as $F_{\Delta q \Delta q}$, that describes extracting two longitudinally polarized quarks. While a non-vanishing distribution for a single longitudinal quark requires a polarized proton, $F_{\Delta q \Delta q}$ describes spin correlations of the two partons in an unpolarized proton. The sum over polarizations is included in the sum over flavors, e.g. $a_1 = \Delta q$ is part of the sum over a_1 .

As an example of color correlations encoded in the superscripts R_1, R_2, R_3, R_4 , two pairs of color-correlated (anti-)quarks can produce two color singlet electroweak bosons, corresponding to a term ${}^{88}F_{qq} {}^{88}F_{\bar{q}\bar{q}}$ in the DPS cross section.³ The tree-level cross section for double Drell-Yan, including spin and color correlations and interference effects, is shown in eq. (43) of ref. [16]. For color correlations, the currents in the DPDs at position 0 and \mathbf{b}_\perp are not color singlets. (The complete operator in the DPD of course is.) Consequently, soft radiation resolving the large distance $\mathbf{b}_\perp \sim 1/\Lambda_{\text{QCD}}$ between the currents must be included. The corresponding soft functions are shown explicitly in ref. [16] but have been absorbed in the DPDs in eq. (3.1). As for the case of TMDs in sec. 2.2, there is an associated rapidity

³Since the proton is colorless, there is no corresponding distribution for single parton scattering. However, the proton is not an electroweak singlet, so there is a corresponding (perturbative) electroweak effect [96].

resummation, for which a corresponding argument ζ_p and $\bar{\zeta}_p$ is included in the DPDs (this is absent for the color-summed DPDs).

DPDs can receive contributions from PDFs in the $\mathbf{b}_\perp \rightarrow 0$ limit [97, 98], known as the double parton splitting singularity [99]. For example, $F_{q\bar{q}}$ receives a contribution from f_g where the gluon splits, $g \rightarrow q\bar{q}$. In particular, one has to make sure to avoid double counting between DPS and SPS. While several proposals for how to address this problem were put forward [15, 100–103], a first complete solution was presented in ref. [19]. This leads to the inclusion of the regulator $\Phi^2(|\mathbf{b}_\perp|\nu)$ in eq. (3.1), which goes to zero for $\mathbf{b}_\perp \rightarrow 0$ and becomes one for large $|\mathbf{b}_\perp|$. This does not play a role in our calculations because we only consider the flavor-non-singlet DPDs and restrict to the one-loop matching. One crucial ingredient in proving factorization is the cancellation of Glauber gluons, which was established for double Drell-Yan in ref. [18].

We will conclude this section by explaining how the “pocket formula” with σ_{eff} arises from eq. (3.1). We assume all spin and color correlations and interferences effects can be ignored, such that we only need to consider $^{11}F_{a_1 a_2}$ and can drop the argument ζ . The following ansatz [11]

$$^{11}F_{a_1 a_2}(x_1, x_2, \mathbf{b}_\perp, \mu) = f_a(x_1, \mu) f_b(x_2, \mu) G(\mathbf{b}_\perp, \mu), \quad (3.2)$$

is then made, where $f_{a,b}$ are the collinear PDFs. Due to the constraint $x_1 + x_2 < 1$, this can only hold if x_i is small (which we assume). This implies

$$\frac{d\sigma_{\text{DPS}}}{dQ_1^2 dY_1 dQ_2^2 dY_2} = \frac{1}{S} \frac{d\sigma}{dQ_1^2 dY_1} \frac{d\sigma}{dQ_2^2 dY_2} \underbrace{\int d\mathbf{b}_\perp \Phi^2(|\mathbf{b}_\perp|\nu) G(\mathbf{b}_\perp, \mu)}_{1/\sigma_{\text{eff}}}, \quad (3.3)$$

so the two partonic scattering can be treated independently. The effective cross section can then be interpreted as a measure of the transverse size of the proton. It will be interesting to confront these assumptions with lattice data, using the LaMET approach.

3.2 Field-theoretical definition of DPDs

Definitions of DPDs as proton matrix elements of operators in quantum field theory, have e.g. been given in refs. [14, 16]. For convenience, we repeat the definition for the quark-quark DPD here.

As for TMDs, the definition of DPDs involve infinite-length light-like Wilson lines and therefore contain rapidity divergences. These divergences cancel in the cross section when the DPDs are combined with their associated soft functions. The DPDs that appear in eq. (3.1) can be defined as the ratio of an unsubtracted DPD and the square root of the corresponding soft function.

Let us now define the unsubtracted quark-quark DPDs, for general color and spin structures:

$$\begin{aligned} F_{ijkl}^{\text{unsub}}(x_1, x_2, \mathbf{b}_\perp, \epsilon, y_B, P^+) \\ = -\pi P^+ \int \frac{db_1^-}{2\pi} \frac{db_2^-}{2\pi} \frac{db_3^-}{2\pi} e^{-ix_1 P^+ b_1^-} e^{-ix_2 P^+ b_2^-} e^{ix_1 P^+ b_3^-} \end{aligned} \quad (3.4)$$

$$\begin{aligned} & \times \langle P | \bar{T} \left\{ \left[\bar{\psi}(b_1) W[b_1 \leftarrow b_\perp - \infty n_B(y_B)] \right]_i \left[\bar{\psi}(b_2) W[b_2 \leftarrow -\infty n_B(y_B)] \right]_j \right\} \\ & \times T \left\{ \left[W[b_\perp - \infty n_B(y_B) \leftarrow b_3] \psi(b_3) \right]_k \left[W[-\infty n_B(y_B) \leftarrow 0] \psi(0) \right]_\ell \right\} | P \rangle. \end{aligned}$$

Here i, j, k, ℓ denote the color *and* spin indices, which are uncontracted, T (\bar{T}) denotes (anti-)time ordering. The coordinates b_i are

$$b_1 = (0^+, b_1^-, \mathbf{b}_\perp), \quad b_2 = (0^+, b_2^-, \mathbf{0}_\perp), \quad b_3 = (0^+, b_3^-, \mathbf{b}_\perp), \quad b_\perp = (0^+, 0^-, \mathbf{b}_\perp), \quad (3.5)$$

The Wilson line W was defined in eq. (2.4), and for definiteness we use the off-lightcone rapidity regulator y_B in eq. (2.10).

The quark-quark DPD as defined above can be decomposed into several color and spin structures. Following the conventions of ref. [20],

$$^{11}F_{q_1 q_2} = (\Gamma_{q_1})_{ik} (\Gamma_{q_2})_{j\ell} F_{ijkl}, \quad (3.6)$$

$$^{88}F_{q_1 q_2} = \frac{2N_c}{\sqrt{N_c^2 - 1}} (\Gamma_{q_1} t^c)_{ik} (\Gamma_{q_2} t^c)_{j\ell} F_{ijkl}, \quad (3.7)$$

where $N_c = 3$ is the number of colors, t^c is the SU(3) generator in the fundamental representation and the Dirac structures $\Gamma_{q_1}, \Gamma_{q_2} \in \{\gamma^+, \gamma^+ \gamma^5, \gamma^+ \gamma_\perp^\mu \gamma^5\}$ are labelled q , Δq and δq , respectively. The free Lorentz index in the δq can be contracted with \mathbf{b}_\perp or the index of another δq .

For the color correlated DPD, the currents at \mathbf{b}_\perp and $\mathbf{0}_\perp$ are not separately gauge invariant and a transverse Wilson line at infinity is required. While this transverse Wilson line can be eliminated in covariant gauges by setting the gauge field at infinity to zero, they will be important when we introduce a lattice calculable quasi-DPD in sec. 4.1. In that case the Wilson lines are located at a finite distance $\tilde{\eta}$ along the z direction, and can no longer be set to unity.

Next we discuss the soft functions needed to obtain the physical DPD from the unsubtracted one in eq. (3.4). For the case of the quark-quark DPDs there are only two soft functions corresponding to the two different color structures: 1S and 8S (in principle there are more when one considers interference contributions). The soft function corresponding to the color-summed DPD is trivial, $^1S = 1$, so in this case no soft subtraction is needed. The (bare) soft function for the color-correlated DPD can be written as

$$\begin{aligned} ^8S(b_\perp, \epsilon, y_A, y_B) = & -\frac{1}{2N_c C_F} + \frac{1}{2N_c C_F} \langle 0 | S_{\gg}^\dagger(b_\perp, -\infty n_B(y_B), -\infty n_A(y_A)) \\ & \times S_{\gg}(b_\perp, -\infty n_B(y_B), -\infty n_A(y_A)) | 0 \rangle, \end{aligned} \quad (3.8)$$

where y_A and y_B are two off-lightcone rapidity regulators and S_{\gg} is the Wilson loop defined in eq. (2.6).

For *general* flavor, spin and color we now define the (bare) DPDs by performing the soft subtraction:

$$R_1 R_2 F_{a_1 a_2}^{\text{bare}}(x_1, x_2, b_\perp, \epsilon, \zeta_p) = \lim_{y_B \rightarrow -\infty} \frac{R_1 R_2 F_{a_1 a_2}^{\text{unsub}}(x_1, x_2, b_\perp, \epsilon, y_B)}{\sqrt{R_1/2} S(b_\perp, \epsilon, y_A, y_B)}. \quad (3.9)$$

This ratio is finite as $y_B \rightarrow -\infty$, but a dependence on a rapidity scale ζ_p remains. This rapidity scale dependence is described by a Collins-Soper evolution [20],

$$\frac{\partial}{\partial \ln \zeta_p} {}^{R_1 R_2} F_{a_1 a_2}^{\text{bare}}(x_1, x_2, b_\perp, \epsilon, \zeta_p) = \frac{1}{2} {}^{R_1/2} J^{\text{bare}}(b_\perp, \epsilon) {}^{R_1 R_2} F_{a_1 a_2}^{\text{bare}}(x_1, x_2, b_\perp, \epsilon, \zeta_p), \quad (3.10)$$

with a similar equation being satisfied by the renormalized DPDs. Here ${}^R J$ is the rapidity anomalous dimension or rapidity evolution kernel. This kernel depends only on the dimension of the representation R with $|R_1| = |R_2|$ being implied. The rapidity evolution kernels are related to the familiar Collins-Soper kernel by a color factor. Note that in contrast to the TMD case in eq. (2.16), the rapidity scale associated to DPDs contains no momentum fractions,

$$\zeta_p = 2(P^+)^2 e^{-2y_n}. \quad (3.11)$$

This general form will be used in sec. 4, but in our actual calculations in sec. 5 we will only consider the color-summed ($R_1 = R_2 = 1$) and color-correlated ($R_1 = R_2 = 8$) quark-quark DPDs.

3.3 Renormalization of DPDs

The bare DPDs defined in eq. (3.9) contain UV divergences and need to be renormalized. The reason for discussing renormalization in some detail here is that the structure of the renormalization group equations will play a key role in constructing the matching relation between the lightcone- and quasi-DPDs. This renormalization has been discussed extensively in refs. [20, 104–106], and includes results at order α_s^2 .

The renormalization of DPDs can be performed either in position or momentum space. These *bare* DPDs are related by a Fourier transform

$${}^{R_1 R_2} F_{a_1 a_2}^{\text{bare}}(x_1, x_2, \Delta_\perp, \epsilon, \zeta) = \int d^{d-2} \mathbf{b}_\perp e^{i \mathbf{b}_\perp \cdot \Delta_\perp} {}^{R_1 R_2} F_{a_1 a_2}^{\text{bare}}(x_1, x_2, b_\perp, \epsilon, \zeta). \quad (3.12)$$

This same formula does not hold for the renormalized DPDs, because of the double parton splitting singularity which occurs in the $\mathbf{b}_\perp \rightarrow 0$ limit (see the discussion of the function Φ in eq. (3.1)).

In position space, the currents that enter the definition of the bare DPDs are separated by a distance \mathbf{b}_\perp . Because of this transverse separation, the two operators renormalize separately⁴,

$$F = Z \otimes_1 Z \otimes_2 F^{\text{bare}}. \quad (3.13)$$

Explicitly, this reads

$${}^{R_1 R_2} F_{a_1 a_2}(x_1, x_2, b_\perp, \mu, \zeta_p) = \sum_{a'_1, a'_2} \sum_{R'_1, R'_2} \int \frac{dx'_1}{x'_1} \frac{dx'_2}{x'_2} {}^{R_1 \bar{R}'_1} Z_{a_1 a'_1} \left(\frac{x_1}{x'_1}, \mu, x_1^2 \zeta_p \right) \quad (3.14)$$

⁴In principle one could consider two separate renormalization scales for the two operators as they renormalize independently.

$$\times {}^{R_2\bar{R}_2'}Z_{a_2a_2'}\left(\frac{x_2}{x_2'}, \mu, x_2'^2\zeta_p\right) {}^{R_1' R_2'}F_{a_1'a_2'}^{\text{bare}}(x_1', x_2', b_\perp, \mu, \zeta_p).$$

Here it is clear why ζ_p is defined without momentum fractions, since they differ in the various terms. For color-summed DPDs the rapidity scale dependence drops out.

In momentum space, additional singularities are generated due to the $1 \rightarrow 2$ splitting mechanism. This leads to mixing with single PDFs,

$$F = Z \otimes_1 Z \otimes_2 F^{\text{bare}} + Z_s \otimes f^{\text{bare}}. \quad (3.15)$$

Explicitly,

$$\begin{aligned} {}^{R_1 R_2}F_{a_1 a_2}(x_1, x_2, \Delta_\perp, \mu, \zeta_p) &= \sum_{a_1', a_2'} \sum_{R_1', R_2'} \int \frac{dx_1'}{x_1'} \frac{dx_2'}{x_2'} {}^{R_1 \bar{R}_1'}Z_{a_1 a_1'}\left(\frac{x_1}{x_1'}, \mu, x_1'^2\zeta_p\right) \\ &\quad \times {}^{R_2 \bar{R}_2'}Z_{a_2 a_2'}\left(\frac{x_2}{x_2'}, \mu, x_2'^2\zeta_p\right) {}^{R_1' R_2'}F_{a_1' a_2'}^{\text{bare}}(x_1', x_2', \Delta_\perp, \mu, \zeta_p) \\ &\quad + \sum_{a'} \int \frac{dx'}{(x')^2} {}^{R_1 R_2}Z_{a_1 a_2, a'}\left(\frac{x_1}{x'}, \frac{x_2}{x'}, \mu, x_1 x_2 \zeta_p\right) f_{a'}^{\text{bare}}(x', \mu, \epsilon). \end{aligned} \quad (3.16)$$

Because the renormalization of DPDs is different in position space and momentum space, the matching with quasi-DPDs will also be different in position space and momentum space. Note that this only affects the mixing with single PDFs, which is absent from our explicit one-loop calculations that are limited to the flavor-non-singlet case.

4 Quasi-double parton distributions

In this section we take the first steps in extending the quasi-PDF approach to the case of double parton distributions. We define quasi-DPDs in sec. 4.1, which are related to the physical lightcone-DPD by an infinite Lorentz boost. The lattice-calculability of the DPD soft function is discussed in sec. 4.2 (paralleling the discussion in sec. 2.5 for the TMD soft function). In sec. 4.3, we construct a matching relation between the physical and quasi-DPD. Although we do not prove the matching relation in this work, we verify its consistency to one-loop order in sec. 5 for the flavor non-singlet quark-quark DPD.

4.1 Defining quasi-DPDs

First we define (bare and unsubtracted) quasi-DPDs. Their definition can be obtained straightforwardly from their lightcone counterparts by essentially replacing all appearances of n_a and n_b by \hat{z} and $-\hat{z}$. For the quark-quark DPD with spin and color indices i, j, k, ℓ uncontracted, we obtain

$$\begin{aligned} \tilde{F}_{ijkl}^{\text{unsub}}(x_1, x_2, \mathbf{b}_\perp, a, \tilde{\eta}, \tilde{P}^z) &= -\pi \tilde{P}^z \int \frac{db_1^z}{2\pi} \frac{db_2^z}{2\pi} \frac{db_3^z}{2\pi} e^{ix_1 \tilde{P}^z b_1^z} e^{ix_2 \tilde{P}^z b_2^z} e^{-ix_1 \tilde{P}^z b_3^z} \\ &\quad \times \langle \tilde{P} | \left[\bar{\psi}(b_1) W[b_1 \leftarrow b_\perp + \tilde{\eta} \hat{z}] \right]_i \left[\bar{\psi}(b_2) W[b_2 \leftarrow \tilde{\eta} \hat{z}] \right]_j \\ &\quad \times \left[W[b_\perp + \tilde{\eta} \hat{z} \leftarrow b_3] \psi(b_3) \right]_k \left[W[\tilde{\eta} \hat{z} \leftarrow 0] \psi(0) \right]_\ell | \tilde{P} \rangle, \end{aligned} \quad (4.1)$$

as the quasi-analogue of eq. (3.4). The coordinates b_i are now

$$b_1 = (0, \mathbf{b}_\perp, b_1^z), \quad b_2 = (0, \mathbf{0}_\perp, b_2^z), \quad b_3 = (0, \mathbf{b}_\perp, b_3^z), \quad b_\perp = (0, \mathbf{b}_\perp, 0), \quad (4.2)$$

so (anti-)time ordering is no longer relevant. The Wilson line W is defined in eq. (2.4), and we replaced the off-lightcone rapidity regulator in eq. (3.4) by a finite length $\tilde{\eta}$ of the Wilson lines, i.e. $-\infty n_B(y_B) \rightarrow \tilde{\eta}\hat{z}$. This is necessary as the quasi-DPD is calculated on a lattice of finite size.

The color and spin decomposition of quasi-DPDs is essentially the same as for lightcone-DPDs. For definiteness, the decomposition of the quark-quark quasi-DPDs is given by

$${}^{11}\tilde{F}_{q_1 q_2}^{\text{unsub}}(x_1, x_2, b_\perp, a, \tilde{\eta}, \tilde{P}^z) \quad (4.3)$$

$$= -\pi \tilde{P}^z \int \frac{db_1^z}{2\pi} \frac{db_2^z}{2\pi} \frac{db_3^z}{2\pi} e^{ix_1 \tilde{P}^z b_1^z} e^{ix_2 \tilde{P}^z b_2^z} e^{-ix_1 \tilde{P}^z b_3^z} \\ \times \langle \tilde{P} | \bar{\psi}(b_1) \tilde{\Gamma}_{q_1} W[b_1 \leftarrow b_3] \psi(b_3) \bar{\psi}(b_2) \tilde{\Gamma}_{q_2} W[b_2 \leftarrow 0] \psi(0) | \tilde{P} \rangle,$$

$${}^{88}\tilde{F}_{q_1 q_2}^{\text{unsub}}(x_1, x_2, b_\perp, a, \tilde{\eta}, \tilde{P}^z) \quad (4.4)$$

$$= -\pi \tilde{P}^z \int \frac{db_1^z}{2\pi} \frac{db_2^z}{2\pi} \frac{db_3^z}{2\pi} e^{ix_1 \tilde{P}^z b_1^z} e^{ix_2 \tilde{P}^z b_2^z} e^{-ix_1 \tilde{P}^z b_3^z} \\ \times \langle \tilde{P} | \bar{\psi}(b_1) \tilde{\Gamma}_{q_1} W[b_1 \leftarrow b_\perp + \tilde{\eta}\hat{z}] t^c W[b_\perp + \tilde{\eta}\hat{z} \leftarrow b_3] \psi(b_3) \\ \times \bar{\psi}(b_2) \tilde{\Gamma}_{q_2} W[b_2 \leftarrow \tilde{\eta}\hat{z}] t^c W[\tilde{\eta}\hat{z} \leftarrow 0] \psi(0) | \tilde{P} \rangle.$$

Note that q_i denotes both the flavor of the quark field ψ as well as the Dirac structure $\tilde{\Gamma}_{q_i}$. These Dirac structures are related to those of the lightcone-DPD by

$$\frac{1}{p^z} \bar{u}(p) \tilde{\Gamma} u(p) = \frac{1}{p^+} \bar{u}(p) \Gamma u(p), \quad (4.5)$$

with $u(p)$ the spinor for a massless quark with momentum in the z direction. Note that in this equation, the overall magnitude of p is irrelevant because it cancels in the ratio, so p can be replaced by \tilde{p} if necessary. In principle there exists a universality class of valid choices of $\tilde{\Gamma}$, obtained by replacing γ^+ in the lightcone-DPD definition by a linear combination of γ^0 and γ^z (except for $\gamma^0 - \gamma^z$). For definiteness, we take $\tilde{\Gamma} = \gamma^z, \gamma^z \gamma^5, \gamma^z \gamma_\perp \gamma^5$ for unpolarized (q), helicity (Δq) and transversity (δq), respectively.

We note that the color non-singlet distribution ${}^{88}\tilde{F}$ as written in eq. (4.3) is not automatically gauge invariant due to the appearance of SU(3) generators t^c in between the Wilson lines. While this issue could be ignored for the DPD in sec. 3.2 (at least as long as covariant gauges are used), here we need to be more careful. We address this by first applying completeness relations for the generators which reconnects the color indices of the end-points of the Wilson lines, and then introducing transverse gauge links at spatial infinity where needed. As an example, in the quark-quark case we first use

$$t_{ij}^a t_{kl}^a = T_F \left(\delta_{il} \delta_{kj} - \frac{1}{N_c} \delta_{ij} \delta_{kl} \right), \quad (4.6)$$

and then add the missing transverse Wilson lines between $\tilde{\eta}\hat{z}$ and $b_\perp + \tilde{\eta}\hat{z}$. This leads to the following gauge invariant definition of the color-correlated quark-quark quasi-DPD

$${}^{88}\tilde{F}_{q_1 q_2}^{\text{unsub}}(x_1, x_2, b_\perp, a, \tilde{\eta}, \tilde{P}^z)$$

$$\begin{aligned}
&= -\frac{T_F}{N} {}^{11}\tilde{F}_{q_1 q_2}^{\text{unsub}}(x_1, x_2, b_\perp, a, \tilde{\eta}, \tilde{P}^z) - \pi \tilde{P}^z \int \frac{db_1^z}{2\pi} \frac{db_2^z}{2\pi} \frac{db_3^z}{2\pi} e^{ix_1 \tilde{P}^z b_1^z} e^{ix_2 \tilde{P}^z b_2^z} e^{-ix_1 \tilde{P}^z b_3^z} \\
&\times \langle \tilde{P} | \left[(\bar{\psi}(b_1) \tilde{\Gamma}_{q_1})_\alpha W[b_1 \leftarrow b_\perp + \tilde{\eta} \hat{z} \leftarrow \tilde{\eta} \hat{z} \leftarrow 0] \psi_\beta(0) \right] \\
&\times \left[(\bar{\psi}(b_2) \tilde{\Gamma}_{q_2})_\beta W[b_2 \leftarrow \tilde{\eta} \hat{z} \leftarrow b_\perp + \tilde{\eta} \hat{z} \leftarrow b_3] \psi_\alpha(b_3) \right] | \tilde{P} \rangle, \tag{4.7}
\end{aligned}$$

where α, β denote the spin indices. (Note that we already used this approach to obtain a gauge-invariant soft function in eq. (3.8).)

Next we define a quasi-DPS soft function. As for the TMD soft function, it is not possible to define a matrix element that is both time-independent and is related to the lightcone soft function by a boost. To make sure that the quasi- and lightcone distributions possess the same infrared behaviour, we follow the same approach as in sec. 2.4 for TMDs, defining the quasi-soft function as the off-lightcone regularized soft function with finite-length Wilson lines. Explicitly, the DPS quasi-soft function can be obtained by taking the off-lightcone regularized soft function and making the replacement

$$\infty n_A(y_A) \rightarrow \tilde{\eta} \frac{n_A(y_A)}{|n_A(y_A)|}, \quad \infty n_B(y_B) \rightarrow \tilde{\eta} \frac{n_B(y_B)}{|n_B(y_B)|}. \tag{4.8}$$

For the quark-quark case, the color-summed quasi-soft function is ${}^1\tilde{S} = 1$ and the color-correlated quasi-soft function is defined as

$$\begin{aligned}
{}^8\tilde{S}(b_\perp, a, \tilde{\eta}, y_A, y_B) &= -\frac{1}{2N_c C_F} + \frac{1}{2N_c C_F} \langle 0 | S_\otimes^\dagger \left(b_\perp, -\tilde{\eta} \frac{n_B(y_B)}{|n_B(y_B)|}, -\tilde{\eta} \frac{n_A(y_A)}{|n_A(y_A)|} \right) \\
&\times S_\otimes \left(b_\perp, -\tilde{\eta} \frac{n_B(y_B)}{|n_B(y_B)|}, -\tilde{\eta} \frac{n_A(y_A)}{|n_A(y_A)|} \right) | 0 \rangle, \tag{4.9}
\end{aligned}$$

with S_\otimes defined in eq. (2.6).

We now define quasi-DPDs, which we will match onto the physical lightcone-DPDs in the next section. First we use the quasi-soft functions to subtract the singularities for $\tilde{\eta} \rightarrow \infty$ (known as pinch-pole singularities) from the unsubtracted quasi-DPDs, and then we perform the renormalization,

$${}^{R_1 R_2} \tilde{F}_{a_1 a_2}(x_1, x_2, b_\perp, \mu, \tilde{\zeta}_p, \tilde{P}^z) = \lim_{\substack{a \rightarrow 0 \\ \tilde{\eta} \rightarrow \infty}} {}^{R_1 R_2} \tilde{Z}_{a_1, a_2}(a, \mu, y_A, y_B) \frac{{}^{R_1 R_2} \tilde{F}_{a_1 a_2}(x_1, x_2, b_\perp, a, \tilde{\eta}, \tilde{P}^z)}{\sqrt{{}^R \tilde{S}(b_\perp, a, \tilde{\eta}, y_A, y_B)}}, \tag{4.10}$$

Note that, as in the case of quasi-PDFs and quasi-TMDs, quasi-DPDs can be renormalized multiplicatively. This is in contrast to the lightcone-DPDs, which are renormalized by a convolution in the two momentum fractions, see eq. (3.14).

4.2 Lattice calculability of the DPD quasi-soft function

The quasi-DPD as defined above cannot be calculated directly on the lattice because the matrix element defining the quasi-soft function is time-dependent. Therefore, analogous to the TMD case in sec. 2.5, we define naive quasi-DPDs, which can be calculated on the lattice directly and can be related to the proper quasi-DPDs via an intrinsic soft function.

For the quark-quark DPD, we simply have $^1S_{\text{naive}} = 1$ in the color-summed case, while for the color-correlated case we define the (bare) naive soft function as

$$^8S_{\text{naive}}(b_\perp, a, \tilde{\eta}) = -\frac{1}{2N_c C_F} + \frac{1}{2N_c C_F} \langle 0 | S_{\gg}^\dagger[\mathbf{b}_\perp, -\tilde{\eta}\hat{z}, \tilde{\eta}\hat{z}] S_{\gg}[\mathbf{b}_\perp, -\tilde{\eta}\hat{z}, \tilde{\eta}\hat{z}] | 0 \rangle. \quad (4.11)$$

We then define the naive quasi-DPDs as

$$^{R_1 R_2} \tilde{F}_{a_1 a_2}^{\text{naive}}(x_1, x_2, b_\perp, \mu, \tilde{P}^z) = \lim_{\substack{a \rightarrow 0 \\ \tilde{\eta} \rightarrow \infty}} ^{R_1 R_2} \tilde{Z}_{a_1 a_2}(a, \mu, y_A, y_B) \frac{^{R_1 R_2} \tilde{F}_{a_1 a_2}(x_1, x_2, \mathbf{b}_\perp, a, \tilde{\eta}, \tilde{P}^z)}{\sqrt{^R \tilde{S}_{\text{naive}}(b_\perp, a, \tilde{\eta})}}, \quad (4.12)$$

The naive quasi-DPD does not possess the correct IR behaviour to be used to in the matching relation, as it is not related to the lightcone-DPD by a boost. However, it can be used in lattice calculations to subtract the pinch-pole singularities of the unsubtracted quasi-DPD, that appear as divergences in the limit $\tilde{\eta} \rightarrow \infty$.

To relate the naive quasi-DPD to the quasi-DPD that is used in the matching to physical DPDs, we need to define an analogue of the intrinsic soft function of (2.31) for the double parton case. To define an intrinsic soft function it is necessary that the rapidity divergences exponentiate, which was proven to be the case in [107]. This allows us to define an intrinsic soft function for the DPD case by⁵

$$^R S(b_\perp, \mu, y_A, y_B) = ^R S_I(b_\perp, \mu) e^{(y_A - y_B) ^R J(b_\perp, \mu)}. \quad (4.13)$$

Following the same arguments as for the TMD case, we then find the following relation between the quasi- and the naive quasi-DPDs,

$$\begin{aligned} \tilde{F}(x_1, x_2, b_\perp, \tilde{P}^z, \mu, \tilde{\zeta}) &= \tilde{F}_{\text{naive}}(x_1, x_2, b_\perp, \tilde{P}^z, \mu, \tilde{\zeta}) \sqrt{\frac{^R \tilde{S}_{\text{naive}}(b_\perp, \mu)}{^R S_I(b_\perp, \mu)}} \\ &\times \exp \left[-\frac{1}{4} ^R J(b_\perp, \mu) \ln \left(\frac{(2x_1 \tilde{P}^z)^2}{x_1^2 \tilde{\zeta}_p} \right) - \frac{1}{4} ^R J(b_\perp, \mu) \ln \left(\frac{(2x_2 \tilde{P}^z)^2}{x_2^2 \tilde{\zeta}_p} \right) \right]. \end{aligned} \quad (4.14)$$

4.3 Factorization for quasi-DPDs

We will now present a matching relation between quasi-DPDs and the physical DPDs for *general* flavor, color and spin. In position space the matching relation reads

$$\begin{aligned} ^{R_1 R_2} \tilde{F}_{a_1 a_2}(x_1, x_2, b_\perp, \mu, \tilde{\zeta}_p, \tilde{P}^z) \\ = \sum_{R'_1, R'_2} \sum_{a'_1, a'_2} \int_0^1 \frac{dx'_1}{x'_1} \frac{dx'_2}{x'_2} ^{R_1 R'_1} C_{a_1 a'_1} \left(\frac{x_1}{x'_1}, x'_1 \tilde{P}^z, \mu \right) ^{R_2 R'_2} C_{a_2 a'_2} \left(\frac{x_2}{x'_2}, x'_2 \tilde{P}^z, \mu \right) \\ \times \exp \left[\frac{1}{2} ^{R'_1 R'_2} J(b_\perp, \mu) \ln \left(\frac{\tilde{\zeta}_p}{\zeta_p} \right) \right] ^{R'_1 R'_2} F_{a'_1 a'_2}(x'_1, x'_2, b_\perp, \mu, \zeta_p), \end{aligned} \quad (4.15)$$

⁵Note that we assume a basis where mixing between different soft functions under rapidity evolution is absent.

while in momentum space the matching relation reads

$$\begin{aligned}
& {}^{R_1 R_2} \tilde{F}_{a_1 a_2}(x_1, x_2, \Delta_\perp, \mu, \tilde{\zeta}_p, \tilde{P}^z) \\
&= \sum_{R'_1, R'_2} \sum_{a'_1, a'_2} \int_0^1 \frac{dx'_1}{x'_1} \frac{dx'_2}{x'_2} {}^{R_1 R'_1} C_{a_1 a'_1} \left(\frac{x_1}{x'_1}, x'_1 \tilde{P}^z, \mu \right) {}^{R_2 R'_2} C_{a_2 a'_2} \left(\frac{x_2}{x'_2}, x'_2 \tilde{P}^z, \mu \right) \\
&\quad \times {}^{R'_1 R'_2} F_{a'_1 a'_2}(x'_1, x'_2, \Delta_\perp, \mu, \tilde{\zeta}_p) \\
&\quad + \sum_{a'} \int_0^1 \frac{dx'}{x'^2} {}^{R_1 R_2} C_{a_1 a_2, a'} \left(\frac{x_1}{x'}, \frac{x_2}{x'}, x' \tilde{P}^z, \mu \right) f_{a'}(x', \mu).
\end{aligned} \tag{4.16}$$

Here, ${}^{RR'} C_{aa'}$ and ${}^{RR'} C_{a_1 a_2, a'}$ are perturbative matching kernels. The rapidity evolution kernel ${}^R J$ only depends on the dimensionality of the representation, and $|R_1| = |R_2|$ is necessary to have a non-vanishing DPD. In the momentum-space matching the lightcone- and quasi-DPD are evaluated at the same rapidity scale, to avoid the more complicated momentum-space rapidity evolution. Furthermore we wish to stress that the position space and momentum space matching relations eq. (4.15) and eq. (4.16) are not equivalent due to the single-PDF contribution that arises at vanishing transverse separation.

As we will now show, the above matching relations are consistent with the renormalization group evolution and the rapidity evolution of the lightcone- and quasi-DPDs. The rapidity evolution is satisfied trivially, as both the lightcone- and the quasi-DPD satisfy a Collins-Soper evolution. Note that this relies on the fact there is no matching between quasi-DPDs onto lightcone-DPDs with a different rapidity anomalous dimension and that the matching kernels are rapidity-scale independent.

To show that the matching relation is also consistent with renormalization group evolution, we start by presenting the structure of evolution equations for the quasi-DPD. Their evolution can be inferred from eq. (4.14) by using the fact that the unsubtracted quasi-DPDs have a multiplicative renormalization and the quasi-soft soft function satisfies eq. (4.13). This leads to the following evolution equation for the quasi-DPDs,

$$\begin{aligned}
& \frac{d}{d \ln \mu^2} {}^{R_1 R_2} \tilde{F}_{a_1 a_2}(x_1, x_2, b_\perp, \mu, \tilde{\zeta}_p, \tilde{P}^z) \\
&= \left[{}^{R_1} \gamma_{a_1} + \frac{1}{4} {}^{R_1} \gamma_J \ln \left(\frac{(2x_1 \tilde{P}^z)^2}{x_1^2 \tilde{\zeta}_p} \right) + (1 \leftrightarrow 2) \right] {}^{R_1 R_2} \tilde{F}_{a_1 a_2}(x_1, x_2, b_\perp, \mu, \tilde{\zeta}_p, \tilde{P}^z).
\end{aligned} \tag{4.17}$$

Here ${}^R \gamma_a$ corresponds to the anomalous dimension of one of the current operators in the unsubtracted quasi-DPD and ${}^R \gamma_J$ is the anomalous dimension of the rapidity evolution kernel,

$$\frac{d}{d \ln \mu^2} {}^R J(b_\perp, \mu) = -{}^R \gamma_J(\mu). \tag{4.18}$$

On the other hand, for the physical DPDs in position space, the renormalization scale dependence is given by [20, 105]

$$\frac{d}{d \ln \mu^2} {}^{R_1 R_2} F_{a_1 a_2}(x_1, x_2, b_\perp, \mu, \zeta_p) \tag{4.19}$$

$$\begin{aligned}
&= \sum_{R'_1 R'_2} \sum_{a'_1, a'_2} \int \frac{dx'_1}{x'_1} \frac{dx'_2}{x'_2} \left[{}^{R_1 \bar{R}_1} P_{a_1 a'_1} \left(\frac{x_1}{x'_1}, \mu, x_1^2 \zeta_p \right) \delta_{R'_2 R_2} \delta_{a'_2 a_2} \delta \left(1 - \frac{x_2}{x'_2} \right) + (1 \leftrightarrow 2) \right] \\
&\quad \times {}^{R'_1 R'_2} F_{a'_1 a'_2} (x'_1, x'_2, \mathbf{b}_\perp, \mu, \zeta_p),
\end{aligned}$$

where the ${}^{R \bar{R}'} P_{aa'}$ are referred to as the color-dependent DGLAP splitting kernels. These kernels can be split up into a rapidity-independent part \hat{P} and rapidity-dependent part,

$${}^{R \bar{R}'} P_{aa'}(x, \mu, \zeta) = {}^{R \bar{R}'} \hat{P}_{aa'}(x, \mu) - \frac{1}{4} \delta_{R \bar{R}'} \delta_{aa'} \delta(1-x) {}^R \gamma_J \ln \left(\frac{\zeta}{\mu^2} \right). \quad (4.20)$$

Using these evolution equations, one can see that the matching relation is consistent with the UV and large rapidity behaviour of the lightcone- and quasi-DPDs. Furthermore, one can conclude that the matching kernels satisfy,

$$\begin{aligned}
\frac{d}{d \ln \mu^2} {}^{R \bar{R}'} C_{aa'} \left(\frac{x}{x'}, x' \tilde{P}^z, \mu \right) &= \left[{}^R \gamma_a + \frac{1}{4} {}^R \gamma_J \ln \left(\frac{(2x' \tilde{P}^z)^2}{\mu^2} \right) \right] {}^{R \bar{R}'} C_{aa'} \left(\frac{x}{x'}, x' \tilde{P}^z, \mu \right) \\
&\quad - \sum_{R''} \sum_{a''} \int_0^1 \frac{dx''}{|x''|} {}^{R'' \bar{R}'} \hat{P}_{a'' a'} \left(\frac{x''}{x'}, \mu \right) {}^{R \bar{R}''} C_{aa'} \left(\frac{x}{x''}, x'' \tilde{P}^z, \mu \right).
\end{aligned} \quad (4.21)$$

In this paper we do not provide a proof for the matching relation. However, for the color-summed case, the proof for the single-PDF case [58], which makes use of the operator product expansion (OPE), directly carries over for the position-space matching in eq. (4.15). This is because the operator that defines the color-summed DPDs consists of two copies of the single-PDF operators separated by a finite distance \mathbf{b}_\perp . The finite transverse separation ensures that no additional terms can arise in the OPE and so one can apply the OPE to each current operator separately. This leads to the conclusion that the matching kernels for the color-summed DPDs will be identical to the matching kernels of the single parton case,

$${}^{11} C_{aa'} \left(\frac{x}{x'}, x' \tilde{P}^z, \mu \right) = \mathcal{C}_{aa'} \left(\frac{x}{x'}, \frac{\mu}{|x'| \tilde{P}^z} \right), \quad (4.22)$$

where the $\mathcal{C}_{aa'}$ are the matching kernels that appear in (2.18). Note that this proof does not directly carry over to the momentum-space matching relation of eq. (4.16), as the OPE relies on the position-space formulation where \mathbf{b}_\perp is taken to be finite, whereas the mixing term involving single PDFs arises from the region where $\mathbf{b}_\perp \rightarrow 0$.

For DPDs with a non-trivial color structure the proof would be more complicated. In principle, one could extend the proof of the TMD matching relation in ref. [65] to the case of color-correlated DPDs. This proof was based on the decomposition of the hadronic correlator in terms of all available Lorentz structures, which was used to show that the correlators describing the quasi- and LR scheme TMDs agree in the infinite boost limit, up to higher twist terms. An extension of this proof to the case of DPDs would require an analysis of the Lorentz decomposition of the hadronic correlator defining DPDs. Furthermore, this proof cannot be carried over directly to our case because DPDs have a substantially different UV behaviour.

5 One-loop matching for the flavor-non-singlet case

In this section we will calculate the quark-quark DPD matching kernel ${}^{RR'}C_{qq'}$ for all color and spin structures to one-loop order. We consider the flavor non-singlet DPDs, which can be defined as

$${}^{R_1 R_2}F_{q_1 q_2}^{\text{NS}} = {}^{R_1 R_2}F_{u_1 u_2} - {}^{R_1 R_2}F_{u_1 d_2} - {}^{R_1 R_2}F_{d_1 u_2} + {}^{R_1 R_2}F_{d_1 d_2}. \quad (5.1)$$

Here q_i denote the spin structure $q, \Delta q, \delta q$ and *not* the quark flavor, while u_i and d_i denote different quark flavors and have the same spin structure as the corresponding q_i . By considering the flavor non-singlet case, we do not need to consider mixing with different flavors, but mixing with color and spin is still present. In this case the matching relation of eq. (4.15) simplifies to

$$\begin{aligned} & {}^{R_1 R_2}\tilde{F}_{q_1 q_2}^{\text{NS}}(x_1, x_2, b_\perp, \mu, \tilde{\zeta}_p, \tilde{P}^z) \\ &= \sum_{R'_1, R'_2} \sum_{q'_1, q'_2} \int_0^1 \frac{dx'_1}{x'_1} \frac{dx'_2}{x'_2} {}^{R_1 R'_1}C_{q_1 q'_1}\left(\frac{x_1}{x'_1}, x'_1 \tilde{P}^z, \mu\right) {}^{R_2 R'_2}C_{q_2 q'_2}\left(\frac{x_2}{x'_2}, x'_2 \tilde{P}^z, \mu\right) \\ &\quad \times \exp\left[\frac{1}{2} {}^{R_1/2}J(b_\perp, \mu) \ln\left(\frac{\tilde{\zeta}_p}{\zeta_p}\right)\right] {}^{R'_1 R'_2}F_{q'_1 q'_2}^{\text{NS}}(x'_1, x'_2, b_\perp, \mu, \zeta_p). \end{aligned} \quad (5.2)$$

where the sum on q'_i runs only over the spin structures, not quark flavors. The only nonvanishing color structures are $R_1 = R_2$ and $R'_1 = R'_2$ which can be either 1 or 8.

The one-loop matching kernels can be extracted from the one-loop corrections to the lightcone- and quasi-DPDs with the proton replaced by partonic states. As we discuss in sec. 5.1, the use of partonic states leads to ill-defined expressions. We resolve this by using different in- and out-states, only taking them equal at the end of the calculation. The “master formula” for extracting the one-loop matching kernel from the various ingredients is derived in sec. 5.2. Next, sec. 5.3 provides an example calculation for one of the diagrams contributing to the one-loop lightcone- and quasi-DPD, with our conventions for plus distributions given in app. A. The results for all one-loop diagrams are presented in app. B. Finally, in sec. 5.4 we obtain the one-loop matching coefficients and verify their perturbative nature by showing that they are free of infrared logarithms. We also provide the one-loop expressions for the remaining ingredients that enter the matching relation: the lightcone- and quasi-soft functions, the rapidity evolution kernel and the relevant renormalization factors.

5.1 Handling divergences in calculating DPDs for partonic states

The matching kernel in eq. (5.2) is independent of the external state $|P\rangle$. We can therefore replace the proton by a suitable partonic state to calculate the matching kernel in perturbation theory. However, the DPDs as defined in the previous section are not well-suited for partonic states. This is because the definition of DPDs leads to the square of a delta function when applied to identical partonic in- and out-states. Here we demonstrate how this issue arises, and how it can be resolved by using different in- and out states in intermediate steps of the calculation.

The simplest state that gives a non-trivial result for the DPDs is a di-quark state where the quarks have definite (on-shell) momenta p_1 and p_2 . Neglecting the transverse momentum of the two quarks, we take

$$p_1 = \omega_1 p, \quad p_2 = \omega_2 p, \quad \text{with} \quad \omega_1 + \omega_2 = 1, \quad (5.3)$$

where $p = (p^+, 0^-, \mathbf{0}) = (p^z, \mathbf{0}, p^z)$, and we will use lowercase p for partonic momenta throughout the calculation.

Since we calculate the matching kernels for all color and spin structures, we do not average over the color and spin of the external partons. For notation convenience, we denote products of spinors as

$$\bar{u}(p_1) \Gamma_{q_1} T_{R_1} u(p_1) \bar{u}(p_2) \Gamma_{q_2} T_{R_2} u(p_2) \equiv (T_{R_1} \otimes T_{R_2}) \Gamma_{q_1} \otimes \Gamma_{q_2}, \quad (5.4)$$

where T_{R_i} are the generators in the representation R_i and Γ_{q_i} are Dirac structures.

When calculated on di-parton states, the DPDs defined in eq. (3.4) diverge. Explicitly, for the color-summed DPD at tree-level, using the di-quark state in eq. (5.3)

$$\begin{aligned} {}^{11}F_{qq}^{(0)}(x_1, x_2) = & -\pi p^+ \int \frac{db_1^-}{2\pi} \frac{db_2^-}{2\pi} \frac{db_3^-}{2\pi} e^{-ix_1 p^+ b_1^-} e^{-ix_2 p^+ b_2^-} e^{ix_1 p^+ b_3^-} \\ & \times \bar{u}(p_1) e^{i\omega_1 p^+ b_1^-} \gamma^+ e^{-i\omega_1 p^+ b_3^-} u(p_1) \bar{u}(p_2) e^{i\omega_2 p^+ b_1^-} \gamma^+ u(p_2). \end{aligned} \quad (5.5)$$

The Fourier transforms over b_1^- and b_2^- result in delta functions of the two momentum fractions,

$${}^{11}F_{qq}^{(0)}(x_1, x_2) = -\pi(1 \otimes 1) \frac{\gamma^+ \otimes \gamma^+}{p_1^+ p_2^+} \delta\left(1 - \frac{x_1}{\omega_1}\right) \delta\left(1 - \frac{x_2}{\omega_2}\right) \int \frac{d(p^+ b_3^-)}{2\pi} e^{i(x_1 - \omega_1)p^+ b_3^-}. \quad (5.6)$$

The combination of Dirac matrices and p_i^+ is chosen to match the form in eq. (4.5). The remaining b_3^- integral gives a delta function involving x_1 , which has already been fixed to $x_1 = \omega_1$ by the Fourier transform over b_1^- , therefore resulting in a square of a delta function.

To avoid this extra delta function, we introduce slightly different in- and out states, which we use in intermediate steps of the calculation of the matching coefficients. Specifically, we temporarily change the in-state to

$$|p_1 p_2\rangle \rightarrow \int d\omega_3 \Psi(\omega_3) |p_3 p_4\rangle, \quad (5.7)$$

with $p_3 = \omega_3 p$ and $p_4 = \omega_4 p = (1 - \omega_3)p$, while keeping the out-state as $\langle p_1 p_2|$. The above in-state replaces the unwanted extra delta function by $\Psi(\omega_1)$:

$${}^{11}F_{qq}^{(0)}(x_1, x_2) = -\pi(1 \otimes 1) \frac{\gamma^+ \otimes \gamma^+}{p_1^+ p_2^+} \Psi(\omega_1) \delta\left(1 - \frac{x_1}{\omega_1}\right) \delta\left(1 - \frac{x_2}{\omega_2}\right). \quad (5.8)$$

In the limit that the in- and out-states are identical, i.e. when $\Psi(\omega_3)$ is narrowly peaked around $\omega_3 = \omega_1$, the above factor $\Psi(\omega_1)$ can be treated as an infinite normalization factor. Because the tree-level lightcone- and the quasi-DPD share this normalization factor, it directly drops out of the matching coefficient at this order, see eq. (5.12) below. Beyond tree-level care should be taken in treating $\Psi(\omega_3)$ as narrowly peaked, as we will see in our one-loop calculation in sec. 5.3. In practice, we will set ω_3 equal to ω_1 whenever that is possible without generating a divergence.

5.2 Constructing the one-loop matching kernel

Here we lay out the details that enter the calculation of the one-loop matching kernel in eq. (5.2). We denote the perturbative expansion of the matching kernels by

$$C = C^{(0)} + \frac{\alpha_s}{4\pi} C^{(1)} + \mathcal{O}(\alpha_s^2), \quad (5.9)$$

and use a similar notation for the perturbative expansion of the other objects. At tree-level, the matching kernel can be constructed from the tree-level lightcone- and quasi-DPDs, which respectively read

$$R_1 R_2 F_{q_1 q_2}^{(0)}(x_1, x_2) = -\pi \Psi(\omega_1) \delta\left(1 - \frac{x_1}{\omega_1}\right) \delta\left(1 - \frac{x_2}{\omega_2}\right) (T_{R_1} \otimes T_{R_2}) \frac{\Gamma_{q_1} \otimes \Gamma_{q_2}}{p_1^+ p_2^+}, \quad (5.10)$$

$$R_1 R_2 \tilde{F}_{q_1 q_2}^{(0)}(x_1, x_2) = -\pi \Psi(\omega_1) \delta\left(1 - \frac{x_1}{\omega_1}\right) \delta\left(1 - \frac{x_2}{\omega_2}\right) (T_{R_1} \otimes T_{R_2}) \frac{\tilde{\Gamma}_{q_1} \otimes \tilde{\Gamma}_{q_2}}{p_1^z p_2^z}. \quad (5.11)$$

The tree-level matching kernel is then

$${}^{RR'}C_{qq'}^{(0)}\left(\frac{x}{\omega}, \omega \tilde{p}^z, \mu\right) = \delta_{RR'} \delta_{qq'} \delta\left(1 - \frac{x}{\omega}\right). \quad (5.12)$$

Using these tree-level results in the expansion of eq. (5.2) to one-loop order, leads to

$$\begin{aligned} & R_1 R_2 \tilde{F}_{q_1 q_2}^{(1)}(x_1, x_2, b_\perp, \mu, \tilde{\zeta}_p, \tilde{p}^z) \\ &= R_1 R_2 F_{q_1 q_2}^{(1)}(x_1, x_2, b_\perp, \mu, \zeta_p) \\ &\quad - \sum_{R'_1} \sum_{q'_1} \pi \Psi(\omega_1) \delta\left(1 - \frac{x_2}{\omega_2}\right) (T_{R'_1} \otimes T_{R_2}) \frac{\Gamma_{q'_1} \otimes \Gamma_{q_2}}{p_1^+ p_2^+} R_1 R'_1 C_{q_1 q'_1}^{(1)}\left(\frac{x_1}{\omega_1}, \omega_1 p^z, \mu\right) \\ &\quad - \sum_{R'_2} \sum_{q'_2} \pi \Psi(\omega_1) \delta\left(1 - \frac{x_1}{\omega_1}\right) (T_{R_1} \otimes T_{R'_2}) \frac{\Gamma_{q_1} \otimes \Gamma_{q'_2}}{p_1^+ p_2^+} R_2 R'_2 C_{q_2 q'_2}^{(1)}\left(\frac{x_2}{\omega_2}, \omega_2 p^z, \mu\right) \\ &\quad - \pi \Psi(\omega_1) \delta\left(1 - \frac{x_1}{\omega_1}\right) \delta\left(1 - \frac{x_2}{\omega_2}\right) (T_{R_1} \otimes T_{R_2}) \frac{\Gamma_{q_1} \otimes \Gamma_{q_2}}{p_1^+ p_2^+} \frac{1}{2} R_J^{(1)}(b_\perp, \mu) \ln\left(\frac{\tilde{\zeta}_p}{\zeta_p}\right). \end{aligned} \quad (5.13)$$

The one-loop corrections to the DPDs that appear in this expression are the renormalized subtracted DPDs. Following eqs. (3.9), (3.14) and (4.10), these one-loop corrections can be written in terms of the *bare unsubtracted* DPDs $R_1 R_2 F_{q_1 q_2}^{\text{unsub}}$ and $R_1 R_2 \tilde{F}_{q_1 q_2}^{\text{unsub}}$ as

$$\begin{aligned} & R_1 R_2 F_{q_1 q_2}^{(1)}(x_1, x_2, b_\perp, \mu, \zeta_p) = \lim_{\epsilon \rightarrow 0} \lim_{\delta^+ \rightarrow 0} \left\{ R_1 R_2 F_{q_1 q_2}^{\text{unsub}(1)}(x_1, x_2, b_\perp, \epsilon, \delta^+, p^+) \right. \\ &\quad + \pi \Psi(\omega_1) \delta\left(1 - \frac{x_1}{\omega_1}\right) \delta\left(1 - \frac{x_2}{\omega_2}\right) (T_{R_1} \otimes T_{R_2}) \frac{\Gamma_{q_1} \otimes \Gamma_{q_2}}{p_1^+ p_2^+} \frac{1}{2} R_S^{(1)}(b_\perp, \epsilon, \delta^+, e^{2y_n} \delta^+) \\ &\quad - \pi \Psi(\omega_1) \delta\left(1 - \frac{x_2}{\omega_2}\right) (T_{R'_1} \otimes T_{R_2}) \frac{\Gamma_{q'_1} \otimes \Gamma_{q_2}}{p_1^+ p_2^+} R_1 \bar{R}'_1 Z_{q_1 q'_1}^{(1)}\left(\frac{x_1}{\omega_1}, \mu, x_1^2 \zeta_p\right) \\ &\quad \left. - \pi \Psi(\omega_1) \delta\left(1 - \frac{x_1}{\omega_1}\right) (T_{R_1} \otimes T_{R'_2}) \frac{\Gamma_{q_1} \otimes \Gamma_{q'_2}}{p_1^+ p_2^+} R_2 \bar{R}'_2 Z_{q_2 q'_2}^{(1)}\left(\frac{x_2}{\omega_2}, \mu, x_2^2 \zeta_p\right) \right\}, \end{aligned} \quad (5.14)$$

$$R_1 R_2 \tilde{F}_{q_1 q_2}^{(1)}(x_1, x_2, b_\perp, \mu, \tilde{\zeta}_p, \tilde{p}^z) = \lim_{\tilde{\eta} \rightarrow \infty} \lim_{\epsilon \rightarrow 0} \left\{ R_1 R_2 \tilde{F}_{q_1 q_2}^{\text{unsub}(1)}(x_1, x_2, b_\perp, \epsilon, \tilde{\eta}, \tilde{p}^z) \right\} \quad (5.15)$$

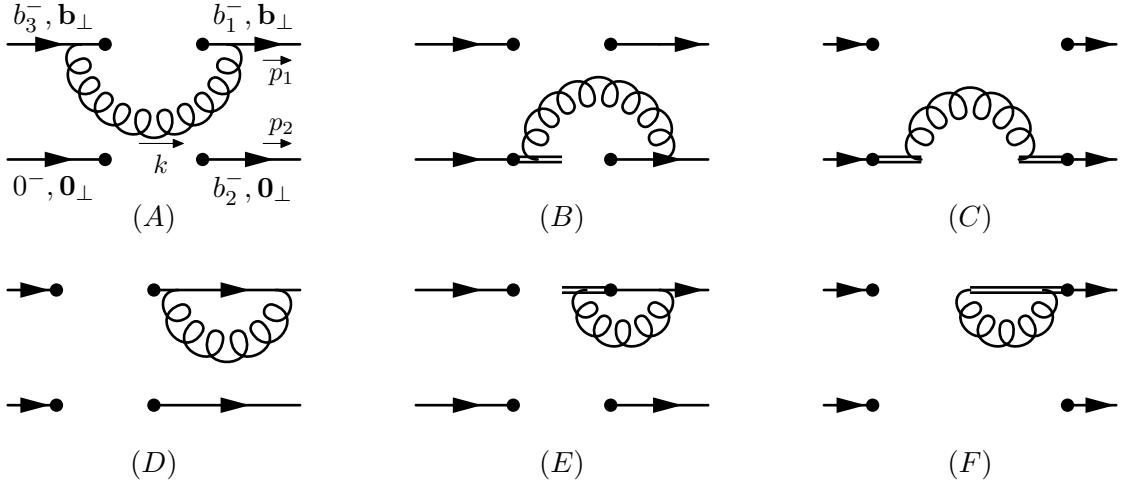


Figure 1. The one-loop corrections to the quark-quark quasi-DPD that involve only a single quark line. For the corresponding lightcone diagrams, a cut should be inserted vertically in the middle of the diagram. The top and bottom row have different color factors for the color-correlated DPD, and consequently require a rapidity regulator.

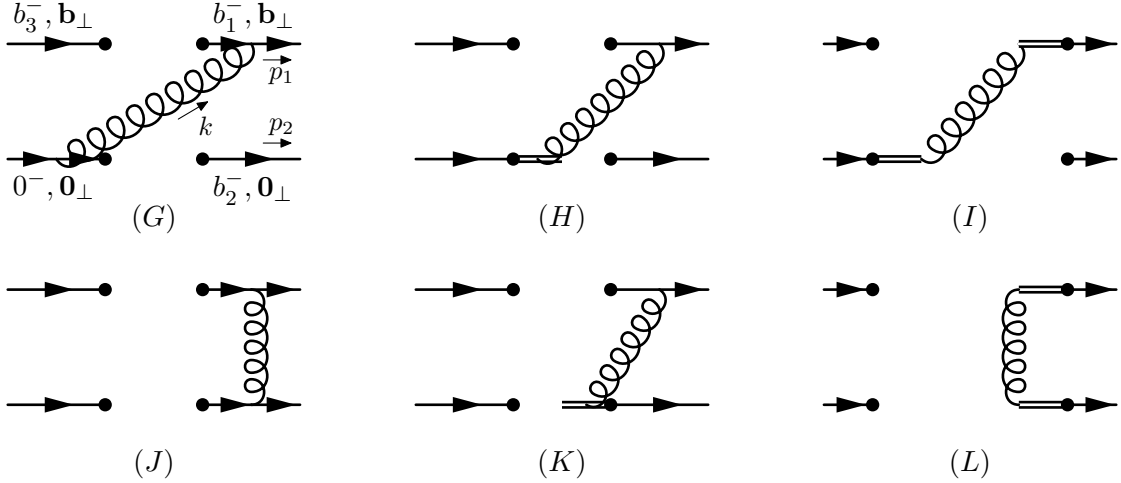


Figure 2. The one-loop corrections to the quark-quark quasi-DPD that involve a gluon exchange between the two quark lines. For the corresponding lightcone diagrams, a cut should be inserted vertically in the middle of the diagram.

$$\begin{aligned}
& + \pi \Psi(\omega_1) \delta\left(1 - \frac{x_1}{\omega_1}\right) \delta\left(1 - \frac{x_2}{\omega_2}\right) (T_{R_1} \otimes T_{R_2}) \frac{\tilde{\Gamma}_{q_1} \otimes \tilde{\Gamma}_{q_2}}{\tilde{p}_1^z \tilde{p}_2^z} \frac{1}{2} R \tilde{S}^{(1)}(b_\perp, \epsilon, \tilde{\eta}, y_A, y_B) \\
& - \pi \Psi(\omega_1) \delta\left(1 - \frac{x_1}{\omega_1}\right) \delta\left(1 - \frac{x_2}{\omega_2}\right) (T_{R_1} \otimes T_{R_2}) \frac{\tilde{\Gamma}_{q_1} \otimes \tilde{\Gamma}_{q_2}}{\tilde{p}_1^z \tilde{p}_2^z} R_1 R_2 \tilde{Z}_{q_1 q_2}^{(1)}(\epsilon, \mu, y_A, y_B) \Big\}.
\end{aligned}$$

Here we switched from the off-lightcone regulator in eq. (2.9) to the delta regulator in eq. (2.11).

The diagrams for the one-loop corrections to the bare unsubtracted DPDs are shown in figures 1 and 2. For simplicity, we only show the diagrams belonging to the quasi-DPD,

as those for the lightcone-DPD look identical up to a vertical cut through the middle of the diagram due to the time-ordering prescription in eq. (3.4). For identical quark flavors one could also consider “crossing” quark lines, but this turns out to be irrelevant. The one-loop corrections can be classified as diagrams where only a single quark line is involved (fig. 2) and diagrams where a gluon connects the two quark lines (fig. 1). This classification is useful, as the diagrams in the first category are identical to the one-loop corrections to regular PDFs, up to an overall normalization and the presence of the other quark line. Note however that these diagrams must be calculated with a rapidity regulator, as the diagrams in the top and bottom row receive different color factors for the color-correlated DPD, preventing the cancellation of rapidity divergences. The diagrams shown do not include the contributions of the transverse Wilson line that are necessary to ensure gauge invariance of the color-correlated quasi-DPD (see eq. (4.4) vs. eq. (4.7)). However, we have explicitly verified that at one-loop order the contribution of the transverse Wilson line cancels between the unsubtracted quasi-DPD and the quasi-soft function.

It is useful to separate the color structure from the rest of the diagram such that the resulting expressions can be used to calculate both the color-summed and color-correlated DPDs:

$$R_1 R_2 F_{q_1 q_2}^{\text{unsub}(1)} = \sum_{i \in \text{diagrams}} \sum_{R'_1, R'_2} \sum_{q'_1, q'_2} R_1 R_2, R'_1 R'_2 c^i [F_{q_1 q_2}^i]_{q'_1 q'_2} (T_{R'_1} \otimes T_{R'_2}) \frac{\Gamma_{q'_1} \otimes \Gamma_{q'_2}}{p_1^+ p_2^+}. \quad (5.16)$$

Here $F_{q_1 q_2}^i$ is the expression for diagram i contributing to $R_1 R_2 F_{q_1 q_2}^{(1)}$ with color factors absorbed into $R_1 R_2, R'_1 R'_2 c^i$. Conveniently, the diagrams in figures 1 and 2 are ordered such that diagrams in each row have an identical color structure. We furthermore use $[F_{q_1 q_2}^i]_{q'_1 q'_2}$ to denote its contribution to the spin structure $\Gamma_{q'_1} \otimes \Gamma_{q'_2}$. A similar expression holds for the quasi-DPDs \tilde{F} , with the appropriate replacement of Γ and p_i^+ , see eq. (4.5).

Before writing down an expression for the one-loop matching kernel, let us discuss how the divergent factor $\Psi(\omega_1)$ drops out of the matching kernel. The individual expressions for the one-loop lightcone- and quasi-DPDs contain non-trivial integrals involving $\Psi(\omega_3)$. However, in constructing the matching kernel, these terms cancel between the lightcone- and the quasi-DPDs. Even at the level of individual diagrams, the difference between the one-loop corrections to the lightcone- and quasi-DPDs factors as

$$\begin{aligned} \lim_{p_3, p_4 \rightarrow p_1, p_2} [\tilde{F}_{q_1 q_2}^i]_{q'_1 q'_2}(x_1, x_2, b_\perp, \epsilon, \tilde{\eta}, \tilde{p}^z) - [F_{q_1 q_2}^i]_{q'_1 q'_2}(x_1, x_2, b_\perp, \epsilon, \delta^+, p^+) \\ = -\pi \Psi(\omega_1) [\Delta_{q_1 q_2}^i]_{q'_1 q'_2}(x_1, x_2, b_\perp, \epsilon, \{\tilde{\eta}, \tilde{p}^z\}, \{\delta^+, p^+\}), \end{aligned} \quad (5.17)$$

such that the divergent factor $\Psi(\omega_1)$ drops out of the matching kernel.

Combining all the perturbative expansions and organizing by color and spin structures, the one-loop matching kernels for the flavor non-singlet case can be expressed as

$$\begin{aligned} \delta_{R_2 R'_2} \delta_{q_2 q'_2} \delta\left(1 - \frac{x_2}{\omega_2}\right) R_1 R'_1 C_{q_1 q'_1}^{(1)}\left(\frac{x_1}{\omega_1}, \omega_1 \tilde{p}^z, \mu\right) + (1 \leftrightarrow 2) \\ = \lim_{\tilde{\eta} \rightarrow \infty} \lim_{\epsilon \rightarrow 0} \lim_{\delta^+ \rightarrow 0} \left\{ \sum_i R_1 R_2, R'_1 R'_2 c^i [\Delta_{q_1 q_2}^i]_{q'_1 q'_2}(x_1, x_2, b_\perp, \epsilon, \{\tilde{\eta}, \tilde{p}^z\}, \{\delta^+, p^+\}) \right\} \end{aligned} \quad (5.18)$$

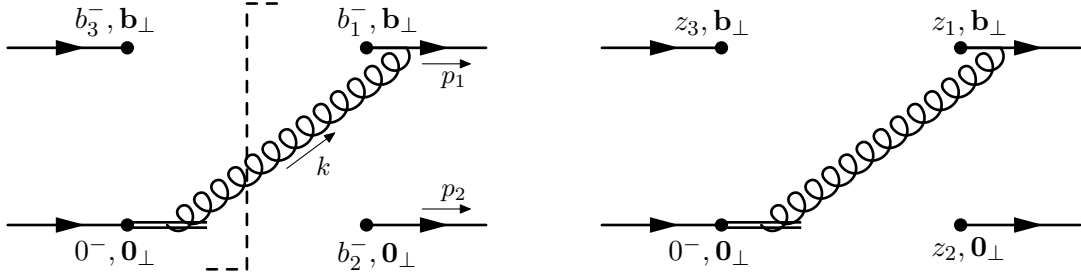


Figure 3. Diagram H for the lightcone- (left) and quasi-DPD (right).

$$\begin{aligned}
& + \frac{1}{2} \delta_{R_1 R'_1} \delta_{R_2 R'_2} \delta_{q_1 q'_1} \delta_{q_2 q'_2} \delta\left(1 - \frac{x_1}{\omega_1}\right) \delta\left(1 - \frac{x_2}{\omega_2}\right) \\
& \times \left[R\tilde{S}^{(1)}(b_\perp, \epsilon, \delta^+, e^{2y_n} \delta^+) - R\tilde{S}^{(1)}(b_\perp, \epsilon, \tilde{\eta}, y_A, y_B) - R^J^{(1)}(b_\perp, \mu) \ln\left(\frac{\tilde{\zeta}_p}{\zeta_p}\right) \right] \\
& + \delta_{R_1 R'_1} \delta_{R_2 R'_2} \delta_{q_1 q'_1} \delta_{q_2 q'_2} \delta\left(1 - \frac{x_1}{\omega_1}\right) \delta\left(1 - \frac{x_2}{\omega_2}\right) R_1 R_2 \tilde{Z}_{q_1 q_2}^{(1)}(\epsilon, \mu, y_A, y_B) \\
& - \delta_{R_2 R'_2} \delta_{q_2 q'_2} R_1 \tilde{R}'_1 Z_{q_1 q'_1}^{(1)}\left(\frac{x_1}{\omega_1}, \mu, x_1^2 \zeta_p\right) \delta\left(1 - \frac{x_2}{\omega_2}\right) \\
& - \delta_{R_1 R'_1} \delta_{q_1 q'_1} R_2 \tilde{R}'_2 Z_{q_2 q'_2}^{(1)}\left(\frac{x_2}{\omega_2}, \mu, x_2^2 \zeta_p\right) \delta\left(1 - \frac{x_1}{\omega_1}\right) \Big\}.
\end{aligned}$$

The order of the $\tilde{\eta}$ and ϵ limits does not matter [65].

5.3 Lightcone- and quasi-DPDs at one-loop

Here we will provide an example calculation of one of the diagrams that contributes to the one-loop lightcone- and quasi-DPDs. A complete overview of the results of all diagrams is given in app. B. The diagram we will calculate here is diagram H , also shown in fig. 3. This diagram exhibits most features that distinguish DPDs from PDFs and TMDs, as it involves both quark lines.

First we calculate the lightcone diagram, shown on the left in fig. 3. To keep the notation compact, we will use the shorthand for the graph labelled with n

$$F^n = \frac{\alpha_s}{4\pi} \sum_{q'_1, q'_2} [F_{q_1 q_2}^n]_{q'_1 q'_2} \frac{\Gamma_{q'_1} \otimes \Gamma_{q'_2}}{p_1^+ p_2^+}, \quad (5.19)$$

and \tilde{F}^n for the corresponding quasi-DPDs. From the Feynman rules one can derive the following expression,

$$\begin{aligned}
F^H &= -\pi p^+ \mu_0^{2\epsilon} \int d\omega_3 \Psi(\omega_3) \int \frac{d^d k}{(2\pi)^d} e^{i\mathbf{k}_\perp \cdot \mathbf{b}_\perp} \left[(ig\gamma^\mu) \frac{i}{\not{p}_1 - \not{k}} \Gamma_{q_1} \otimes \Gamma_{q_2} (ign_a^\nu) \frac{i}{\not{k}^+ + i\delta^+} \right] \\
&\quad \times (-g_{\mu\nu}) 2\pi \delta(k^2) \theta(k^0) \delta[x_1 p^+ - (p_1^+ - k^+)] \delta[x_2 p^+ - p_2^+] \delta[x_1 p^+ - p_3^+] \\
&= -\alpha_s \Psi(x_1) \delta\left(1 - \frac{x_2}{\omega_2}\right) \frac{\gamma^+ \gamma_\mu \Gamma_{q_1} \otimes \Gamma_{q_2}}{p_1^+ p_2^+} \frac{1}{(\omega_1 - x_1) p^+ + i\delta^+}
\end{aligned}$$

$$\times 4\pi^3 \mu_0^{2\epsilon} \int \frac{d^d k}{(2\pi)^d} e^{i\mathbf{k}_\perp \cdot \mathbf{b}_\perp} \frac{(p_1 - k)^\mu}{k^-} \delta(k^2) \theta(k^0) \delta[k^+ - (\omega_1 - x_1)p^+] , \quad (5.20)$$

where μ_0 is the scale associated with dimensional regularization. The remaining momentum integral in eq. (5.20) can be simplified by considering the contribution of each component of $(p_1 - k)^\mu$ separately: First, since $(\gamma^+)^2 = 0$, the contribution of $(p_1 - k)^-$ vanishes. Second, since γ_\perp^μ can be anti-commuted through γ^+ , and because $\gamma^+ \Gamma = 0$ for all $\Gamma \in \{\gamma^+, \gamma^+ \gamma^5, \gamma^+ \gamma^\perp \gamma^5\}$ the contribution of $(p_1 - k)_\perp^\mu$ vanishes as well. This leaves us only with the combination $\gamma^-(p_1 - k)^+ = x_1 p^+ \gamma^-$, which gives

$$F^H = -\frac{\alpha_s}{4\pi} \Psi(x_1) \delta\left(1 - \frac{x_2}{\omega_2}\right) \frac{\Gamma_{q_1} \otimes \Gamma_{q_2}}{p_1^+ p_2^+} \frac{2x_1}{(\omega_1 - x_1) + i\delta^+/p^+} \times (4\pi^2 \mu_0^2)^\epsilon \int d^d k e^{i\mathbf{k}_\perp \cdot \mathbf{b}_\perp} \frac{1}{k^-} \delta(k^2) \theta(k^0) \delta[k^+ - (\omega_1 - x_1)p^+] . \quad (5.21)$$

The remaining integral is given in eq. (B.3), resulting in

$$F^H = -\frac{\alpha_s}{4\pi} \pi \Psi(x_1) \delta\left(1 - \frac{x_2}{\omega_2}\right) \frac{\Gamma_{q_1} \otimes \Gamma_{q_2}}{p_1^+ p_2^+} \frac{2x_1}{(\omega_1 - x_1) + i\delta^+/p^+} \frac{2\sqrt{\pi}\Gamma(-2\epsilon_{\text{ir}})}{\Gamma(\frac{1}{2} - \epsilon)} (4\pi\mu_0^2 \mathbf{b}_\perp^2)^\epsilon , \quad (5.22)$$

where $d = 4 - 2\epsilon_{\text{ir/uv}}$ and we only sometimes add the subscript “ir” or “uv” to indicate the origin of the poles. Finally, introducing a plus distribution using the convention in app. A, and expanding in ϵ and dropping terms of $\mathcal{O}(\epsilon)$

$$F^H = \frac{\alpha_s}{4\pi} 2\pi \Psi(x_1) \delta\left(1 - \frac{x_2}{\omega_2}\right) \frac{\Gamma_{q_1} \otimes \Gamma_{q_2}}{p_1^+ p_2^+} \left[\frac{1}{\epsilon_{\text{ir}}} + \ln\left(\frac{\mu^2 \mathbf{b}_\perp^2}{b_0^2}\right) \right] \times \left\{ \left[\frac{\frac{x_1}{\omega_1}}{1 - \frac{x_1}{\omega_1}} \right]_+^{[0,1]} - \delta\left(1 - \frac{x_1}{\omega_1}\right) \left[1 + \ln\left(\frac{\delta^+}{p_1^+}\right) + \frac{i\pi}{2} \right] \right\} , \quad (5.23)$$

Here the ratio x_1/ω_1 is the variable of the plus distribution, i.e. integrating it over the interval $[0, 1]$ will give zero. The μ_0 is related to the $\overline{\text{MS}}$ -scale μ and the b_0 is given by

$$\mu_0^2 = \mu^2 \frac{e^{\gamma_E}}{4\pi} , \quad b_0 = 2e^{-\gamma_E} . \quad (5.24)$$

Next we calculate diagram H for the quasi-DPD. This matrix element can be treated as time-ordered and therefore does not include a cut gluon propagator. From the Feynman rules we derive

$$\begin{aligned} \tilde{F}^H &= -\pi p^z \mu_0^{2\epsilon} \int d\omega_3 \Psi(\omega_3) \int \frac{d^d k}{(2\pi)^d} e^{i\mathbf{k}_\perp \cdot \mathbf{b}_\perp} \left[(ig\gamma^\mu) \frac{i}{\not{p}_1 - \not{k}} \tilde{\Gamma}_{q_1} \otimes \tilde{\Gamma}_{q_2} (ig\hat{z}^\nu) \frac{i}{k^z} \right] \\ &\times \frac{-ig_{\mu\nu}}{k^2} (e^{-ik^z \tilde{\eta}} - 1) \delta[x_1 p^z - (p_1^z - k^z)] \delta[x_2 p^z - p_2^z] \delta[x_1 p^z - p_3^z] \\ &= \alpha_s \Psi(x_1) \delta\left(1 - \frac{x_2}{\omega_2}\right) \frac{\gamma^z \gamma_\mu \tilde{\Gamma}_{q_1} \otimes \tilde{\Gamma}_{q_2}}{p_1^z p_2^z} \\ &\times 4i\pi^2 p_1^z \mu_0^{2\epsilon} \int \frac{d^d k}{(2\pi)^d} e^{i\mathbf{k}_\perp \cdot \mathbf{b}_\perp} \frac{(p_1 - k)^\mu}{k^2 (p_1 - k)^2} \frac{1 - e^{-ik^z \tilde{\eta}}}{k^z} \delta[k^z - (\omega_1 - x_1)p^z] . \end{aligned} \quad (5.25)$$

Note that $\hat{z} \cdot p = -p^z$ due to the signature of our metric. To simplify the above expression, we use that for an on-shell quark spinor $u(p)$ with $p = (p^z, 0, 0, p^z)$ we have $\gamma^0 u(p) = \gamma^z u(p)$. Additionally, we can ignore the term $(p_1 - k)_\perp^\mu$ as its contribution is power-suppressed by $1/(|\mathbf{b}_\perp| p^z)$. This leads to

$$\begin{aligned} \tilde{F}^H &= \frac{\alpha_s}{4\pi} 16i\pi^3 \Psi(x_1) \delta\left(1 - \frac{x_2}{\omega_2}\right) \frac{\tilde{\Gamma}_{q_1} \otimes \tilde{\Gamma}_{q_2}}{p_2^z} \\ &\quad \times \mu_0^{2\epsilon} \int \frac{d^d k}{(2\pi)^d} e^{i\mathbf{k}_\perp \cdot \mathbf{b}_\perp} \frac{(p_1 - k)^0 + (p_1 - k)^z}{k^2 (p_1 - k)^2} \frac{1 - e^{-ik^z \tilde{\eta}}}{k^z} \delta[k^z - (\omega_1 - x_1)p^z] . \end{aligned} \quad (5.26)$$

We find it convenient to already introduce a plus distribution at this stage of the calculation. That way we may omit the regulator $\tilde{\eta}$ inside the plus distribution, as the behavior of the function at $x_1 = \omega_1$ is contained in the delta-function term. To calculate the resulting momentum integrals we combine denominators by introducing a Feynman parameter v and use eq. (B.5),

$$\begin{aligned} \tilde{F}^H &= \frac{\alpha_s}{4\pi} \left\{ -\Psi(x_1) \delta\left(1 - \frac{x_2}{\omega_2}\right) \frac{\tilde{\Gamma}_{q_1} \otimes \tilde{\Gamma}_{q_2}}{p_1^z p_2^z} \right. \\ &\quad \times \left(\frac{\mu_0^2}{p_{1z}^2} \right)^\epsilon \left[\frac{1}{1 - \frac{x_1}{\omega_1}} \int_0^1 dv \left(v + \frac{x_1}{\omega_1} \right) \left(\frac{2\pi |\mathbf{b}_\perp| p_1^z}{|v - \frac{x_1}{\omega_1}|} \right)^{\frac{1}{2} + \epsilon} K_{\frac{1}{2} + \epsilon} \left(|v - \frac{x_1}{\omega_1}| |\mathbf{b}_\perp| p_1^z \right) \right]_+ \\ &\quad + \pi \Psi(\omega_1) \delta\left(1 - \frac{x_1}{\omega_1}\right) \delta\left(1 - \frac{x_2}{\omega_2}\right) \frac{\tilde{\Gamma}_{q_1} \otimes \tilde{\Gamma}_{q_2}}{p_1^z p_2^z} \\ &\quad \times 16i\pi^2 p_1^z \mu_0^{2\epsilon} \int_0^1 dv \int_{-\infty}^\infty dy \frac{1 - e^{-iy p_1^z \tilde{\eta}}}{y} \int \frac{d^d \ell}{(2\pi)^d} e^{i\ell_\perp \cdot \mathbf{b}_\perp} \frac{2 - y - v}{\ell^4} \delta[\ell^z - (y - v)p_1^z] \Big\} . \end{aligned} \quad (5.27)$$

Finally, we perform the integral over the Feynman parameter v and expand in ϵ to obtain

$$\begin{aligned} \tilde{F}^H &= \frac{\alpha_s}{4\pi} \left\{ \pi \Psi(x_1) \delta\left(1 - \frac{x_2}{\omega_2}\right) \frac{\tilde{\Gamma}_{q_1} \otimes \tilde{\Gamma}_{q_2}}{p_1^z p_2^z} \left[\frac{1}{\epsilon_{\text{ir}}} + \ln \left(\frac{\mu^2 \mathbf{b}_\perp^2}{b_0^2} \right) \right] \left[\frac{2x_1}{1 - \frac{x_1}{\omega_1}} \right]^{[0,1]}_+ \right. \\ &\quad + \pi \Psi(\omega_1) \delta\left(1 - \frac{x_1}{\omega_1}\right) \delta\left(1 - \frac{x_2}{\omega_2}\right) \frac{\tilde{\Gamma}_{q_1} \otimes \tilde{\Gamma}_{q_2}}{p_1^z p_2^z} \\ &\quad \times 16i\pi^2 p_1^z \mu_0^{2\epsilon} \int_{-\infty}^\infty dy \frac{1 - e^{-iy p_1^z \tilde{\eta}}}{y} \int_0^1 dv \int \frac{d^d \ell}{(2\pi)^d} e^{i\ell_\perp \cdot \mathbf{b}_\perp} \frac{2 - y - v}{\ell^4} \delta[\ell^z - (y - v)p_1^z] \Big\} . \end{aligned} \quad (5.28)$$

While we were able to obtain a closed-form expression for the remaining integral, we find that it substantially simplifies after combining it with other diagrams, so we only present results for the sum. This is discussed at the end of app. B.

Let us now write down the contribution of diagram H to the matching kernel. First, note that as both the lightcone- and quasi diagrams are diagonal in spin, this diagram does not contribute to mixing between spin structures. Second, note that the difference of the two diagrams can be written as eq. (5.17). Including the contributions of the three sister topologies of this diagram, we find that

$$[\Delta_{q_1 q_2}^H]_{q'_1 q'_2}(x_1, x_2, b_\perp, \epsilon, \{\tilde{\eta}, \tilde{P}^z\}, \{\delta^+, p^+\}) \quad (5.29)$$

$$\begin{aligned}
&= -4\delta_{q_1 q'_1} \delta_{q_2 q'_2} \delta\left(1 - \frac{x_1}{\omega_1}\right) \delta\left(1 - \frac{x_2}{\omega_2}\right) \left[\frac{1}{\epsilon_{\text{ir}}} + \ln\left(\frac{\mu^2 \mathbf{b}_\perp^2}{b_0^2}\right) \right] \left[1 + \ln\left(\frac{\delta^+}{p_1^+}\right) \right] \\
&\quad - 2\delta_{q_1 q'_1} \delta_{q_2 q'_2} \delta\left(1 - \frac{x_1}{\omega_1}\right) \delta\left(1 - \frac{x_2}{\omega_2}\right) \\
&\quad \times 16i\pi^2 \tilde{p}_1^z \mu_0^{2\epsilon} \int_{-\infty}^{\infty} dy \frac{1 - \cos(y\tilde{p}_1^z \tilde{\eta})}{y} \int_0^1 dv \int \frac{d^d \ell}{(2\pi)^d} e^{i\ell_\perp \cdot \mathbf{b}_\perp} \frac{2-y-v}{\ell^4} \delta[\ell^z - (y-v)\tilde{p}_1^z] \\
&\quad + (1 \leftrightarrow 2).
\end{aligned}$$

Inserting this into eq. (5.18), gives its contribution to the one-loop matching coefficient.

5.4 Result for one-loop matching kernel

Here we present the one-loop matching kernels for the flavor non-singlet case of eq. (5.1) for all color- and spin structures, which can be calculated from the master formula in eq. (5.18).

Here we list all the one-loop ingredients that are needed to construct the matching kernels. The results for the one-loop diagrams for the lightcone- and quasi-DPDs can be found in app. B. The one-loop soft functions for the lightcone-DPD can be obtained from the TMD case [108] by an appropriate modification of the color factor

$${}^{88}S^{(1)}(b_\perp, \epsilon, \delta^+, \delta^-) = -4C_A \left\{ \frac{1}{\epsilon_{\text{uv}}^2} + \left[\frac{1}{\epsilon_{\text{uv}}} + \ln\left(\frac{\mu^2 \mathbf{b}_\perp^2}{b_0^2}\right) \right] \ln\left(\frac{\mu^2}{2\delta^+ \delta^-}\right) - \frac{1}{2} \ln^2\left(\frac{\mu^2 \mathbf{b}_\perp^2}{b_0^2}\right) - \frac{\pi^2}{12} \right\}, \quad (5.30)$$

We have calculated the corresponding quasi-soft function, obtaining

$${}^{88}\tilde{S}^{(1)}(b_\perp, \epsilon, \tilde{\eta}, y_A, y_B) = 4C_A \left\{ \left[\frac{1}{\epsilon_{\text{uv}}} + \ln\left(\frac{\mu^2 \mathbf{b}_\perp^2}{b_0^2}\right) \right] \left[2 - (y_A - y_B) \right] + \frac{2\pi\tilde{\eta}}{|\mathbf{b}_\perp|} \right\}. \quad (5.31)$$

Note that the above expression for the quasi-soft function does not contain the contribution from the transverse Wilson line. Though non-zero, its contribution cancels between the quasi-soft function and the unsubtracted quasi-DPD. The one-loop rapidity evolution kernel is given by

$${}^8J^{(1)}(b_\perp, \mu) = -4C_A \ln\left(\frac{\mu^2 \mathbf{b}_\perp^2}{b_0^2}\right). \quad (5.32)$$

For completeness we also present the renormalization kernels and factors that define the renormalized distributions. The renormalization kernels for the lightcone-DPD read [106]

$$\begin{aligned}
{}^{11}Z_{qq}^{(1)}(x, \mu, \zeta) &= -\frac{1}{\epsilon_{\text{uv}}} 2C_F \left[\frac{1+x^2}{1-x} \right]_+^{[0,1]}, \\
{}^{11}Z_{\Delta q \Delta q}^{(1)}(x, \mu, \zeta) &= -\frac{1}{\epsilon_{\text{uv}}} 2C_F \left[\frac{1+x^2}{1-x} \right]_+^{[0,1]}, \\
{}^{11}Z_{\delta q \delta q}^{(1)}(x, \mu, \zeta) &= -\frac{1}{\epsilon_{\text{uv}}} C_F \left(4 \left[\frac{x}{1-x} \right]_+^{[0,1]} + \delta(1-x) \right),
\end{aligned} \quad (5.33)$$

for the color-singlet case. Those for the color non-singlet case are related to their color-singlet counterpart by an modification of the color factor and an additional piece

$${}^{88}Z_{qq}^{(1)}(x, \mu, \zeta) = \left(1 - \frac{C_A}{2C_F}\right) {}^{11}Z_{qq}^{(1)}(x, \mu, \zeta) - C_A \delta(1-x) \left\{ \frac{1}{\epsilon_{uv}^2} + \frac{1}{\epsilon_{uv}} \left[\ln\left(\frac{\mu^2}{\zeta}\right) + \frac{3}{2} \right] \right\}. \quad (5.34)$$

For the color-singlet quasi-DPDs, we find that only the transversity distribution needs renormalization,

$$\begin{aligned} {}^{11}\tilde{Z}_{qq}^{(1)}(\epsilon, \mu, y_A, y_B) &= 0, \\ {}^{11}\tilde{Z}_{\Delta q \Delta q}^{(1)}(\epsilon, \mu, y_A, y_B) &= 0, \\ {}^{11}\tilde{Z}_{\delta q \delta q}^{(1)}(\epsilon, \mu, y_A, y_B) &= -\frac{1}{\epsilon_{uv}} 2C_F. \end{aligned} \quad (5.35)$$

In direct analogy to eq. (5.34), the renormalization factors for the color-correlated quasi-DPDs are related to their color-singlet counterpart by

$${}^{88}\tilde{Z}_{qq}^{(1)}(\epsilon, \mu, y_A, y_B) = \left(1 - \frac{C_A}{2C_F}\right) {}^{11}\tilde{Z}_{qq}^{(1)}(\epsilon, \mu, y_A, y_B) - \frac{1}{\epsilon_{uv}} C_A \left[1 + 2(y_A - y_B)\right]. \quad (5.36)$$

Note that all renormalization kernels are diagonal in color- and spin structures.

We find that at one-loop order there is no mixing between color structures. This can be understood from the fact that the matching coefficients are related to the difference between the order of the UV and large rapidity limits (as discussed at the end of sec. 2.4). However, only diagrams where a gluon connects the two quark lines can lead to mixing between color structures, but these do not have UV divergences since the quark lines are separated by b_\perp . It should be noted that individual diagrams of this type can contribute to the matching kernel due to the different treatment of rapidity divergences for the lightcone- and quasi-DPDs, but their contribution should cancel once all diagrams are combined. This argument is expected to hold at higher orders in perturbation theory as well.

For the color-singlet case, we verify that the matching kernel is related to that of the ordinary PDF case, see eq. (4.22). We have verified that this holds, and for completeness we present the matching kernels in the $\overline{\text{MS}}$ scheme,

$$\begin{aligned} {}^{11}C_{qq}^{(1)}(x, \tilde{p}^z, \mu) &= -2C_F \left\{ \left[\frac{1+x^2}{1-x} \left[\ln\left(\frac{\mu^2}{4(1-x)^2 \tilde{p}_z^2}\right) - 1 \right] + \frac{4x}{1-x} \right]_+^{[0,1]} \right. \\ &\quad \left. - \left[\text{sgn}(x) \left(1 + \frac{1+x^2}{1-x} \ln \left| \frac{x}{1-x} \right| \right) \right]_+^{(-\infty, +\infty)} \right\}, \end{aligned} \quad (5.37)$$

$$\begin{aligned} {}^{11}C_{\Delta q \Delta q}^{(1)}(x, \tilde{p}^z, \mu) &= -2C_F \left\{ \left[\frac{1+x^2}{1-x} \left[\ln\left(\frac{\mu^2}{4(1-x)^2 \tilde{p}_z^2}\right) + 3 \right] - \frac{4x}{1-x} \right]_+^{[0,1]} \right. \\ &\quad \left. - \left[\text{sgn}(x) \left(1 + \frac{1+x^2}{1-x} \ln \left| \frac{x}{1-x} \right| \right) \right]_+^{(-\infty, +\infty)} \right\}. \end{aligned} \quad (5.38)$$

$${}^{11}C_{\delta q \delta q}^{(1)}(x, \tilde{p}^z, \mu) = -2C_F \left\{ \left[\frac{2x}{1-x} \left[\ln\left(\frac{\mu^2}{4(1-x)^2 \tilde{p}_z^2}\right) + 1 \right] \right]_+^{[0,1]} \right\} \quad (5.39)$$

$$- \left[\text{sgn}(x) \frac{x}{1-x} \ln \left| \frac{x}{1-x} \right| \right]_+^{(-\infty, +\infty)} \Big\}.$$

The matching kernels for the color-correlated case are identical to those for the color-summed case, up to a color factor and an additional $x\tilde{P}^z$ -dependent piece,

$$\begin{aligned} {}^{88}C_{qq}^{(1)}\left(\frac{x}{x'}, x' \tilde{P}^z, \mu\right) &= \left(1 - \frac{C_A}{2C_F}\right) {}^{11}C_{qq}^{(1)}\left(\frac{x}{x'}, x' \tilde{P}^z, \mu\right) \\ &\quad - \delta\left(1 - \frac{x}{x'}\right) \frac{1}{2} C_A \left[\ln^2\left(\frac{\mu^2}{(2x' \tilde{P}^z)^2}\right) + 2 \ln\left(\frac{\mu^2}{(2x' \tilde{P}^z)^2}\right) + 4 - \frac{\pi^2}{6} \right], \end{aligned} \quad (5.40)$$

where we switched back to expressing partonic momenta as fractions of hadronic momenta. Note that all matching kernels which are off-diagonal in color or spin vanish (though this is not true at the level of individual diagrams). Note also that the form of (5.40) arises because the contribution of all graphs in fig. 2 to the matching kernel is proportional to delta functions in both momentum fractions, although the contribution of some individual graphs to the DPD or quasi-DPD is not.

6 Conclusions

Double parton scattering can significantly affect precision measurements due to the radiation from a secondary partonic collision. For certain processes, such as same-sign WW production, its contribution can be on par with that of single parton scattering. Currently, the double parton distributions (DPDs) that enter in the factorization theorems for these cross sections are poorly constrained experimentally: Essentially only a single number, the effective cross section, has been measured for a range of different processes. At the same time, these DPDs provide a window on a range of interesting correlations of partons inside the proton.

Inspired by the substantial progress in the quasi-PDF approach to extract (single) PDFs from lattice QCD, we have taken the first steps in this paper to extend this approach to DPDs. We have put forward a general matching relation, whose form is constrained using the renormalization group equations. This shares similarities with both the quasi-PDF approach to parton distribution functions (convolutions in momentum fractions and flavor mixing) and transverse momentum distributions (rapidity divergences, requiring a soft function). We have obtained explicit results for the flavor non-singlet quark-quark DPD at one-loop order, showing that the matching coefficients do not involve the infrared scale b_\perp . For the color-summed case, the kernel can directly be expressed in terms of that for the single PDF case.

There are several open questions left that we wish to explore in future work: On the conceptual side, the method to obtain the double-parton scattering soft function from the lattice requires further investigation. On the calculational side, there is the obvious extension to other flavors, for which the mixing with single PDFs may need to be taken into account (in transverse momentum space), as well as the extension to interference DPDs. The following issues related to lattice calculations will also need to be addressed: The nonperturbative renormalization, conversion to the RI/MOM scheme and the mixing

of operators. We expect that in the coming years this effort will lead to a substantial improvement of our understanding of DPDs, that can be confronted with measurements of double parton scattering and unveil more of the fascinating structure of the proton.

Note added: While this manuscript was in preparation, ref. [109] appeared. It discusses the color-singlet quark-quark DPD, showing that the matching can be expressed in terms of that for single PDFs, due to the spatial separation between the currents. We reach the same conclusion, as discussed at the end of sec. 4.3. However, we take a broader perspective, presenting a matching relation for general flavor, spin and color correlations. The latter particularly complicates things due to the presence of rapidity divergences and the need to subtract a soft factor. In our calculations we restrict to the non-singlet quark-quark DPD, but account for general spin and color correlations.

Acknowledgments

We thank Martha Constantinou, Markus Diehl, Florian Fabry, Iain Stewart and Alexey Vladimirov for discussions. This work is supported by the Royal Society through grant URF\R1\201500, the NWO projectruimte 680-91-122, and the D-ITP consortium, a program of NWO that is funded by the Dutch Ministry of Education, Culture and Science (OCW).

A Plus distributions

In this paper we will encounter singularities requiring a plus prescription at $x = 1$. Since quasi-parton distributions have a range outside the domain $[0, 1]$, we have modified the plus prescription such that $[f(x)]_+^I$ only has support on the finite or infinite length interval I (i.e. the theta functions ensuring this are included in the definition of the plus distribution) and satisfies

$$\int_I dx [f(x)]_+^I = 0. \quad (\text{A.1})$$

In practice we decompose a function regulated by e.g. ϵ in terms of plus distributions by writing

$$f(x, \epsilon) = [f(x, \epsilon)]_+^I + \delta(1 - x) \int_I dy f(y, \epsilon), \quad (\text{A.2})$$

and then expanding (with respect to the regulator) the expression *in* the plus distribution and the *result* of the integral. The following identity still holds for these plus distributions

$$\int_I dx g(x) [f(x)]_+^I = \int_I dx [g(x) - g(1)] f(x). \quad (\text{A.3})$$

B One-loop diagrams

In this appendix we present the calculation of the one-loop lightcone- and quasi-DPDs, defined in secs. 3.2 and 4.1. The one-loop diagrams for the quasi-DPD are shown in figs. 1

diagram	$R_1 = 1, R'_1 = 1$	$R_1 = 1, R'_1 = 8$	$R_1 = 8, R'_1 = 1$	$R_1 = 8, R'_1 = 8$
A, B, C	C_F	0	0	$C_F - \frac{C_A}{2}$
D, E, F	C_F	0	0	C_F
G, H, I	0	1	$\frac{C_F}{2N}$	$2C_F - \frac{C_A}{2}$
J, K, L	0	1	$\frac{C_F}{2N}$	$2C_F - C_A$

Table 1. Color factors $R_1 R_2, R'_1 R'_2 c^i$ for the i -th diagram, as defined in eq. (5.16). Note that only $R_1 = R_2$ and $R'_1 = R'_2$ are allowed, which is why we just list R_1 and R'_1 .

and 2. The diagrams for the lightcone-DPD are identical up to a cut that goes vertically through the middle of the diagram. In each figure, the diagrams in the top row correspond to real-emission diagrams while those on the bottom are virtual corrections. These diagrams are decomposed according to eq. (5.16), and the color factors belonging to these diagram are shown in table 1.

The following integrals are convenient for calculating the one-loop corrections to the lightcone-DPD

$$\int d^d k \frac{\delta(k^+ - \xi)}{k^2(k-p)^2} e^{i\mathbf{k}_\perp \cdot \mathbf{b}_\perp} = \frac{i\pi^2}{p^+} \theta(\xi)\theta(p^+ - \xi) \frac{\pi^{\frac{1}{2}-\epsilon} \Gamma(-\epsilon_{\text{ir}})}{\Gamma(\frac{1}{2}-\epsilon)} (\mathbf{b}_\perp^2)^\epsilon, \quad (\text{B.1})$$

$$\int d^d k \frac{\delta(k^+ - \xi)}{k^2(k-p)^2} = \frac{i\pi^2}{p^+} \theta(\xi)\theta(p^+ - \xi) \left(\frac{1}{\epsilon_{\text{uv}}} - \frac{1}{\epsilon_{\text{ir}}} \right), \quad (\text{B.2})$$

$$\int d^d k \delta_+(k^2) \frac{\delta(k^+ - \xi)}{k^-} e^{i\mathbf{k}_\perp \cdot \mathbf{b}_\perp} = \pi\theta(\xi) \frac{2\pi^{\frac{1}{2}-\epsilon} \Gamma(-2\epsilon_{\text{ir}})}{\Gamma(\frac{1}{2}-\epsilon)} (\mathbf{b}_\perp^2)^\epsilon, \quad (\text{B.3})$$

$$\int d^d k \delta_+(k^2) \frac{\delta(k^+ - \xi)}{k^-} = \pi\theta(\xi) \left(\frac{1}{\epsilon_{\text{uv}}} - \frac{1}{\epsilon_{\text{ir}}} \right). \quad (\text{B.4})$$

For the calculation of the one-loop quasi-DPD the integrals below can be used,

$$\int \frac{d^d k}{(2\pi)^d} \frac{\delta(k^z - \xi)}{k^4} e^{i\mathbf{k}_\perp \cdot \mathbf{b}_\perp} = \frac{i}{16\pi^3} \left(\frac{2\pi|\mathbf{b}_\perp|}{|\xi|} \right)^{\frac{1}{2}+\epsilon} K_{\frac{1}{2}+\epsilon}(|\xi||\mathbf{b}_\perp|), \quad (\text{B.5})$$

$$\int \frac{d^d k}{(2\pi)^d} \frac{\delta(k^z - \xi)}{k^4} = \frac{i}{16\pi^2} \frac{(4\pi)^\epsilon \Gamma(\frac{1}{2} + \epsilon)}{\sqrt{\pi}} |\xi|^{-1-2\epsilon}, \quad (\text{B.6})$$

$$\int \frac{d^d k}{(2\pi)^d} \frac{\delta(k^z - \xi)}{k^2} e^{i\mathbf{k}_\perp \cdot \mathbf{b}_\perp} = -\frac{i}{4\pi^2} \left(\frac{2\pi|\mathbf{b}_\perp|}{|\xi|} \right)^{-\frac{1}{2}+\epsilon} K_{-\frac{1}{2}+\epsilon}(|\xi||\mathbf{b}_\perp|), \quad (\text{B.7})$$

$$\int \frac{d^d k}{(2\pi)^d} \frac{\delta(k^z - \xi)}{k^2} = -\frac{i}{8\pi^2} \frac{(4\pi)^\epsilon \Gamma(-\frac{1}{2} + \epsilon)}{\sqrt{4\pi}} |\xi|^{1-2\epsilon}, \quad (\text{B.8})$$

where K denotes the modified Bessel function of the second kind.

We will now discuss each diagram in turn. To keep the notation compact, we will use

the shorthand introduced in eq. (5.19)

$$F^I = \frac{\alpha_s}{4\pi} \sum_{q'_1, q'_2} [F^I_{q_1 q_2}]_{q'_1 q'_2} \frac{\Gamma_{q'_1} \otimes \Gamma_{q'_2}}{p_1^+ p_2^+}. \quad (\text{B.9})$$

In the following we will assume that the arguments of the plus distributions are always the ratios x_i/ω_i .

diagram A

This diagram corresponds to the emission of a real gluon. For the lightcone diagram the gluon propagator is cut and the diagram yields

$$\begin{aligned} F^A &= -\pi p^+ \mu_0^{2\epsilon} \int d\omega_3 \Psi(\omega_3) \int \frac{d^d k}{(2\pi)^d} (ig\gamma^\mu) \frac{i}{\not{p}_1 - \not{k}} \Gamma_{q_1} \frac{i}{\not{p}_3 - \not{k}} (ig\gamma^\nu) \otimes \Gamma_{q_2} \quad (\text{B.10}) \\ &\quad \times (-g_{\mu\nu}) 2\pi\delta_+(k^2) \delta[x_1 p^+ - (p_1^+ - k^+)] \delta[x_2 p^+ - p_2^+] \delta[x_1 p^+ - (p_3^+ - k^+)] \\ &= -\alpha_s \Psi(\omega_1) \delta\left(1 - \frac{x_2}{\omega_2}\right) \frac{\Gamma_{q_1} \otimes \Gamma_{q_2}}{p_1^+ p_2^+} \frac{\rho_{q_1}}{2} \left(\frac{1}{\epsilon_{\text{uv}}} - \frac{1}{\epsilon_{\text{ir}}}\right) \left[1 - \frac{x_1}{\omega_1}\right]_+^{[0,1]} \\ &\quad - \alpha_s \Psi(\omega_1) \delta\left(1 - \frac{x_1}{\omega_1}\right) \delta\left(1 - \frac{x_2}{\omega_2}\right) \frac{\Gamma_{q_1} \otimes \Gamma_{q_2}}{p_1^+ p_2^+} \frac{\rho_{q_1}}{4} \left(\frac{1}{\epsilon_{\text{uv}}} - \frac{1}{\epsilon_{\text{ir}}}\right). \end{aligned}$$

The factors ρ_{q_1} are spin-dependent and given by

$$\rho_q = 1, \quad \rho_{\Delta q} = 1, \quad \rho_{\delta q} = 0. \quad (\text{B.11})$$

In principle these factors include terms of $\mathcal{O}(\epsilon)$ and beyond, but these are irrelevant as they drop out when multiplying with the above combination of ϵ poles.

The range on the plus distribution arises here from two considerations: The upper bound has its origin in one of the intermediate delta distributions, which only has support if $\omega_1 > x_1$. The lower bound is added manually, to separate the quark-DPD from the antiquark-DPD.

For the quasi-diagram the gluon propagator is not cut, as the matrix element defining quasi-DPDs can be treated as time-ordered. The quasi-diagram results in

$$\begin{aligned} \tilde{F}^A &= -\pi \tilde{p}^z \mu_0^{2\epsilon} \int d\omega_3 \Psi(\omega_3) \int \frac{d^d k}{(2\pi)^d} (ig\gamma^\mu) \frac{i}{\not{\tilde{p}}_1 - \not{k}} \tilde{\Gamma}_{q_1} \frac{i}{\not{\tilde{p}}_3 - \not{k}} (ig\gamma^\nu) \otimes \tilde{\Gamma}_{q_2} \quad (\text{B.12}) \\ &\quad \times \frac{-ig_{\mu\nu}}{k^2} \delta[x_1 \tilde{p}^z - (\tilde{p}_1^z - k^z)] \delta[x_2 \tilde{p}^z - \tilde{p}_2^z] \delta[x_1 \tilde{p}^z - (\tilde{p}_3^z - k^z)] \\ &= \alpha_s \Psi(\omega_1) \delta\left(1 - \frac{x_2}{\omega_2}\right) \frac{\tilde{\Gamma}_{q_1} \otimes \tilde{\Gamma}_{q_2}}{\tilde{p}_1^z \tilde{p}_2^z} \\ &\quad \times \frac{\tilde{\rho}_{q_1}}{2} \left[\left(1 - \frac{x_1}{\omega_1}\right) \left(\frac{1}{\epsilon_{\text{ir}}} + 2 + \ln\left(\frac{\mu^2}{4(1 - \frac{x_1}{\omega_1})^2 (\tilde{p}_1^z)^2}\right)\right) \theta\left(\frac{x_1}{\omega_1}\right) \theta\left(1 - \frac{x_1}{\omega_1}\right) \right. \\ &\quad \left. - \text{sgn}\left(\frac{x_1}{\omega_1}\right) \left(1 + \left(1 - \frac{x_1}{\omega_1}\right) \ln\left|\frac{\frac{x_1}{\omega_1}}{1 - \frac{x_1}{\omega_1}}\right|\right) \right]_+^{(-\infty, \infty)} \end{aligned}$$

$$- \alpha_s \Psi(\omega_1) \delta\left(1 - \frac{x_1}{\omega_1}\right) \delta\left(1 - \frac{x_2}{\omega_2}\right) \frac{\Gamma_{q_1} \otimes \Gamma_{q_2}}{p_1^+ p_2^+} \frac{\tilde{\rho}_{q_1}}{4} \left(\frac{1}{\epsilon_{\text{uv}}} - \frac{1}{\epsilon_{\text{ir}}} \right),$$

where we used (4.5) to relate the Dirac structures in the last term to the lightcone ones to highlight the similarity to (B.10). $\tilde{\rho}_{q_1}$ are again spin-dependent factors, given by

$$\tilde{\rho}_q = 1 - 3\epsilon, \quad \tilde{\rho}_{\Delta q} = 1 + \epsilon, \quad \tilde{\rho}_{\delta q} = 0. \quad (\text{B.13})$$

This time the $\mathcal{O}(\epsilon)$ contributions are relevant as they multiply an isolated $1/\epsilon$. The intricate pattern of plus distribution ranges arises from the varying sign possibilities imposed by the absolute values in eq. (B.6).

For both the lightcone and the quasi diagram the infinite normalization factor $\Psi(\omega_1)$ factors out (its argument is ω_1 due to the interplay of the two delta distributions in the first line of eq. (B.12), which enforces $\omega_3 = \omega_1$). Including the corresponding graph where the gluon connects to the other quark line, we obtain, in the notation of eq. (5.17),

$$\begin{aligned} [\Delta_{q_1 q_2}^A]_{q'_1 q'_2} = & -2\delta_{q_1 q'_1} \delta_{q_2 q'_2} \delta\left(1 - \frac{x_2}{\omega_2}\right) \left\{ \frac{\rho_{q_1}}{\epsilon_{\text{uv}}} \left[1 - \frac{x_1}{\omega_1}\right]_+^{[0,1]} + \frac{\tilde{\rho}_{q_1} - \rho_{q_1}}{\epsilon_{\text{ir}}} \left[1 - \frac{x_1}{\omega_1}\right]_+^{[0,1]} \right. \\ & + \tilde{\rho}_{q_1} \left[\left(1 - \frac{x_1}{\omega_1}\right) \left[2 + \ln\left(\frac{\mu^2}{4(1 - \frac{x_1}{\omega_1})^2 (\tilde{p}_1^z)^2}\right) \right] \right]_+^{[0,1]} \\ & \left. - \tilde{\rho}_{q_1} \left[\text{sgn}\left(\frac{x_1}{\omega_1}\right) \left(1 + (1 - x_1) \ln\left|\frac{\frac{x_1}{\omega_1}}{1 - \frac{x_1}{\omega_1}}\right|\right) \right]_+^{(-\infty, +\infty)} \right\} + (1 \leftrightarrow 2). \end{aligned} \quad (\text{B.14})$$

Diagram B

For diagram *B* we need to implement the rapidity regulator. For the lightcone diagram we find

$$\begin{aligned} F^B = & -\pi p^+ \mu_0^{2\epsilon} \int d\omega_3 \Psi(\omega_3) \int \frac{d^d k}{(2\pi)^d} \Gamma_{q_1} \otimes (i\gamma^\mu) \frac{i}{\not{p}_2 - \not{k}} \Gamma_{q_2} (i g n_a^\nu) \frac{i}{k^+ + i\delta^+} \\ & \times (-g_{\mu\nu}) 2\pi \delta_+(k^2) \delta[x_1 p^+ - p_1^+] \delta[x_2 p^+ - (p_2^+ - k^+)] \delta[x_1 p^+ - p_3^+] \\ = & -\alpha_s \Psi(\omega_1) \delta\left(1 - \frac{x_1}{\omega_1}\right) \frac{\Gamma_{q_1} \otimes \Gamma_{q_2}}{p_1^+ p_2^+} \frac{1}{2} \left(\frac{1}{\epsilon_{\text{uv}}} - \frac{1}{\epsilon_{\text{ir}}} \right) \left[\frac{\frac{x_2}{\omega_2}}{1 - \frac{x_2}{\omega_2}} \right]_+^{[0,1]} \\ & + \alpha_s \Psi(\omega_1) \delta\left(1 - \frac{x_1}{\omega_1}\right) \delta\left(1 - \frac{x_2}{\omega_2}\right) \frac{\Gamma_{q_1} \otimes \Gamma_{q_2}}{p_1^+ p_2^+} \frac{1}{2} \left(\frac{1}{\epsilon_{\text{uv}}} - \frac{1}{\epsilon_{\text{ir}}} \right) \left[1 + \ln\left(\frac{\delta^+}{p_2^+}\right) + \frac{i\pi}{2} \right]. \end{aligned} \quad (\text{B.15})$$

For the color-summed DPD, the rapidity divergence ($\ln \delta^+$) of this diagram will cancel against that of diagram *E*. For the quasi-diagram we obtain,

$$\begin{aligned} \tilde{F}^B = & -\pi \tilde{p}^z \mu_0^{2\epsilon} \int d\omega_3 \Psi(\omega_3) \int \frac{d^d k}{(2\pi)^d} \tilde{\Gamma}_{q_1} \otimes (i\gamma^\mu) \frac{i}{\not{\tilde{p}}_2 - \not{k}^z} \tilde{\Gamma}_{q_2} (i g \hat{z}^\nu) \frac{i}{k^z} \\ & \times \frac{-i g_{\mu\nu}}{k^2} \delta[x_1 \tilde{p}^z - \tilde{p}_1^z] (e^{-ik^z \tilde{\eta}} - 1) \delta[x_2 \tilde{p}^z - (\tilde{p}_2^z - k^z)] \delta[x_1 \tilde{p}^z - \tilde{p}_3^z] \\ = & \alpha_s \Psi(\omega_1) \delta\left(1 - \frac{x_1}{\omega_1}\right) \frac{\tilde{\Gamma}_{q_1} \otimes \tilde{\Gamma}_{q_2}}{\tilde{p}_1^z \tilde{p}_2^z} \end{aligned} \quad (\text{B.16})$$

$$\begin{aligned}
& \times \frac{1}{2} \left[\frac{\frac{x_2}{\omega_2}}{1 - \frac{x_2}{\omega_2}} \left(\frac{1}{\epsilon_{\text{ir}}} + \ln \left(\frac{\mu^2}{4(1 - \frac{x_2}{\omega_2})^2 (\tilde{p}_2^z)^2} \right) \right) - 1 \right]_+^{(0,1)} \\
& + \left[\text{sgn} \left(\frac{x_2}{\omega_2} \right) \frac{1}{1 - \frac{x_2}{\omega_2}} \left(\frac{1}{2} - \frac{x_2}{\omega_2} \ln \left| \frac{\frac{x_2}{\omega_2}}{1 - \frac{x_2}{\omega_2}} \right| \right) \right]_+^{(-\infty, \infty)} \\
& + \alpha_s \Psi(\omega_1) \delta \left(1 - \frac{x_1}{\omega_1} \right) \delta \left(1 - \frac{x_2}{\omega_2} \right) \frac{\tilde{\Gamma}_{q_1} \otimes \tilde{\Gamma}_{q_2}}{\tilde{p}_1^z \tilde{p}_2^z} \\
& \times 4i\pi^2 \tilde{p}_2^z \mu_0^{2\epsilon} \int_{-\infty}^{\infty} dy \frac{1 - e^{-iy\tilde{p}_2^z \tilde{\eta}}}{y} \int_0^1 dv \int \frac{d^d \ell}{(2\pi)^d} \frac{2-y-v}{\ell^4} \delta[\ell^z - (y-v)\tilde{p}_2^z].
\end{aligned}$$

While we were able to obtain a closed-form expression for the integral in the last term, it substantially simplifies if we first combine diagrams before performing the integral, which is all we need to calculate the matching. This is discussed at the end of this appendix. The contribution of diagram B and its three sister topologies to the matching kernel is given by

$$\begin{aligned}
[\Delta_{q_1 q_2}^B]_{q'_1 q'_2} = & -4\delta_{q_1 q'_1} \delta_{q_2 q'_2} \delta \left(1 - \frac{x_2}{\omega_2} \right) \left\{ \left[\frac{\frac{x_1}{\omega_1}}{1 - \frac{x_1}{\omega_1}} \left(\frac{1}{\epsilon_{\text{uv}}} + \ln \left(\frac{\mu^2}{4(1 - \frac{x_1}{\omega_1})^2 (\tilde{p}_1^z)^2} \right) \right) - 1 \right]_+^{[0,1]} \right. \\
& + \left[\text{sgn} \left(\frac{x_1}{\omega_1} \right) \frac{1}{1 - \frac{x_1}{\omega_1}} \left(\frac{1}{2} - \frac{x_1}{\omega_1} \ln \left| \frac{\frac{x_1}{\omega_1}}{1 - \frac{x_1}{\omega_1}} \right| \right) \right]_+^{(-\infty, +\infty)} \\
& - \delta \left(1 - \frac{x_1}{\omega_1} \right) \left(\frac{1}{\epsilon_{\text{uv}}} - \frac{1}{\epsilon_{\text{ir}}} \right) \left[1 + \ln \left(\frac{\delta^+}{p_1^+} \right) \right] \\
& + \delta \left(1 - \frac{x_1}{\omega_1} \right) 8i\pi^2 \tilde{p}_1^z \mu_0^{2\epsilon} \\
& \times \int_{-\infty}^{\infty} dy \frac{1 - \cos(y\tilde{p}_1^z \tilde{\eta})}{y} \int_0^1 dv \int \frac{d^d \ell}{(2\pi)^d} \frac{2-y-v}{\ell^4} \delta[\ell^z - (y-v)\tilde{p}_1^z] \Big\} \\
& + (1 \leftrightarrow 2), \tag{B.17}
\end{aligned}$$

where the appearance of the cosine is due to the combination of the two diagrams attaching to the same quark line.

Diagram C

Diagram C vanishes for the lightcone-DPD as both ends of the gluon line are connected to Wilson lines along the n_a direction, leading to $n_a^2 = 0$. For the quasi-DPD it is given by,

$$\begin{aligned}
\tilde{F}^C = & -\pi \tilde{p}^z \mu_0^{2\epsilon} \int d\omega_3 \Psi(\omega_3) \int \frac{d^d k}{(2\pi)^d} \tilde{\Gamma}_{q_1} \otimes \tilde{\Gamma}_{q_2} \frac{i}{k^z} (ig\hat{z}^\mu) \frac{-ig_{\mu\nu}}{k^2} (ig\hat{z}^\nu) \frac{i}{k^z} \delta[x_1 \tilde{p}^z - \tilde{p}_1^z] \\
& \times (1 - e^{-ik^z \tilde{\eta}}) \left\{ \delta[x_2 \tilde{p}^z - (\tilde{p}_2^z - k^z)] - e^{ik^z \tilde{\eta}} \delta[x_2 \tilde{p}^z - \tilde{p}_2^z] \right\} \delta[x_1 \tilde{p}^z - \tilde{p}_3^z] \\
= & \alpha_s \Psi(\omega_1) \delta \left(1 - \frac{x_1}{\omega_1} \right) \frac{\tilde{\Gamma}_{q_1} \otimes \tilde{\Gamma}_{q_2}}{\tilde{p}_1^z \tilde{p}_2^z} \frac{1}{2} \left[\left| \frac{1}{1 - \frac{x_2}{\omega_2}} \right| \right]_+^{(-\infty, \infty)} \\
& + \alpha_s \Psi(\omega_1) \delta \left(1 - \frac{x_1}{\omega_1} \right) \delta \left(1 - \frac{x_2}{\omega_2} \right) \frac{\tilde{\Gamma}_{q_1} \otimes \tilde{\Gamma}_{q_2}}{\tilde{p}_1^z \tilde{p}_2^z} \left[\frac{1}{\epsilon_{\text{uv}}} + 2 + \ln \left(\frac{\mu^2 \tilde{\eta}^2}{b_0^2} \right) \right], \tag{B.18}
\end{aligned}$$

where b_0 and the relation between μ_0 and μ is given in eq. (5.24). Dividing out $\Psi(\omega_1)$, the contribution of diagram C to the matching kernel is

$$\begin{aligned} [\Delta_{q_1 q_2}^C]_{q'_1 q'_2} &= -2\delta_{q_1 q'_1} \delta_{q_2 q'_2} \delta\left(1 - \frac{x_2}{\omega_2}\right) \left\{ \left[\frac{1}{1 - \frac{x_2}{\omega_2}} \right]_+^{(-\infty, \infty)} + 2\delta\left(1 - \frac{x_1}{\omega_1}\right) \left[\frac{1}{\epsilon_{uv}} + 2 + \ln\left(\frac{\mu^2 \tilde{\eta}^2}{b_0^2}\right) \right] \right\} \\ &\quad + (1 \leftrightarrow 2), \end{aligned} \quad (\text{B.19})$$

which also includes the related topology attaching to the other quark line.

Diagram D

This is the quark self-energy diagram and is the same for the lightcone- and quasi-DPD, therefore

$$[\Delta_{q_1 q_2}^D]_{q'_1 q'_2} = 0. \quad (\text{B.20})$$

Diagram E

The lightcone diagram is given by

$$\begin{aligned} F^E &= -\pi p^+ \mu_0^{2\epsilon} \int d\omega_3 \Psi(\omega_3) \int \frac{d^d k}{(2\pi)^d} (ig\gamma^\mu) \frac{i}{\not{p}_1 - \not{k}} \Gamma_{q_1} \frac{-i}{k^+ - i\delta^+} (ign_a^\nu) \otimes \Gamma_{q_2} \quad (\text{B.21}) \\ &\quad \times \frac{-ig_{\mu\nu}}{k^2} \delta[x_1 p^+ - p_1^+] \delta[x_2 p^+ - p_2^+] \delta[x_1 p^+ - p_3^+] \\ &= -\alpha_s \Psi(\omega_1) \delta\left(1 - \frac{x_1}{\omega_1}\right) \delta\left(1 - \frac{x_2}{\omega_2}\right) \frac{\Gamma_{q_1} \otimes \Gamma_{q_2}}{p_1^+ p_2^+} \frac{1}{2} \left(\frac{1}{\epsilon_{uv}} - \frac{1}{\epsilon_{ir}} \right) \left[1 + \ln\left(\frac{\delta^+}{p_1^+}\right) - \frac{i\pi}{2} \right]. \end{aligned}$$

The corresponding quasi-diagram yields,

$$\begin{aligned} \tilde{F}^E &= -\pi \tilde{p}^z \mu_0^{2\epsilon} \int d\omega_3 \Psi(\omega_3) \int \frac{d^d k}{(2\pi)^d} (ig\gamma^\mu) \frac{i}{\not{p}_1 - \not{k}} \tilde{\Gamma}_{q_1} \frac{i}{k^z} (ig\tilde{z}^\nu) \otimes \Gamma_{q_2} \quad (\text{B.22}) \\ &\quad \times \frac{-ig_{\mu\nu}}{k^2} \left\{ \delta[x_1 \tilde{p}^z - \tilde{p}_1^z] - e^{-ik^z \tilde{\eta}} \delta[x_1 \tilde{p}^z - (\tilde{p}_1^z - k^z)] \right\} \delta[x_2 \tilde{p}^z - \tilde{p}_2^z] \delta[x_1 \tilde{p}^z - \tilde{p}_3^z] \\ &= -\alpha_s \Psi(\omega_1) \delta\left(1 - \frac{x_1}{\omega_1}\right) \delta\left(1 - \frac{x_2}{\omega_2}\right) \frac{\tilde{\Gamma}_{q_1} \otimes \tilde{\Gamma}_{q_2}}{\tilde{p}_1^z \tilde{p}_2^z} \\ &\quad \times 4i\pi^2 \tilde{p}_1^z \mu_0^{2\epsilon} \int_{-\infty}^{\infty} dy \frac{1 - e^{-iy\tilde{p}_1^z \tilde{\eta}}}{y} \int_0^1 dv \int \frac{d^d \ell}{(2\pi)^d} \frac{2-y-v}{\ell^4} \delta[\ell^z - (y-v)\tilde{p}_1^z]. \end{aligned}$$

The remaining integral can be carried out but again simplifies when first combined with other diagrams, as discussed at the end of this appendix. The contribution of this diagram and its three sister topologies to the matching kernel is

$$\begin{aligned} [\Delta_{q_1 q_2}^E]_{q'_1 q'_2} &= -4\delta_{q_1 q'_1} \delta_{q_2 q'_2} \delta\left(1 - \frac{x_1}{\omega_1}\right) \delta\left(1 - \frac{x_2}{\omega_2}\right) \left\{ \left(\frac{1}{\epsilon_{uv}} - \frac{1}{\epsilon_{ir}} \right) \left[1 + \ln\left(\frac{\delta^+}{p_1^+}\right) \right] \right. \\ &\quad \left. - 8i\pi^2 \tilde{p}_1^z \mu_0^{2\epsilon} \int_{-\infty}^{\infty} dy \frac{1 - \cos(y\tilde{p}_1^z \tilde{\eta})}{y} \int_0^1 dv \int \frac{d^d \ell}{(2\pi)^d} \frac{2-y-v}{\ell^4} \delta[\ell^z - (y-v)\tilde{p}_1^z] \right\} \\ &\quad + (1 \leftrightarrow 2). \end{aligned} \quad (\text{B.23})$$

Diagram F

Diagram F vanishes for the lightcone-DPD. For the quasi-DPD it is given by

$$\begin{aligned}\tilde{F}^F &= -\pi \tilde{p}^z \mu_0^{2\epsilon} \int d\omega_3 \Psi(\omega_3) \int \frac{d^d k}{(2\pi)^d} \tilde{\Gamma}_{q_1} \frac{i}{k^z} (ig\hat{z}^\mu) \frac{i}{k^z} (ig\hat{z}^\nu) \otimes \tilde{\Gamma}_{q_2} \frac{-ig_{\mu\nu}}{k^2} \\ &\quad \times \delta[x_2 \tilde{p}^z - \tilde{p}_2^z] \delta[x_1 \tilde{p}^z - \tilde{p}_3^z] \left\{ e^{-ik^z \tilde{\eta}} \delta[x_1 \tilde{p}^z - (\tilde{p}_1^z - k^z)] - \delta[x_1 \tilde{p}^z - \tilde{p}_1^z] \right\} \\ &= -\alpha_s \Psi(\omega_1) \delta\left(1 - \frac{x_1}{\omega_1}\right) \delta\left(1 - \frac{x_2}{\omega_2}\right) \frac{\tilde{\Gamma}_{q_1} \otimes \tilde{\Gamma}_{q_2}}{\tilde{p}_1^z \tilde{p}_2^z} \frac{1}{2} \left[\frac{1}{\epsilon_{uv}} + 2 + \ln\left(\frac{\mu^2 \tilde{\eta}^2}{b_0^2}\right) \right].\end{aligned}\quad (\text{B.24})$$

The $\Psi(\omega_1)$ factors out again, and the contribution of diagram F and its three mirror topologies to the matching kernel is given by

$$[\Delta_{q_1 q_2}^F]_{q'_1 q'_2} = 8\delta_{q_1 q'_1} \delta_{q_2 q'_2} \delta\left(1 - \frac{x_1}{\omega_1}\right) \delta\left(1 - \frac{x_2}{\omega_2}\right) \left[\frac{1}{\epsilon_{uv}} + 2 + \ln\left(\frac{\mu^2 \tilde{\eta}^2}{b_0^2}\right) \right]. \quad (\text{B.25})$$

Diagram G

For diagram G one does not need to use the modified partonic states of sec. 5.1, so we can set $\Psi(\omega_3) = \delta(\omega_1 - \omega_3)$ in the calculation of this diagram. The lightcone diagram results in

$$\begin{aligned}F^G &= -\pi p^+ \mu_0^{2\epsilon} \int \frac{d^d k}{(2\pi)^d} e^{i\mathbf{k}_\perp \cdot \mathbf{b}_\perp} (ig\gamma^\mu) \frac{i}{\not{p}_1 - \not{k}} \Gamma_{q_1} \otimes \Gamma_{q_2} \frac{i}{\not{p}_4 - \not{k}} (ig\gamma^\nu) \\ &\quad \times (-g_{\mu\nu}) 2\pi \delta_+(k^2) \delta[x_1 p^+ - (p_1^+ - k^+)] \delta[x_2 p^+ - p_2^+] \delta[x_1 p^+ - p_1^+] \\ &= \alpha_s \delta(\omega_1 - x_1) \delta(\omega_2 - x_2) \frac{1}{p_1^+ p_4^+} \left(g_\perp^{\mu\nu} - 2\epsilon \frac{b^\mu b^\nu}{\mathbf{b}_\perp^2} \right) \gamma_\rho \gamma_\mu \Gamma_{q_1} \otimes \Gamma_{q_2} \gamma_\nu \gamma^\rho \\ &\quad \times \frac{1}{8} \left[\frac{1}{\epsilon_{ir}} + \ln\left(\frac{\mu^2 \mathbf{b}_\perp^2}{b_0^2}\right) \right] (\omega_1 - x_1) \theta(x_1) \theta(\omega_1 - x_1) \\ &= 0.\end{aligned}\quad (\text{B.26})$$

We start by noting that the corresponding quasi-diagram is UV and IR finite. We calculate it by first expanding in $1/(|\mathbf{b}_\perp| p^z)$ (usually we do it the other way around, but that is much more complicated here), leading to

$$\begin{aligned}\tilde{F}^G &= -\pi \tilde{p}^z \mu_0^{2\epsilon} \int d\omega_3 \delta(\omega_3 - \omega_1) \int \frac{d^d k}{(2\pi)^d} e^{i\mathbf{k}_\perp \cdot \mathbf{b}_\perp} (ig\gamma^\mu) \frac{i}{\not{p}_1 - \not{k}} \tilde{\Gamma}_{q_1} \otimes \tilde{\Gamma}_{q_2} \frac{i}{\not{p}_4 - \not{k}} (ig\gamma^\nu) \\ &\quad \times \frac{-ig_{\mu\nu}}{k^2} \delta[x_1 \tilde{p}^z - (\tilde{p}_1^z - k^z)] \delta[x_2 \tilde{p}^z - \tilde{p}_2^z] \delta[x_1 \tilde{p}^z - \tilde{p}_3^z] \\ &= -\alpha_s \delta\left(1 - \frac{x_1}{\omega_1}\right) \delta\left(1 - \frac{x_2}{\omega_2}\right) \frac{1}{\tilde{p}_1^z \tilde{p}_2^z} \gamma_{\perp\rho} \gamma_{\perp\mu} \tilde{\Gamma}_{q_1} \otimes \tilde{\Gamma}_{q_2} \gamma_{\perp\nu} \gamma_{\perp}^\rho \\ &\quad \times 4i\pi^2 \tilde{p}^z \mu_0^{2\epsilon} \frac{\partial}{\partial b_\mu} \frac{\partial}{\partial b_\nu} \int \frac{d^d k}{(2\pi)^d} e^{i\mathbf{k}_\perp \cdot \mathbf{b}_\perp} \frac{1}{k^2 (k - \tilde{p}_1)^2 (k - \tilde{p}_4)^2} \delta(k^z).\end{aligned}\quad (\text{B.27})$$

The precise expression for this diagram is ultimately not relevant for the calculation of the matching kernel, as the difference between the lightcone and quasi diagrams gets divided

by the infinite normalization factor from the tree-level DPDs, so

$$[\Delta_{q_1 q_2}^G]_{q'_1 q'_2} = 0. \quad (\text{B.28})$$

Diagram H

Since this diagram involves a gluon being connected to a Wilson line, its calculation requires the implementation of a rapidity regulator. The lightcone diagram yields

$$\begin{aligned} F^H &= -\pi p^+ \mu_0^{2\epsilon} \int d\omega_3 \Psi(\omega_3) \int \frac{d^d k}{(2\pi)^d} e^{i\mathbf{k}_\perp \cdot \mathbf{b}_\perp} (ig\gamma^\mu) \frac{i}{\not{p}_1 - \not{k}} \Gamma_{q_1} \otimes \Gamma_{q_2} (ign_a^\nu) \frac{i}{k^+ + i\delta^+} \\ &\quad \times (-g_{\mu\nu}) 2\pi\delta_+(k^2) \delta[x_1 p^+ - (p_1^+ - k^+)] \delta[x_2 p^+ - p_2^+] \delta[x_1 p^+ - p_3^+] \\ &= \alpha_s \Psi(x_1) \delta\left(1 - \frac{x_2}{\omega_2}\right) \frac{\Gamma_{q_1} \otimes \Gamma_{q_2}}{p_1^+ p_2^+} \frac{1}{2} \left[\frac{1}{\epsilon_{\text{ir}}} + \ln\left(\frac{\mu^2 \mathbf{b}_\perp^2}{b_0^2}\right) \right] \left[\frac{\frac{x_1}{\omega_1}}{1 - \frac{x_1}{\omega_1}} \theta\left(\frac{x_1}{\omega_1}\right) \theta\left(1 - \frac{x_1}{\omega_1}\right) \right. \\ &\quad \left. - \alpha_s \Psi(\omega_1) \delta\left(1 - \frac{x_1}{\omega_1}\right) \delta\left(1 - \frac{x_1}{\omega_1}\right) \frac{\Gamma_{q_1} \otimes \Gamma_{q_2}}{p_1^+ p_2^+} \frac{1}{2} \left[\frac{1}{\epsilon_{\text{ir}}} + \ln\left(\frac{\mu^2 \mathbf{b}_\perp^2}{b_0^2}\right) \right] \left[1 + \ln\left(\frac{\delta^+}{p_1^+}\right) + \frac{i\pi}{2} \right] \right]. \end{aligned} \quad (\text{B.29})$$

The calculation of the quasi diagram is more complicated because the divergences that arise when the gluon momentum goes to zero is regulated by both ϵ and $\tilde{\eta}$,

$$\begin{aligned} \tilde{F}^H &= -\pi \tilde{p}^z \mu_0^{2\epsilon} \int d\omega_3 \Psi(\omega_3) \int \frac{d^d k}{(2\pi)^d} e^{i\mathbf{k}_\perp \cdot \mathbf{b}_\perp} (ig\gamma^\mu) \frac{i}{\not{\tilde{p}}_1 - \not{k}} \tilde{\Gamma}_{q_1} \otimes \tilde{\Gamma}_{q_2} (ig\hat{z}^\nu) \frac{i}{k^z} \\ &\quad \times \frac{-ig_{\mu\nu}}{k^2} \delta[x_1 \tilde{p}^z - (\tilde{p}_1^z - k^z)] \delta[x_2 \tilde{p}^z - \tilde{p}_2^z] \delta[x_1 \tilde{p}^z - \tilde{p}_3^z] (e^{-ik^z \tilde{\eta}} - 1) \\ &= \alpha_s \Psi(x_1) \delta\left(1 - \frac{x_2}{\omega_2}\right) \frac{\tilde{\Gamma}_{q_1} \otimes \tilde{\Gamma}_{q_2}}{\tilde{p}_1^z \tilde{p}_2^z} \frac{1}{2} \left[\frac{1}{\epsilon_{\text{ir}}} + \ln\left(\frac{\mu^2 \mathbf{b}_\perp^2}{b_0^2}\right) \right] \left[\frac{\frac{x_1}{\omega_1}}{1 - \frac{x_1}{\omega_1}} \theta\left(\frac{x_1}{\omega_1}\right) \theta\left(1 - \frac{x_1}{\omega_1}\right) \right]_+ \\ &\quad + \alpha_s \Psi(\omega_1) \delta\left(1 - \frac{x_1}{\omega_1}\right) \delta\left(1 - \frac{x_2}{\omega_2}\right) \frac{\tilde{\Gamma}_{q_1} \otimes \tilde{\Gamma}_{q_2}}{\tilde{p}_1^z \tilde{p}_2^z} \\ &\quad \times 4i\pi^2 \tilde{p}_1^z \mu_0^{2\epsilon} \int_{-\infty}^{\infty} dy \frac{1 - e^{-iy\tilde{p}_1^z \tilde{\eta}}}{y} \int_0^1 dv \int \frac{d^d \ell}{(2\pi)^d} e^{i\ell_\perp \cdot \mathbf{b}_\perp} \frac{2-y-v}{\ell^4} \delta[\ell^z - (y-v)\tilde{p}_1^z]. \end{aligned} \quad (\text{B.30})$$

The remaining integral can be carried out but again simplifies when first combined with other diagrams, as discussed at the end of this appendix.

A special comment concerning the wave function Ψ : In eq. (5.17) we must factor out $\Psi(\omega_1)$, and so far this has not been a problem: Either this arose naturally (e.g. in diagram A), or we encountered the combination $\Psi(x_1)\delta(1 - \frac{x_1}{\omega_1})$, which is essentially the same. Here for the first time $\Psi(x_1)$ appears with a non-trivial function of x_1 , naively precluding the extraction. However, the lightcone and quasi diagrams share the same non-trivial x -dependence. Therefore, after subtracting the two diagrams only a delta function term remains and we can factor out the normalization constant $\Psi(\omega_1)$ as before. The contribution of this diagram to the matching kernel is then given by

$$[\Delta_{q_1 q_2}^H]_{q'_1 q'_2} = -4\delta_{q_1 q'_1} \delta_{q_2 q'_2} \delta\left(1 - \frac{x_1}{\omega_1}\right) \delta\left(1 - \frac{x_2}{\omega_2}\right) \left\{ \left[\frac{1}{\epsilon_{\text{ir}}} + \ln\left(\frac{\mu^2 \mathbf{b}_\perp^2}{b_0^2}\right) \right] \left[1 + \ln\left(\frac{\delta^+}{p_1^+}\right) \right] \right\}$$

$$\begin{aligned}
& + 8i\pi^2 \tilde{p}_1^z \mu_0^{2\epsilon} \int_{-\infty}^{\infty} dy \frac{1 - \cos(y\tilde{p}_1^z \tilde{\eta})}{y} \int_0^1 dv \int \frac{d^d \ell}{(2\pi)^d} \\
& \times e^{i\ell_{\perp} \cdot \mathbf{b}_{\perp}} \frac{2 - y - v}{\ell^4} \delta[\ell^z - (y - v)\tilde{p}_1^z] \Big\} + (1 \leftrightarrow 2). \tag{B.31}
\end{aligned}$$

Diagram I

This diagram vanishes for the lightcone-DPD as it involves a gluon line whose both ends are connected to Wilson lines in the n_a direction. For the quasi-DPD this diagram gives

$$\begin{aligned}
\tilde{F}^I &= -\pi \tilde{p}^z \mu_0^{2\epsilon} \int d\omega_3 \Psi(\omega_3) \int \frac{d^d k}{(2\pi)^d} e^{i\mathbf{k}_{\perp} \cdot \mathbf{b}_{\perp}} \frac{i}{k^z} (ig\hat{z}^{\mu}) \tilde{\Gamma}_{q_1} \otimes \tilde{\Gamma}_{q_2} (ig\hat{z}^{\nu}) \frac{i}{k^z} \frac{-ig_{\mu\nu}}{k^2} \tag{B.32} \\
& \times (1 - e^{-ik^z \tilde{\eta}}) \Big\{ \delta[x_1 \tilde{p}^z - (\tilde{p}_1^z - k^z)] - e^{ik^z \tilde{\eta}} \delta[x_1 \tilde{p}^z - \tilde{p}_1^z] \Big\} \delta[x_2 \tilde{p}^z - \tilde{p}_2^z] \delta[x_1 \tilde{p}^z - \tilde{p}_3^z] \\
& = \alpha_s \delta\left(1 - \frac{x_1}{\omega_1}\right) \delta\left(1 - \frac{x_2}{\omega_2}\right) \frac{\tilde{\Gamma}_{q_1} \otimes \tilde{\Gamma}_{q_2}}{\tilde{p}_1^z \tilde{p}_2^z} \left[\ln\left(\frac{\tilde{\eta}^2}{b_{\perp}^2}\right) + 2 - \frac{\pi \tilde{\eta}}{b_{\perp}} \right].
\end{aligned}$$

The contribution to the matching kernel is then

$$[\Delta_{q_1 q_2}^I]_{q'_1 q'_2} = -4\delta_{q_1 q'_1} \delta_{q_2 q'_2} \delta\left(1 - \frac{x_1}{\omega_1}\right) \delta\left(1 - \frac{x_2}{\omega_2}\right) \left[\ln\left(\frac{\tilde{\eta}^2}{\mathbf{b}_{\perp}^2}\right) + 2 - \frac{\pi \tilde{\eta}}{|\mathbf{b}_{\perp}|} \right] + (1 \leftrightarrow 2). \tag{B.33}$$

Diagram J

For this diagram we can set $\Psi(\omega_3) = \delta(\omega_1 - \omega_3)$ from the beginning, as no squared delta functions show up here. The lightcone diagram can be calculated directly and results in

$$\begin{aligned}
F^J &= -\pi p^+ \mu_0^{2\epsilon} \int d\omega_3 \Psi(\omega_3) \int \frac{d^d k}{(2\pi)^d} e^{i\mathbf{k}_{\perp} \cdot \mathbf{b}_{\perp}} (ig\gamma^{\mu}) \frac{i}{\not{p}_1 - \not{k}} \Gamma_{q_1} \otimes (ig\gamma^{\nu}) \frac{i}{\not{p}_2 + \not{k}} \Gamma_{q_2} \\
& \times \frac{-ig_{\mu\nu}}{k^2} \delta[x_1 p^+ - (p_1^+ - k^+)] \delta[x_2 p^+ - (p_2^+ + k^+)] \delta[x_1 p^+ - p_3^+] \\
& = -\alpha_s \delta\left(1 - \frac{x_1}{\omega_1}\right) \delta\left(1 - \frac{x_2}{\omega_2}\right) \frac{\gamma_{\perp} \rho \gamma_{\perp} \mu \Gamma_{q_1} \otimes \gamma_{\perp}^{\rho} \gamma_{\perp} \nu \Gamma_{q_2}}{p_1^+ p_2^+} \left(g_{\perp}^{\mu\nu} - 2\epsilon \frac{b^{\mu} b^{\nu}}{\mathbf{b}_{\perp}^2} \right) \\
& \times \frac{1}{8} \left[\frac{1}{\epsilon_{\text{ir}}} + \ln\left(\frac{\mu^2 \mathbf{b}_{\perp}^2}{b_0^2}\right) \right]
\end{aligned}$$

As for diagram G, the calculation of the quasi diagram is more complicated and so we first expanding in $1/(|\mathbf{b}_{\perp}|p^z)$, leading to

$$\begin{aligned}
\tilde{F}_c &= -\pi \tilde{p}^+ \mu_0^{2\epsilon} \int d\omega_3 \Psi(\omega_3) \int \frac{d^d k}{(2\pi)^d} e^{i\mathbf{k}_{\perp} \cdot \mathbf{b}_{\perp}} (ig\gamma^{\mu}) \frac{i}{\not{\tilde{p}}_1 - \not{k}} \tilde{\Gamma}_{q_1} \otimes (ig\gamma^{\nu}) \frac{i}{\not{\tilde{p}}_2 + \not{k}} \tilde{\Gamma}_{q_2} \\
& \times \frac{-ig_{\mu\nu}}{k^2} \delta[x_1 \tilde{p}^z - (\tilde{p}_1^z - k^z)] \delta[x_2 \tilde{p}^z - (\tilde{p}_2^z + k^z)] \delta[x_1 \tilde{p}^z - \tilde{p}_3^z] \\
& = -\alpha_s \delta\left(1 - \frac{x_1}{\omega_1}\right) \delta\left(1 - \frac{x_2}{\omega_2}\right) \frac{\gamma_{\rho} \gamma_{\mu} \tilde{\Gamma}_{q_1} \otimes \gamma^{\rho} \gamma_{\nu} \tilde{\Gamma}_{q_2}}{\tilde{p}_1^z \tilde{p}_2^z} \left(\frac{1}{8} \frac{1}{\epsilon_{\text{ir}}} g_{\perp}^{\mu\nu} + \mathcal{O}(\epsilon^0) \right).
\end{aligned}$$

Because the lightcone and quasi diagram share the same IR poles, their difference is finite. Dividing by the infinite normalization constant $\Psi(\omega_1)$ yields

$$[\Delta_{q_1 q_2}^J]_{q'_1 q'_2} = 0. \tag{B.34}$$

Diagram K

For lightcone diagram K we have

$$\begin{aligned}
F^K &= -\pi p^+ \mu_0^{2\epsilon} \int d\omega_3 \Psi(\omega_3) \int \frac{d^d k}{(2\pi)^d} e^{i\mathbf{k}_\perp \cdot \mathbf{b}_\perp} (ig\gamma^\mu) \frac{i}{\not{p}_1 - \not{k}} \Gamma_{q_1} \otimes \Gamma_{q_2} \frac{-i}{-k^+ - i\delta^+} (-ign_a^\nu) \\
&\quad \times \frac{-ig_{\mu\nu}}{k^2} \delta[x_1 p^+ - (p_1^+ - k^+)] \delta[x_2 p^+ - (p_2^+ + k^+)] \delta[x_1 p^+ - p_3^+] \\
&= -\alpha_s \Psi(x_1) \delta(1 - x_1 - x_2) \frac{\Gamma_{q_1} \otimes \Gamma_{q_2}}{p_1^+ p_2^+} \frac{1}{2} \left[\frac{1}{\epsilon_{\text{ir}}} + \ln \left(\frac{\mu^2 \mathbf{b}_\perp^2}{b_0^2} \right) \right] \left[\frac{\omega_2 \frac{x_1}{\omega_1}}{1 - \frac{x_1}{\omega_1}} \theta \left(\frac{x_1}{\omega_1} \right) \theta \left(1 - \frac{x_1}{\omega_1} \right) \right]_+ \\
&\quad + \alpha_s \Psi(\omega_1) \delta \left(1 - \frac{x_1}{\omega_1} \right) \delta \left(1 - \frac{x_2}{\omega_2} \right) \frac{\Gamma_{q_1} \otimes \Gamma_{q_2}}{p_1^+ p_2^+} \frac{1}{2} \left[\frac{1}{\epsilon_{\text{ir}}} + \ln \left(\frac{\mu^2 \mathbf{b}_\perp^2}{b_0^2} \right) \right] \left[1 + \ln \left(\frac{\delta^+}{p_1^+} \right) + \frac{i\pi}{2} \right].
\end{aligned} \tag{B.35}$$

For the quasi diagram we have,

$$\begin{aligned}
\tilde{F}^K &= -\pi \tilde{p}^z \mu_0^{2\epsilon} \int d\omega_3 \Psi(\omega_3) \int \frac{d^d k}{(2\pi)^d} e^{i\mathbf{k}_\perp \cdot \mathbf{b}_\perp} (ig\gamma^\mu) \frac{i}{\not{\tilde{p}}_1 - \not{k}} \tilde{\Gamma}_{q_1} \otimes \tilde{\Gamma}_{q_2} \frac{i}{k^z} (ig\hat{z}^\nu) \\
&\quad \times \frac{-ig_{\mu\nu}}{k^2} \delta[x_1 \tilde{p}^z - (\tilde{p}_1^z - k^z)] \left\{ \delta[x_2 \tilde{p}^z - (\tilde{p}_2^z + k^z)] - e^{-ik^z \tilde{\eta}} \delta[x_2 \tilde{p}^z - \tilde{p}_2^z] \right\} \delta[x_1 \tilde{p}^z - \tilde{p}_3^z] \\
&= -\alpha_s \Psi(x_1) \delta(1 - x_1 - x_2) \frac{\tilde{\Gamma}_{q_1} \otimes \tilde{\Gamma}_{q_2}}{\tilde{p}_1^z \tilde{p}_2^z} \frac{1}{2} \left[\frac{1}{\epsilon_{\text{ir}}} + \ln \left(\frac{\mu^2 \mathbf{b}_\perp^2}{b_0^2} \right) \right] \left[\frac{\omega_2 \frac{x_1}{\omega_1}}{1 - \frac{x_1}{\omega_1}} \theta \left(\frac{x_1}{\omega_1} \right) \theta \left(1 - \frac{x_1}{\omega_1} \right) \right]_+ \\
&\quad - \alpha_s \Psi(\omega_1) \delta \left(1 - \frac{x_1}{\omega_1} \right) \delta \left(1 - \frac{x_2}{\omega_2} \right) \frac{\tilde{\Gamma}_{q_1} \otimes \tilde{\Gamma}_{q_2}}{\tilde{p}_1^z \tilde{p}_2^z} \\
&\quad \times 4i\pi^2 \tilde{p}_1^z \mu_0^{2\epsilon} \int_{-\infty}^{\infty} dy \frac{1 - e^{-iy\tilde{p}_1^z \tilde{\eta}}}{y} \int_0^1 dv \int \frac{d^d \ell}{(2\pi)^d} e^{i\ell_\perp \cdot \mathbf{b}_\perp} \frac{2-y-v}{\ell^4} \delta[\ell^z - (y-v)\tilde{p}_1^z].
\end{aligned} \tag{B.36}$$

Upon subtracting the lightcone and quasi diagrams, the non-trivial x -dependence cancels between the two and $\Psi(\omega_1)$ can be factored out, to yield

$$\begin{aligned}
[\Delta_{q_1 q_2}^K]_{q'_1 q'_2} &= 4\delta_{q_1 q'_1} \delta_{q_2 q'_2} \delta \left(1 - \frac{x_1}{\omega_1} \right) \delta \left(1 - \frac{x_2}{\omega_2} \right) \left\{ \left[\frac{1}{\epsilon_{\text{ir}}} + \ln \left(\frac{\mu^2 \mathbf{b}_\perp^2}{b_0^2} \right) \right] \left[1 + \ln \left(\frac{\delta^+}{p_1^+} \right) \right] \right. \\
&\quad + 8i\pi^2 \tilde{p}_1^z \mu_0^{2\epsilon} \int_{-\infty}^{\infty} dy \frac{1 - \cos(y\tilde{p}_1^z \tilde{\eta})}{y} \int_0^1 dv \int \frac{d^d \ell}{(2\pi)^d} \\
&\quad \times e^{i\ell_\perp \cdot \mathbf{b}_\perp} \frac{2-y-v}{\ell^4} \delta[\ell^z - (y-v)\tilde{p}_1^z] \left. \right\} + (1 \leftrightarrow 2).
\end{aligned} \tag{B.37}$$

Diagram L

For the lightcone-DPD, diagram L vanishes due to the gluon line being connected to two Wilson lines in the n_a direction. For the quasi diagram we find

$$\begin{aligned}
\tilde{F}^L &= -\pi \tilde{p}^z \mu_0^{2\epsilon} \int d\omega_3 \Psi(\omega_3) \int \frac{d^d k}{(2\pi)^d} e^{i\mathbf{k}_\perp \cdot \mathbf{b}_\perp} \tilde{\Gamma}_{q_1} \frac{i}{k^z} (ig\hat{z}^\mu) \otimes \tilde{\Gamma}_{q_2} \frac{-i}{k^z} (ig\hat{z}^\nu) \frac{-ig_{\mu\nu}}{k^2} \\
&\quad \times \delta[x_1 \tilde{p}^z - \tilde{p}_3^z] \left\{ \delta[x_1 \tilde{p}^z - (\tilde{p}_1^z - k^z)] - e^{-ik^z \tilde{\eta}} \delta[x_1 \tilde{p}^z - \tilde{p}_1^z] \right\}
\end{aligned} \tag{B.38}$$

$$\begin{aligned}
& \times \left\{ \delta[x_2 \tilde{p}^z - (\tilde{p}_2^z + k^z)] - e^{+ik^z \tilde{\eta}} \delta[x_2 \tilde{p}^z - \tilde{p}_2^z] \right\} \\
& = -\alpha_s \Psi(\omega_1) \delta\left(1 - \frac{x_1}{\omega_1}\right) \delta\left(1 - \frac{x_2}{\omega_2}\right) \frac{\tilde{\Gamma}_{q_1} \otimes \tilde{\Gamma}_{q_2}}{\tilde{p}_1^z \tilde{p}_2^z} \left[\ln\left(\frac{\tilde{\eta}^2}{b_\perp^2}\right) + 2 - \frac{\pi \tilde{\eta}}{b_\perp} \right]. \tag{B.39}
\end{aligned}$$

Dividing out $\Psi(\omega_1)$, we find that the contribution of diagram L to the matching kernel is given by

$$[\Delta_{q_1 q_2}^L]_{q'_1 q'_2} = 4\delta_{q_1 q'_1} \delta_{q_2 q'_2} \delta\left(1 - \frac{x_1}{\omega_1}\right) \delta\left(1 - \frac{x_2}{\omega_2}\right) \left[\ln\left(\frac{\tilde{\eta}^2}{b_\perp^2}\right) + 2 - \frac{\pi \tilde{\eta}}{b_\perp} \right] + (1 \leftrightarrow 2). \tag{B.40}$$

Remaining integrals in $\Delta^B, \Delta^H, \Delta^E, \Delta^K$

For the color-summed DPD, the remaining integrals cancel between Δ^B and Δ^E . For the color-correlated DPDs, this cancellation no longer holds, due to the different color factors in table 1. In that case, the combination of all four diagrams leads to the following integral,

$$\mathcal{I}(\tilde{p}^z) = \tilde{p}^z \mu_0^{2\epsilon} \int_{-\infty}^{\infty} dy \frac{1 - \cos(y \tilde{p}^z \tilde{\eta})}{y} \int_0^1 dv \int \frac{d^d \ell}{(2\pi)^d} (1 - e^{i\ell_\perp \cdot \mathbf{b}_\perp}) \frac{2 - y - v}{\ell^4} \delta[\ell^z - (y - v)\tilde{p}^z]. \tag{B.41}$$

Note that this integral does not contain any IR divergences due to factor of $1 - e^{i\mathbf{b}_\perp \cdot \mathbf{1}_\perp}$. However, we cannot set $d = 4$ because the term proportional to y in the numerator of the momentum integral results in a UV divergence for $y \rightarrow \pm\infty$. However, this term is finite as $y \rightarrow 0$ and so we can take $\tilde{\eta} \rightarrow \infty$ in this term, leading to trivial integrals over y and v . Splitting off this term, we can rewrite the above integral as

$$\begin{aligned}
\mathcal{I}(\tilde{p}^z) &= \tilde{p}^z \int_{-\infty}^{\infty} dy \frac{1 - \cos(y \tilde{p}^z \tilde{\eta})}{y} \int_0^1 dv (2 - v) \int \frac{d^4 \ell}{(2\pi)^4} \frac{1 - e^{i\ell_\perp \cdot \mathbf{b}_\perp}}{\ell^4} \delta[\ell^z - (y - v)\tilde{p}^z] \\
&\quad - \mu_0^{2\epsilon} \int \frac{d^d \ell}{(2\pi)^d} \frac{1 - e^{i\ell_\perp \cdot \mathbf{b}_\perp}}{\ell^4}. \tag{B.42}
\end{aligned}$$

The integral in the second line is straightforward to compute. To calculate the momentum integral in the first line we first perform a Wick rotation, integrate over all components of the momentum perpendicular to the plane spanned by \mathbf{b}_\perp and \hat{z} , and lastly integrate over the component of ℓ that is parallel to \mathbf{b}_\perp . The result is

$$\begin{aligned}
\mathcal{I}(\tilde{p}^z) &= \frac{i}{16\pi^2} \int_{-\infty}^{\infty} dy \frac{1 - \cos(y \tilde{p}^z \tilde{\eta})}{y} \int_0^1 dv \frac{2 - v}{|y - v|} (1 - e^{-|y - v| b_\perp \tilde{p}^z}) \\
&\quad - \frac{i}{16\pi^2} \left(\frac{1}{\epsilon_{uv}} + L_b \right), \tag{B.43}
\end{aligned}$$

with L_b defined in eq. (B.46). To perform the remaining integral over y and v , we first change the integration bound of the y integral to $[0, \infty)$ by symmetrizing the integrand. The resulting integrand is finite as $y \rightarrow 0$ and so we can drop the regulator $\tilde{\eta}$, leading to

$$\mathcal{I}(\tilde{p}^z) = \frac{i}{16\pi^2} \int_0^\infty dy \frac{1}{y} \int_0^1 dv (2 - v) \left(\frac{1 - e^{-|y - v| b_\perp \tilde{p}^z}}{|y - v|} - \frac{1 - e^{-|y + v| b_\perp \tilde{p}^z}}{|y + v|} \right) \tag{B.44}$$

$$-\frac{i}{16\pi^2}\left(\frac{1}{\epsilon_{uv}}+L_b\right).$$

The remaining integrals over y and v can then be performed. For large $|\mathbf{b}_\perp|\tilde{p}^z$ the result can be written as

$$\mathcal{I}(\tilde{p}^z) = -\frac{i}{16\pi^2}\left(\frac{1}{\epsilon_{uv}} + 2L_b - L_b L_p - 2 + L_p - \frac{1}{2}L_b^2 - \frac{1}{2}L_p^2\right), \quad (\text{B.45})$$

where

$$L_b = \ln\left(\frac{\mu^2 \mathbf{b}_\perp^2}{b_0^2}\right), \quad L_p = \ln\left(\frac{4(\tilde{p}^z)^2}{\mu^2}\right). \quad (\text{B.46})$$

References

- [1] T. Sjostrand and M. van Zijl, *A Multiple Interaction Model for the Event Structure in Hadron Collisions*, *Phys. Rev. D* **36** (1987) 2019.
- [2] J. M. Butterworth, J. R. Forshaw, and M. H. Seymour, *Multiparton interactions in photoproduction at HERA*, *Z. Phys. C* **72** (1996) 637–646, [[hep-ph/9601371](#)].
- [3] T. Sjostrand and P. Z. Skands, *Transverse-momentum-ordered showers and interleaved multiple interactions*, *Eur. Phys. J. C* **39** (2005) 129–154, [[hep-ph/0408302](#)].
- [4] J. Bellm, S. Gieseke, and P. Kirchgaesser, *Improving the description of multiple interactions in Herwig*, *Eur. Phys. J. C* **80** (2020), no. 5 469, [[arXiv:1911.13149](#)].
- [5] M. Dasgupta, K. Khelifa-Kerfa, S. Marzani, and M. Spannowsky, *On jet mass distributions in Z +jet and dijet processes at the LHC*, *JHEP* **10** (2012) 126, [[arXiv:1207.1640](#)].
- [6] I. W. Stewart, F. J. Tackmann, and W. J. Waalewijn, *Dissecting Soft Radiation with Factorization*, *Phys. Rev. Lett.* **114** (2015), no. 9 092001, [[arXiv:1405.6722](#)].
- [7] P. V. Landshoff and J. C. Polkinghorne, *Calorimeter Triggers for Hard Collisions*, *Phys. Rev. D* **18** (1978) 3344.
- [8] C. Goebel, F. Halzen, and D. M. Scott, *Double Drell-Yan Annihilations in Hadron Collisions: Novel Tests of the Constituent Picture*, *Phys. Rev. D* **22** (1980) 2789.
- [9] F. Takagi, *Multiple Production of Quark Jets Off Nuclei*, *Phys. Rev. Lett.* **43** (1979) 1296.
- [10] M. Mekhfi, *Correlations in Color and Spin in Multiparton Processes*, *Phys. Rev. D* **32** (1985) 2380.
- [11] N. Paver and D. Treleani, *Multi-Quark Scattering and Large p_T Jet Production in Hadronic Collisions*, *Nuovo Cim. A* **70** (1982) 215.
- [12] B. Blok, Y. Dokshitzer, L. Frankfurt, and M. Strikman, *The Four jet production at LHC and Tevatron in QCD*, *Phys. Rev. D* **83** (2011) 071501, [[arXiv:1009.2714](#)].
- [13] M. Diehl and A. Schafer, *Theoretical considerations on multiparton interactions in QCD*, *Phys. Lett. B* **698** (2011) 389–402, [[arXiv:1102.3081](#)].
- [14] M. Diehl, D. Ostermeier, and A. Schafer, *Elements of a theory for multiparton interactions in QCD*, *JHEP* **03** (2012) 089, [[arXiv:1111.0910](#)]. [Erratum: JHEP 03, 001 (2016)].
- [15] M. G. Ryskin and A. M. Snigirev, *A Fresh look at double parton scattering*, *Phys. Rev. D* **83** (2011) 114047, [[arXiv:1103.3495](#)].

- [16] A. V. Manohar and W. J. Waalewijn, *A QCD Analysis of Double Parton Scattering: Color Correlations, Interference Effects and Evolution*, *Phys. Rev. D* **85** (2012) 114009, [[arXiv:1202.3794](#)].
- [17] B. Blok, Y. Dokshitzer, L. Frankfurt, and M. Strikman, *Perturbative QCD correlations in multi-parton collisions*, *Eur. Phys. J. C* **74** (2014) 2926, [[arXiv:1306.3763](#)].
- [18] M. Diehl, J. R. Gaunt, D. Ostermeier, P. Plöchl, and A. Schäfer, *Cancellation of Glauber gluon exchange in the double Drell-Yan process*, *JHEP* **01** (2016) 076, [[arXiv:1510.08696](#)].
- [19] M. Diehl, J. R. Gaunt, and K. Schönwald, *Double hard scattering without double counting*, *JHEP* **06** (2017) 083, [[arXiv:1702.06486](#)].
- [20] M. G. A. Buffing, M. Diehl, and T. Kasemets, *Transverse momentum in double parton scattering: factorisation, evolution and matching*, *JHEP* **01** (2018) 044, [[arXiv:1708.03528](#)].
- [21] P. Bartalini and J. R. Gaunt, eds., *Multiple Parton Interactions at the LHC*, vol. 29. WSP, 2019.
- [22] **Axial Field Spectrometer** Collaboration, T. Åkesson et al., *Double Parton Scattering in pp Collisions at $\sqrt{s} = 63\text{-GeV}$* , *Z. Phys. C* **34** (1987) 163.
- [23] **CDF** Collaboration, F. Abe et al., *Study of four jet events and evidence for double parton interactions in $p\bar{p}$ collisions at $\sqrt{s} = 1.8\text{ TeV}$* , *Phys. Rev. D* **47** (1993) 4857–4871.
- [24] **CDF** Collaboration, F. Abe et al., *Measurement of double parton scattering in $p\bar{p}$ collisions at $\sqrt{s} = 1.8\text{ TeV}$* , *Phys. Rev. Lett.* **79** (1997) 584–589.
- [25] **D0** Collaboration, V. M. Abazov et al., *Double Parton Interactions in $\gamma + 3\text{ Jet}$ and $\gamma + b/c\text{jet} + 2\text{ Jet}$ Events in $p\bar{p}$ Collisions at $\sqrt{s} = 1.96\text{ TeV}$* , *Phys. Rev. D* **89** (2014), no. 7 072006, [[arXiv:1402.1550](#)].
- [26] **LHCb** Collaboration, R. Aaij et al., *Observation of double charm production involving open charm in pp collisions at $\sqrt{s} = 7\text{ TeV}$* , *JHEP* **06** (2012) 141, [[arXiv:1205.0975](#)]. [Addendum: *JHEP* **03**, 108 (2014)].
- [27] **ATLAS** Collaboration, G. Aad et al., *Measurement of hard double-parton interactions in $W(\rightarrow l\nu) + 2\text{ jet}$ events at $\sqrt{s} = 7\text{ TeV}$ with the ATLAS detector*, *New J. Phys.* **15** (2013) 033038, [[arXiv:1301.6872](#)].
- [28] **CMS** Collaboration, S. Chatrchyan et al., *Study of Double Parton Scattering Using $W + 2\text{-Jet}$ Events in Proton-Proton Collisions at $\sqrt{s} = 7\text{ TeV}$* , *JHEP* **03** (2014) 032, [[arXiv:1312.5729](#)].
- [29] **D0** Collaboration, V. M. Abazov et al., *Observation and Studies of Double J/ψ Production at the Tevatron*, *Phys. Rev. D* **90** (2014), no. 11 111101, [[arXiv:1406.2380](#)].
- [30] **LHCb** Collaboration, R. Aaij et al., *Production of associated Y and open charm hadrons in pp collisions at $\sqrt{s} = 7$ and 8 TeV via double parton scattering*, *JHEP* **07** (2016) 052, [[arXiv:1510.05949](#)].
- [31] **ATLAS** Collaboration, M. Aaboud et al., *Study of hard double-parton scattering in four-jet events in pp collisions at $\sqrt{s} = 7\text{ TeV}$ with the ATLAS experiment*, *JHEP* **11** (2016) 110, [[arXiv:1608.01857](#)].
- [32] **LHCb** Collaboration, R. Aaij et al., *Measurement of the J/ψ pair production cross-section*

- in pp collisions at $\sqrt{s} = 13$ TeV, *JHEP* **06** (2017) 047, [[arXiv:1612.07451](#)]. [Erratum: *JHEP* **10**, 068 (2017)].
- [33] CMS Collaboration, A. M. Sirunyan et al., *Constraints on the double-parton scattering cross section from same-sign W boson pair production in proton-proton collisions at $\sqrt{s} = 8$ TeV*, *JHEP* **02** (2018) 032, [[arXiv:1712.02280](#)].
 - [34] CMS Collaboration, A. Tumasyan et al., *Study of Z boson plus jets events using variables sensitive to double-parton scattering in pp collisions at 13 TeV*, *JHEP* **10** (2021) 176, [[arXiv:2105.14511](#)].
 - [35] CMS Collaboration, A. Tumasyan et al., *Measurement of double-parton scattering in inclusive production of four jets with low transverse momentum in proton-proton collisions at $\sqrt{s} = 13$ TeV*, *JHEP* **01** (2022) 177, [[arXiv:2109.13822](#)].
 - [36] CMS Collaboration, *Observation of same-sign WW production from double parton scattering in proton-proton collisions at $\sqrt{s} = 13$ TeV*, [[arXiv:2206.02681](#)].
 - [37] J. R. Gaunt and W. J. Stirling, *Double Parton Distributions Incorporating Perturbative QCD Evolution and Momentum and Quark Number Sum Rules*, *JHEP* **03** (2010) 005, [[arXiv:0910.4347](#)].
 - [38] M. Diehl, J. R. Gaunt, D. M. Lang, P. Plöchl, and A. Schäfer, *Sum rule improved double parton distributions in position space*, *Eur. Phys. J. C* **80** (2020), no. 5 468, [[arXiv:2001.10428](#)].
 - [39] M. Diehl and T. Kasemets, *Positivity bounds on double parton distributions*, *JHEP* **05** (2013) 150, [[arXiv:1303.0842](#)].
 - [40] M. Diehl, J. R. Gaunt, P. Pichini, and P. Plöchl, *Double parton distributions out of bounds in colour space*, *Eur. Phys. J. C* **81** (2021), no. 11 1033, [[arXiv:2109.14304](#)].
 - [41] H.-M. Chang, A. V. Manohar, and W. J. Waalewijn, *Double Parton Correlations in the Bag Model*, *Phys. Rev. D* **87** (2013), no. 3 034009, [[arXiv:1211.3132](#)].
 - [42] M. Rinaldi, S. Scopetta, and V. Vento, *Double parton correlations in constituent quark models*, *Phys. Rev. D* **87** (2013) 114021, [[arXiv:1302.6462](#)].
 - [43] W. Broniowski and E. Ruiz Arriola, *Valence double parton distributions of the nucleon in a simple model*, *Few Body Syst.* **55** (2014) 381–387, [[arXiv:1310.8419](#)].
 - [44] M. Rinaldi, S. Scopetta, M. Traini, and V. Vento, *Double parton correlations and constituent quark models: a Light Front approach to the valence sector*, *JHEP* **12** (2014) 028, [[arXiv:1409.1500](#)].
 - [45] M. Rinaldi, S. Scopetta, M. Traini, and V. Vento, *Double parton scattering: a study of the effective cross section within a Light-Front quark model*, *Phys. Lett. B* **752** (2016) 40–45, [[arXiv:1506.05742](#)].
 - [46] T. Kasemets and A. Mukherjee, *Quark-gluon double parton distributions in the light-front dressed quark model*, *Phys. Rev. D* **94** (2016), no. 7 074029, [[arXiv:1606.05686](#)].
 - [47] W. Broniowski, E. Ruiz Arriola, and K. Golec-Biernat, *Generalized Valon Model for Double Parton Distributions*, *Few Body Syst.* **57** (2016), no. 6 405–410, [[arXiv:1602.00254](#)].
 - [48] G. S. Bali, P. C. Bruns, L. Castagnini, M. Diehl, J. R. Gaunt, B. Gläsel, A. Schäfer, A. Sternbeck, and C. Zimmermann, *Two-current correlations in the pion on the lattice*, *JHEP* **12** (2018) 061, [[arXiv:1807.03073](#)].

- [49] A. Courtoy, S. Noguera, and S. Scopetta, *Two-current correlations in the pion in the Nambu and Jona-Lasinio model*, *Eur. Phys. J. C* **80** (2020), no. 10 909, [[arXiv:2006.05300](#)].
- [50] G. S. Bali, L. Castagnini, M. Diehl, J. R. Gaunt, B. Gläkle, A. Schäfer, and C. Zimmermann, *Double parton distributions in the pion from lattice QCD*, *JHEP* **02** (2021) 067, [[arXiv:2006.14826](#)].
- [51] X. Ji, *Parton Physics on a Euclidean Lattice*, *Phys. Rev. Lett.* **110** (2013) 262002, [[arXiv:1305.1539](#)].
- [52] X. Ji, *Parton Physics from Large-Momentum Effective Field Theory*, *Sci. China Phys. Mech. Astron.* **57** (2014) 1407–1412, [[arXiv:1404.6680](#)].
- [53] Y.-Q. Ma and J.-W. Qiu, *Extracting Parton Distribution Functions from Lattice QCD Calculations*, *Phys. Rev. D* **98** (2018), no. 7 074021, [[arXiv:1404.6860](#)].
- [54] A. V. Radyushkin, *Quasi-parton distribution functions, momentum distributions, and pseudo-parton distribution functions*, *Phys. Rev. D* **96** (2017), no. 3 034025, [[arXiv:1705.01488](#)].
- [55] K. Orginos, A. Radyushkin, J. Karpie, and S. Zafeiropoulos, *Lattice QCD exploration of parton pseudo-distribution functions*, *Phys. Rev. D* **96** (2017), no. 9 094503, [[arXiv:1706.05373](#)].
- [56] X. Ji, Y.-S. Liu, Y. Liu, J.-H. Zhang, and Y. Zhao, *Large-momentum effective theory*, *Rev. Mod. Phys.* **93** (2021), no. 3 035005, [[arXiv:2004.03543](#)].
- [57] J.-H. Zhang, X. Ji, A. Schäfer, W. Wang, and S. Zhao, *Accessing Gluon Parton Distributions in Large Momentum Effective Theory*, *Phys. Rev. Lett.* **122** (2019), no. 14 142001, [[arXiv:1808.10824](#)].
- [58] T. Izubuchi, X. Ji, L. Jin, I. W. Stewart, and Y. Zhao, *Factorization Theorem Relating Euclidean and Light-Cone Parton Distributions*, *Phys. Rev. D* **98** (2018), no. 5 056004, [[arXiv:1801.03917](#)].
- [59] X. Xiong, X. Ji, J.-H. Zhang, and Y. Zhao, *One-loop matching for parton distributions: Nonsinglet case*, *Phys. Rev. D* **90** (2014), no. 1 014051, [[arXiv:1310.7471](#)].
- [60] X. Ji, L.-C. Jin, F. Yuan, J.-H. Zhang, and Y. Zhao, *Transverse momentum dependent parton quasidistributions*, *Phys. Rev. D* **99** (2019), no. 11 114006, [[arXiv:1801.05930](#)].
- [61] M. A. Ebert, I. W. Stewart, and Y. Zhao, *Determining the Nonperturbative Collins-Soper Kernel From Lattice QCD*, *Phys. Rev. D* **99** (2019), no. 3 034505, [[arXiv:1811.00026](#)].
- [62] M. A. Ebert, I. W. Stewart, and Y. Zhao, *Towards Quasi-Transverse Momentum Dependent PDFs Computable on the Lattice*, *JHEP* **09** (2019) 037, [[arXiv:1901.03685](#)].
- [63] X. Ji, Y. Liu, and Y.-S. Liu, *TMD soft function from large-momentum effective theory*, *Nucl. Phys. B* **955** (2020) 115054, [[arXiv:1910.11415](#)].
- [64] X. Ji, Y. Liu, and Y.-S. Liu, *Transverse-momentum-dependent parton distribution functions from large-momentum effective theory*, *Phys. Lett. B* **811** (2020) 135946, [[arXiv:1911.03840](#)].
- [65] M. A. Ebert, S. T. Schindler, I. W. Stewart, and Y. Zhao, *Factorization connecting continuum & lattice TMDs*, *JHEP* **04** (2022) 178, [[arXiv:2201.08401](#)].
- [66] S. T. Schindler, I. W. Stewart, and Y. Zhao, *One-loop matching for gluon lattice TMDs*, *JHEP* **08** (2022) 084, [[arXiv:2205.12369](#)].

- [67] A. A. Vladimirov and A. Schäfer, *Transverse momentum dependent factorization for lattice observables*, *Phys. Rev. D* **101** (2020), no. 7 074517, [[arXiv:2002.07527](#)].
- [68] O. del Río and A. Vladimirov, *Quasi Transverse Momentum Dependent Distributions at Next-to-Next-to-Leading order*, [arXiv:2304.14440](#).
- [69] **LPC Collaboration**, J.-C. He, M.-H. Chu, J. Hua, X. Ji, A. Schäfer, Y. Su, W. Wang, Y. Yang, J.-H. Zhang, and Q.-A. Zhang, *Unpolarized Transverse-Momentum-Dependent Parton Distributions of the Nucleon from Lattice QCD*, [arXiv:2211.02340](#).
- [70] **Lattice Parton Collaboration**, Q.-A. Zhang et al., *Lattice-QCD Calculations of TMD Soft Function Through Large-Momentum Effective Theory*, *Phys. Rev. Lett.* **125** (2020), no. 19 192001, [[arXiv:2005.14572](#)].
- [71] P. Shanahan, M. Wagman, and Y. Zhao, *Collins-Soper kernel for TMD evolution from lattice QCD*, *Phys. Rev. D* **102** (2020), no. 1 014511, [[arXiv:2003.06063](#)].
- [72] M. A. Ebert, I. W. Stewart, and Y. Zhao, *Renormalization and matching for the collins-soper kernel from lattice qcd*, *Journal of High Energy Physics* **2020** (Mar, 2020).
- [73] M. Schlemmer, A. Vladimirov, C. Zimmermann, M. Engelhardt, and A. Schäfer, *Determination of the Collins-Soper Kernel from Lattice QCD*, *JHEP* **08** (2021) 004, [[arXiv:2103.16991](#)].
- [74] J.-y. Chiu, A. Fuhrer, A. H. Hoang, R. Kelley, and A. V. Manohar, *Soft-Collinear Factorization and Zero-Bin Subtractions*, *Phys. Rev. D* **79** (2009) 053007, [[arXiv:0901.1332](#)].
- [75] T. Becher and M. Neubert, *Drell-Yan Production at Small q_T , Transverse Parton Distributions and the Collinear Anomaly*, *Eur. Phys. J. C* **71** (2011) 1665, [[arXiv:1007.4005](#)].
- [76] J. Collins, *Foundations of perturbative QCD*, vol. 32. Cambridge University Press, 11, 2013.
- [77] J.-y. Chiu, A. Jain, D. Neill, and I. Z. Rothstein, *The Rapidity Renormalization Group*, *Phys. Rev. Lett.* **108** (2012) 151601, [[arXiv:1104.0881](#)].
- [78] T. Becher and G. Bell, *Analytic Regularization in Soft-Collinear Effective Theory*, *Phys. Lett. B* **713** (2012) 41–46, [[arXiv:1112.3907](#)].
- [79] M. G. Echevarria, I. Scimemi, and A. Vladimirov, *Universal transverse momentum dependent soft function at NNLO*, *Phys. Rev. D* **93** (2016), no. 5 054004, [[arXiv:1511.05590](#)].
- [80] Y. Li, D. Neill, and H. X. Zhu, *An exponential regulator for rapidity divergences*, *Nucl. Phys. B* **960** (2020) 115193, [[arXiv:1604.00392](#)].
- [81] A. V. Manohar and I. W. Stewart, *The Zero-Bin and Mode Factorization in Quantum Field Theory*, *Phys. Rev. D* **76** (2007) 074002, [[hep-ph/0605001](#)].
- [82] X.-d. Ji, J.-p. Ma, and F. Yuan, *QCD factorization for semi-inclusive deep-inelastic scattering at low transverse momentum*, *Phys. Rev. D* **71** (2005) 034005, [[hep-ph/0404183](#)].
- [83] A. Idilbi and T. Mehen, *On the equivalence of soft and zero-bin subtractions*, *Phys. Rev. D* **75** (2007) 114017, [[hep-ph/0702022](#)].
- [84] S. Mantry and F. Petriello, *Factorization and Resummation of Higgs Boson Differential Distributions in Soft-Collinear Effective Theory*, *Phys. Rev. D* **81** (2010) 093007, [[arXiv:0911.4135](#)].

- [85] L.-B. Chen, W. Wang, and R. Zhu, *Next-to-Next-to-Leading Order Calculation of Quasiparton Distribution Functions*, *Phys. Rev. Lett.* **126** (2021), no. 7 072002, [[arXiv:2006.14825](#)].
- [86] Z.-Y. Li, Y.-Q. Ma, and J.-W. Qiu, *Extraction of Next-to-Next-to-Leading-Order Parton Distribution Functions from Lattice QCD Calculations*, *Phys. Rev. Lett.* **126** (2021), no. 7 072001, [[arXiv:2006.12370](#)].
- [87] W. Wang, J.-H. Zhang, S. Zhao, and R. Zhu, *Complete matching for quasidistribution functions in large momentum effective theory*, *Phys. Rev. D* **100** (2019), no. 7 074509, [[arXiv:1904.00978](#)].
- [88] X. Gao, A. D. Hanlon, J. Holligan, N. Karthik, S. Mukherjee, P. Petreczky, S. Syritsyn, and Y. Zhao, *Unpolarized proton PDF at NNLO from lattice QCD with physical quark masses*, *Phys. Rev. D* **107** (2023), no. 7 074509, [[arXiv:2212.12569](#)].
- [89] Z. Fan, W. Good, and H.-W. Lin, *Gluon Parton Distribution of the Nucleon from $2+1+1$ -Flavor Lattice QCD in the Physical-Continuum Limit*, [arXiv:2210.09985](#).
- [90] **HadStruc** Collaboration, T. Khan et al., *Unpolarized gluon distribution in the nucleon from lattice quantum chromodynamics*, *Phys. Rev. D* **104** (2021), no. 9 094516, [[arXiv:2107.08960](#)].
- [91] **HadStruc** Collaboration, C. Egerer et al., *Toward the determination of the gluon helicity distribution in the nucleon from lattice quantum chromodynamics*, *Phys. Rev. D* **106** (2022), no. 9 094511, [[arXiv:2207.08733](#)].
- [92] K. Cichy et al., *Generalized Parton Distributions from Lattice QCD*, 4, 2023. [arXiv:2304.14970](#).
- [93] X. Ji, Y. Liu, A. Schäfer, and F. Yuan, *Single Transverse-Spin Asymmetry and Sivers Function in Large Momentum Effective Theory*, *Phys. Rev. D* **103** (2021), no. 7 074005, [[arXiv:2011.13397](#)].
- [94] Q.-A. Zhang, J. Hua, Y. Huo, X. Ji, Y. Liu, Y.-S. Liu, M. Schlemmer, A. Schäfer, P. Sun, W. Wang, and et al., *Lattice qcd calculations of transverse-momentum-dependent soft function through large-momentum effective theory*, *Physical Review Letters* **125** (Nov, 2020).
- [95] M. Luszczak, R. Maciula, and A. Szczurek, *Production of two $c\bar{c}$ pairs in double-parton scattering*, *Phys. Rev. D* **85** (2012) 094034, [[arXiv:1111.3255](#)].
- [96] A. V. Manohar and W. J. Waalewijn, *Electroweak Logarithms in Inclusive Cross Sections*, *JHEP* **08** (2018) 137, [[arXiv:1802.08687](#)].
- [97] R. Kirschner, *Generalized Lipatov-Altarelli-Parisi Equations and Jet Calculus Rules*, *Phys. Lett. B* **84** (1979) 266–270.
- [98] V. P. Shelest, A. M. Snigirev, and G. M. Zinovev, *The Multiparton Distribution Equations in QCD*, *Phys. Lett. B* **113** (1982) 325.
- [99] Z. Nagy and D. E. Soper, *Numerical integration of one-loop Feynman diagrams for N -photon amplitudes*, *Phys. Rev. D* **74** (2006) 093006, [[hep-ph/0610028](#)].
- [100] B. Blok, Y. Dokshitzer, L. Frankfurt, and M. Strikman, *p QCD physics of multiparton interactions*, *Eur. Phys. J. C* **72** (2012) 1963, [[arXiv:1106.5533](#)].
- [101] M. G. Ryskin and A. M. Snigirev, *Double parton scattering in double logarithm approximation of perturbative QCD*, *Phys. Rev. D* **86** (2012) 014018, [[arXiv:1203.2330](#)].

- [102] B. Blok and M. Strikman, *Multiparton pp and pA Collisions: From Geometry to Parton-Parton Correlations*, *Adv. Ser. Direct. High Energy Phys.* **29** (2018) 63–99, [[arXiv:1709.00334](#)].
- [103] A. V. Manohar and W. J. Waalewijn, *What is Double Parton Scattering?*, *Phys. Lett. B* **713** (2012) 196–201, [[arXiv:1202.5034](#)].
- [104] M. Diehl, J. R. Gaunt, P. Plöchl, and A. Schäfer, *Two-loop splitting in double parton distributions*, *SciPost Phys.* **7** (2019), no. 2 017, [[arXiv:1902.08019](#)].
- [105] M. Diehl, J. R. Gaunt, and P. Ploessl, *Two-loop splitting in double parton distributions: the colour non-singlet case*, *JHEP* **08** (2021) 040, [[arXiv:2105.08425](#)].
- [106] M. Diehl, F. Fabry, and A. Vladimirov, *Two-loop evolution kernels for colour dependent double parton distributions*, [[arXiv:2212.11843](#)].
- [107] A. Vladimirov, *Structure of rapidity divergences in multi-parton scattering soft factors*, *JHEP* **04** (2018) 045, [[arXiv:1707.07606](#)].
- [108] M. G. Echevarría, A. Idilbi, and I. Scimemi, *Soft and Collinear Factorization and Transverse Momentum Dependent Parton Distribution Functions*, *Phys. Lett. B* **726** (2013) 795–801, [[arXiv:1211.1947](#)].
- [109] J.-H. Zhang, *Double Parton Distributions from Euclidean Lattice*, [[arXiv:2304.12481](#)].